Characterization and interpretation of cardiovascular and cardiorespiratory dynamics in cardiomyopathy patients

Javier Rodriguez Benitez

Universitat Politècnica de Catalunya (UPC)
Institut de Bioenginyeria de Catalunya (IBEC)

Doctoral program: Biomedical Engineering

Doctoral thesis

Characterization and interpretation of cardiovascular and cardiorespiratory dynamics in cardiomyopathy patients

by

Javier Rodriguez Benitez

Thesis advisor
Dr. Beatriz F. Giraldo Giraldo

Biomedical Signal Processing and Interpretation (BIOSPIN) group,
IBEC - UPC
Departament d'Enginyeria de Sistemes, Automàtica i
Informàtica Industrial (ESAII), UPC

Barcelona, July 2020

Abstract

Characterization and interpretation of cardiovascular and cardiorespiratory dynamics in cardiomyopathy patients

Javier Rodriguez Benitez
Biomedical Signal Processing and Interpretation (BIOSPIN) group, IBEC
Departament d'Enginyeria de Sistemes, Automàtica i Informàtica Industrial (ESAII), UPC

Doctoral thesis

The main objective of this thesis was to study and characterize the variability of the cardiac, respiratory and vascular systems through electrocardiographic, respiratory flow and blood pressure signals, in patients with idiopathic, dilated, or ischemic disease. The aim of this work was to introduce new indices that could contribute to understanding, describing and characterizing these diseases. With these new indices, we propose methods to classify cardiomyopathy patients according to their cardiovascular risk or etiology. The sudden cardiac death risk stratification of cardiomyopathy patients, including patients with idiopathic dilated cardiomyopathy, remains a clinical challenge. In addition, due to the possible presence of similar symptoms and comorbidities, there are still inaccuracies in the diagnosis of patients based on their etiology. These diagnostic limitations could complicate treatment, and therefore hinder patient prognosis. Our purpose is to introduce new indices with which to characterize the cardiovascular and cardiorespiratory interactions under pathological conditions. More specifically, these analyses focus on the study of ischemic and dilated cardiomyopathy patients associated with sudden cardiac risk stratification. All this new information could facilitate the future diagnosis of cardiomyopathy patients. These studies have been conducted using biomedical signal analysis. Thus, prior to studying these signals, a processing step should be considered to ensure that they are analyzed under optimal conditions. Therefore, a new tool is proposed to reconstruct artifacts in biomedical signals, when needed. This process allows information unrelated to the clinical study that could distort its results to be removed.

In this research, we used four different datasets: the Heris, ART, WeanDB, and Healthy databases. These databases contain electrocardiographic (ECG), blood pressure (BP), and respiratory flow (FLW) signals from which different

data series were extracted: beat to beat intervals (BBI, s), from the ECG signal; systolic and diastolic blood pressure (SBP and DBP, mmHg), from the BP signal; and breathing duration (TT, s), from the FLW signal. We employed the Heris, WeanDB, and Healthy databases to test the artifact reconstruction tool. The Heris database was used with the Poincaré plot analysis for the cardiovascular risk stratification of cardiomyopathy patients according to their left ventricular ejection fraction. The ART database was used for cardiovascular coupling analysis research. The Heris dataset was also used for the cardiorespiratory and vascular variability analysis to classify cardiomyopathy patients based on their cardiorespiratory response associated with vascular activity. In order to contrast all these results, the Healthy database was used as a reference to compare the indices studied.

In the first part of this work, we propose a novel artifact reconstruction method applied to biomedical signals made up of physiological pseudo-cycles. The reconstruction process makes use of information from neighboring events while maintaining the dynamics of the original signal. The method is based on detecting the cycles and artifacts, identifying the number of cycles to reconstruct, and predicting the cycles used to replace the artifact segments. It works by comparing the morphology of the areas under the curve of each event analyzed. The Θ_E parameter is defined as the difference between the areas under the curve when two events are compared. The value of this parameter is low when two events are similar, whereas it is high when the events are dissimilar, such as a physiological cycle and an artifact. Then, an adaptive threshold was defined to identify the artifact episodes. Afterwards, the number of cycles to be reconstructed was generated considering the same number of physiological cycles as in neighbouring signals to the left and right of the original signal. Finally, we tested the method's performance by comparing the number of events and artifacts detected and their correct reconstruction.

The method was tested using ECG, BP and FLW signals. The results showed that most of the artifacts were correctly detected and successfully reconstructed. Physiological cycles were incorrectly detected as artifacts in fewer than 1% of the cases. The application of a reconstruction step, if necessary, allowed us to treat artifacts and interruptions, improving the information from these signals, and therefore, the expected results of the study.

The second part of the study is related to the cardiac death risk stratification of patients based on their left ventricular ejection (LVEF) using the Poincaré plot analysis. The patients where stratified according to their left ventricular ejection fraction and classified as low (LVEF $> 35\%$) or high (LVEF $\leq 35\%$) risk. The BBI, SBP, and TT time series of 46 cardiomyopathy patients from the Heris dataset were used to explore this method. Indices that describe the scatterplot of Poincaré method, related to short- and long- term variabilities, acceleration

and deceleration of the dynamic system, and the complex correlation index were extracted. The linear discriminant analysis (LDA) and support vector machines (SVM) classification methods were used to analyze the results of the extracted parameters. The models were optimized in terms of accuracy.

When comparing low risk vs high risk, the best accuracy (98.12%) was obtained with an SVM model using the ANOVA kernel. When comparing control vs patient groups, the best accuracy (97.01%) was obtained using an SVM model with a Laplacian kernel. Our results suggest that a dysfunction in the vagal activity could prevent the body from correctly maintaining circulatory homeostasis. This reduction in vagal activity and increase in the sympathetic influence could expose the cardiovascular system to frequent states of stress, which could contribute to further worsening the condition over time. Through analyzing the morphology of the Poincaré plot, we were able to introduce indices that allow the cardiorespiratory system dynamics to be characterized. These indices, related to cardiorespiratory and vascular variabilities, are proposed as a means to characterize patients and predict their cardiovascular risk based on their left ventricular ejection fraction.

Next, we studied cardio-vascular couplings based on heart rate variability (HRV) and blood pressure variability (BPV) analyses in order to introduce new indices for noninvasive risk stratification in idiopathic dilated cardiomyopathy patients (IDC). The method was explored through the high-resolution electrocardiogram (ECG) and continuous noninvasive blood pressure (BP) signals of 91 IDC patients from the ART database, and 49 healthy subjects (CON) from the Healthy database. The patients were stratified by their sudden cardiac death (SCD) risk as: high risk (IDC_{HR}), when after two years the subject either died or suffered life-threatening complications, and low risk (IDC_{LR}), when the subject remained stable during this period. Several indices were extracted from the beat-to-beat interval and systolic and diastolic blood pressure, and analyzed using the segmented Poincaré plot analysis (SPPA), the high-resolution joint symbolic dynamics (HRJSD), and the normalized short time partial directed coherence (NSTPDC) methods. Support vector machines (SVM) models were built to classify these patients based on their SCD risk.

Our results suggest that IDC_{HR} patients have decreased HRV and increased BPV compared to both the IDC_{LR} patients and the control subjects, suggesting a decrease in their vagal activity and the compensation of sympathetic activity. The strength of both cardio-systolic and cardio-diastolic coupling was higher in high-risk patients than in low-risk patients. The cardio-systolic coupling analysis revealed that the systolic influence on heart rate gets weaker as the risk increases. The SVM IDC_{LR} vs IDC_{HR} model achieved 98.9% accuracy with an area under the curve (AUC) of 0.96. The IDC and the CON groups obtained 93.6% accuracy and 0.94 AUC. To simulate a circumstance in which the original status of the sub-

ject is unknown, a cascade model was built to merge the aforementioned models, and achieved 94.4% accuracy. The coupling analysis-based indices introduced could be suitable for the sudden cardiac death risk stratification of idiopathic cardiomyopathy patients.

Lastly, we analyzed the cardiorespiratory interaction associated with the systems related to ischemic (ICM) and dilated (DCM) cardiomyopathies. We propose a three-dimensional analysis considering the relation between the cardiac, respiratory and vascular systems. Based on vascular activity as the input and output of the baroreflex response, we evaluated the variability of these systems through the geometrical distribution analyzing the bivariate behavior of the cardiorespiratory interaction in function of the dynamical changes of the vascular activity. The aim of this study was to analyze the suitability of cardiorespiratory and vascular interactions for the classification of ICM and DCM patients. To do this, we studied 41 cardiomyopathy patients from the Heris dataset. All patients selected had a New York heart association index (NYHA) of ≥ 2, and were diagnosed with either ICM (24 patients) or DCM (17 patients). In addition, 39 healthy subjects (CON) from the Healthy data set were used as a reference. In this study, we explored the BBI, TT, SBP and DBP time series.

Vascular activity was determined by defining thresholds associated with the increase, decrease or absence of change in SBP or DBP variability. To analyze this variability, three new sub-spaces were defined based on thresholds: 'up' referred to increasing values; 'no change' referred to values between the negative and positive threshold, and 'down' was used for decreasing values. To evaluate the variability of the cardiorespiratory activity associated with the vascular behavior, a three-dimensional representation was created for each sub-space. This representation was then characterized statistically and morphologically and the resulting indices were used to classify the patients by their etiology through SVM models. The results were validated using leave-one-out cross-validation.

The optimal SVM model for the comparison of ICM vs DCM patients achieved 92.7% accuracy, 94.1% sensitivity and 91.7% specificity. The optimal model for the comparison of cardiomyopathy patients vs CON groups obtained 86.2% accuracy, 82.9% sensitivity, and 89.7% specificity. The optimal model for the comparison of ICM patients vs CON subjects achieved 88.9% accuracy, 87.5% sensitivity, and 89.7% specificity; and for DCM patients vs CON subjects, 87.5% accuracy, 76.5% sensitivity, and 92.3% specificity. The results reflected a more pronounced deterioration of the autonomous regulation in dilated cardiomyopathy patients. In general, the cardiac and respiratory variabilities showed lower values in patients compared to control subjects. Therefore, the analysis of the interaction between cardiac and respiratory activity and blood pressure could provide new insight into the classification of patients by etiology, introducing new information related to the homeostatic control system and other internal relationships. The proposed method not only contributes to analyzing the behavior of ischemic and dilated cardiomyopathy patients, but also introduces a new procedure with which to analyze the dynamic behavior among other related systems.

The research presented in this work should be replicated in larger databases. Therefore, our results are more of a hypothesis-generating nature than confirmatory.

Acknowledgements

This thesis has been developed in the BIOSPIN (Recognized Research Group [GRC], 2009 SGR 722) research group at the Institute for Bioengineering of Catalonia (IBEC), led by Dr. Raimon Jané. I am truly grateful for all the help and advice given during my time with the group, and for the partial financial support I was granted.

First, I would like to express my gratitude to my supervisor Dr. Beatriz F. Giraldo for all the encouragement, nurturing, and patience given throughout my pre-doctoral process. Her support has been critical for the production of this thesis. I thank her for teaching me her art, and for providing the tools that allowed me to grow as a researcher. For all of this, I will be forever in her debt. I would also like to thank the people from the Department of Automatic Control (ESAII) of the Universitat Politècnica de Catalunya (UPC) for their support and advice.

I am grateful to Dr. Andreas Voß and the people from the Department of Medical Engineering at the University of Applied Sciences Jena, Germany, for all their support, guidance, and resources, which were vital for the development of this thesis, and for granting me the opportunity to complete a research stay with their group. It was a rewarding experience, which allowed me to grow both as a researcher and as a person, and for that I thank them. Special thanks to Steffen Schulz for his support and contribution to this thesis. The research stays were funded by both IBEC foundation and the "La Caixa" foundation, and I thank them for their support.

I want to thank Colciencias and Colfuturo foundation for funding my doctoral studies in Barcelona. Your support was critical to the success of the entire thesis.

I would like to give a big warm thanks to my dear colleagues and friends at the UPC and IBEC, I will always cherish the time we spent together enjoying conversations during dinner, exciting times at different congresses, playing darts, and in general all the great times we spent together. I will always remember them all.

A big thank to all my friends back at Jena. I thank them for their warm welcome and making me feel at home. Thanks to them, my time there was incredible.

I want to thank all my friends for all their patience and emotional support. I thank them for always being there whenever I needed. I am really lucky to have them in my life.

I want to thank the whole Rodriguez family for their support and good wishes. A special mention to my nephew Nicolas, for inspiring me to become the best version of myself.

Deep thanks to my mother, father, and brothers for always being there supporting me, for all their love, and for helping me overcome the most difficult times. This thesis would not have been possible without their support.

I owe the deepest of thanks to my sister Ines for pushing me to start this process. I thank her for teaching me her discipline, resilience, and persistence. I thank her for believing in me, even before I did, and for continually and patiently supporting me all the way. She can count on me, always.

Thanks to all of you. This thesis would not have been possible without all your help and support.

Contents

List of Tables

List of Figures

1
Introduction

1.1 Introduction

Recent technological advancements have positively impacted medical practice, and have fostered the development of new tools. These novel advances can not only help physicians to improve their knowledge of pathologies, enabling more accurate diagnoses but they can also have a direct impact on the quality of life of the patient.

According to the World Health Organization, heart disease is the leading cause of death in the world, responsible for 15-20% of mortality worldwide [31]. It is estimated that half of these deaths correspond to sudden cardiac death (SCD). Often, sudden cardiac arrest takes place when the electrical system of the heart malfunctions and becomes erratic. In some cases, the heart starts beating outside homeostatic values and ventricular fibrillation occurs, reducing blood flow to dangerous levels, and often causing death [19]. The cardiovascular risk stratification of these patients still represents a major challenge for cardiologists. In this work, we propose analyzing the cardiac, respiratory and vascular systems to yield new information that can contribute to improving the diagnosis and risk stratification of patients with chronic heart failure.

The majority of SCD incidents occur in patients who are unaware of their heart condition. Early detection of SCD is especially difficult due to the asymptomaticity of some patients [33]. The relevant risk factors include the onset of ischemic heart disease or dilated cardiomyopathy. Likewise, the left ventricular ejection fraction (LVEF) is one of the clinical indices used to assess the heart activity in a patient. In addition, the possible presence of a range of comorbidities, especially in elderly patients, may add complexity into the task of stratification. Consequently, the diagnosis of cardiomyopathies poses a variety of challenges that are currently being investigated.

Despite the differences between the etiologies of these diseases, the symptoms experienced can be similar, contributing to a possible inaccurate diagnosis by means of traditional methods. For instance, ischemic cardiomyopathy (ICM) is related to coronary artery disease [23], while dilated cardiomyopathy (DCM) is characterized by the enlargement and weakening of the left ventricle [30]. On the other hand, some patients with heart failure disease could present relatively normal LVEF levels [12]. New knowledge could lead to more accurate patient treatment and prognosis, and contribute to the improvement of their quality of life.

Notwithstanding the similarities in the physical limitations and symptoms experienced by patients with different cardiomyopathies, there are possible dissimilarities in the functionality and regulation of their cardiovascular systems, including the baroreflex mechanism. These differences are not likely to be assessed through a physical examination or the use of imaging techniques. The development of new clinical tools related to the exploration of cardiovascular and cardiorespiratory systems variability, and the homeostatic regulation processes involved, could contribute to the expansion of the current body of knowledge about these systems in pathological conditions.

Tools based on the analysis of biomedical signals could analyze information that is unreachable by means of other medical examination methods. Biomedical signals are recorded directly from the patients under controlled conditions. These recordings reflect the behavior of the physiological systems, their state and dynamics. More specifically, information related to the time series of these records could contribute to analyzing the cardiovascular and cardiorespiratory behavior of these patients. Consequently, mathematical models could be used to define, characterize and analyze patterns associated with the response of these physiological systems.

On the other hand, biomedical signal recordings can be affected by different types of interference unrelated to the physiological process. These recordings sometimes require a preprocessing stage in order to minimize the effects of this interference. Biomedical signal preprocessing is used to remove interference due to factors such as the electrical network, outliers, spikes or physiological interferences, among others. In other cases, these records could present other undesired events that would require the use of more specific techniques in order to reconstruct them and maintain the dynamic of the physiological system.

1.2 State of the art

For the purpose of analyzing, characterizing and interpreting the functionality of cardiovascular and cardiorespiratory dynamics in patients with chronic heart failure, we present the following brief description of previously published relevant research. These works are mainly related to cardiovascular risk stratification, and the characterization of cardiomyopathies. Research related to artifact reconstruction in biomedical signals is also presented.

1.2.1 Processing of artifacts in biomedical signals

In order to extract relevant information from a biomedical signal, components that are not related to the physiological process must be removed or attenuated. These components, referred to as artifacts, can have different lengths, shapes and sources. Reconstructing these corrupted segments can prevent potential mistakes during the analysis of the signal.

Several studies have reported solutions to the artifact interference issue. For instance, the Bayesian filter has been used to estimate a new state space, with the assumption that the dynamic of the system is Markovian [13]. Some authors have developed methods for removing transcranial magnetic stimulation-induced artifacts from electroencephalographic (EEG) and photoplethysmographic (PPG) signals using a two-part estimation Bayesian filter (*a priori - a posteriori*) [22, 21, 29]. Other authors have implemented a power spectral density-based wavelet Wiener filter to minimize the mean square error between the original ECG signals and their estimation [41].

Some researchers have used a template to analyze the morphological features of a signal divided in segments [15, 16]. Multiple synchronized signals were considered to compare synchronized segments with artifacts using a template, and then the reconstruction was performed based on the past information from that segment of the template.

The approach taken by other authors was to train a neural network model with uncorrupted signals and then predict the output of the affected segments during the reconstruction step [28]. Independent component analysis (ICA) has also been explored as an artifact detection and reconstruction technique [3, 27, 17]. Canonical correlation analysis was successfully used to remove muscle artifacts from EEGs, by reconstructing the signal from components without muscle artifact sources [8]. Morphological correlation analysis, which divides the signal into components that have different morphological characteristics, has also been explored as a means to remove artifacts from EEG recordings [50]. Other works have studied the suitability of local singular spectrum analysis to remove low-frequency and high-amplitude artifacts from EEG recordings [44]. The fast ICA method was studied as a means to eliminate ocular artifacts from EEG and magnetoencephalogram signals [20]. Additionally, stationary sub-space analysis has been considered as a method for removing optical artifacts in EEG recordings [51].

In addition, wavelet methods have been tried on ECG and BP signals through the application of reconstructed wavelets to replace the affected segments of the signal [3, 11]. Other methods developed are based on empirical mode decomposition in respiratory flow (FLW), PPG, and ECG signals, which consists of decomposing the recordings into instantaneous frequency series, achieving reconstruction when the artifacts are present several times over the full length of the signal [27, 46, 26]. Motion artifacts in the heart rate signal have been reconstructed using time-varying spectral analysis, by calculating the power spectral density of the signals and comparing the time-varying spectra and the accelerometer data to distinguish the motion artifacts from the PPG spectrum [36].

1.2.2 Cardiovascular risk stratification

Cardiovascular diseases are one of the main causes of death in first world countries. They commonly manifest as sudden cardiac death (SCD), caused by unexpected loss of cardiac function [31]. According to L. Saxon., (2019) [37], SCD is responsible for half of all heart disease related deaths. The introduction of new indices related to the complex cardiovascular and cadiorespiratory interactions under pathological conditions could improve SCD risk stratification, as well as the early detection of patients at high risk of SCD.

Previous studies have hypothesized various strategies to assess SCD risk based on clinical tests data, imaging techniques, and signal processing methods, among others. In the ECG signal, the corrected QT interval was tested in elderly subjects and was associated with SCD risk [32]. Other authors have analyzed T-wave inversions, wide QRS-T angle, and the left bundle branch block, and suggested that it prolonged the ability of QRS to predict all-cause mortality, including SCD, but despite being useful for prediction, it does not seem to predict individual risk [2]. Some research suggests that sympathetic dominance of the autonomic nervous system in conjunction with pro-arrhythmic processes increases the probability of

SCD in patients with ventricular fibrillation problems [40].

In other research, peak oxygen uptake was evaluated during exercise to stratify cardiovascular risk in ambulatory patients with heart failure with ischemic and dilated cardiomyopathies. The authors claim that a predicted absolute peak oxygen uptake of over 50% could provide a good short-term prognosis in patients undergoing medical treatment [42]. Ventricular arrhythmias have been studied to stratify mortality risk among patients with severe ischemic and non-ischemic dilated cardiomyopathy, suggesting that complex ventricular arrhythmias represent an independent mortality risk factor [18].

Cardiac imaging of the myocardial scar, including the infarction border zone, has also been analyzed to stratify SCD risk. The quantification of the total myocardial scar was explored as a possible index with which to determine an appropriate implantable cardioverter defibrillator (ICD) therapy in comparison with the left ventricular ejection fraction measure (LVEF) [4]. Other studies have demonstrated that the image-based analysis of myocardial scars can contribute to the decision to implant ICDs in SCD patients [35, 38, 48].

Heart rate variability (HRV) has also been studied as a measure of autonomic tone. Higher vagal tone activity is related to increased spontaneous variations in heart rate, and multiple non-linear techniques have been applied to study it [47, 43, 10, 49, 14]. Lower indices related to this variability have been associated with patients at risk of SCD, regardless of their LVEF [24, 25, 34]. Another index that has been explored is heart rate turbulence as a measure of autonomic function. This index may be capable of predicting SCD-related mortality by assessing the absence of this behavior [39]. The dynamics of the cardiovascular system behave in a highly complex way through the interplays of different linear and non-linear subsystems [45]. Changes in blood pressure are reflected in changes in heart-rate regulation, and vice versa [9].

1.2.3 Ischemic and dilated cardiomyopathy characterization

Heart failure is a complex cardiovascular disease brought on by functional or structured cardiac disorders. Heart failure patients often have multiple comorbidities that can make diagnosis, and therefore treatment, challenging. More accurate identification of this pathology can lead to an improvement in the patient's quality of life.

In one study, calcium release during the excitation-contraction coupling of the heart was investigated in both ischemic and dilated cardiomyopathy patients [6].

The authors found that the calcium release channel of the sarcoplasmic reticulum levels was 28% lower in ICM patients, suggesting that ischemic hearts exhibit diminished calcium release during excitation-contraction. This pathological behavior could be caused by the abnormal calcium processing of myopathic cardiac muscle in ischemic heart disease.

Other authors have measured the behavior of components of the β-adrenergic receptor-G protein-adenylate cyclase complex and adrenergic neurotransmitter levels in the left and right ventricular myocardium of patients with ischemic and dilated cardiomyopathy. They revealed differences between the regulatory β-receptor-effector related mechanisms in ICM vs DCM patients [7]. ICM patients were characterized by less β-adrenergic receptor downregulation in both ventricles, a decreased coupling of β-adrenergic receptors mediating a contractile response in right ventricular tissue, and decreased coupling of β-adrenergic receptors mediating adenylate cyclase stimulation in the left ventricular tissue.

Another study compared the myocardial tissue from ischemic and dilated cardiomyopathy patients [5]. The authors found a reduction in positive inotropic effects, leading to weaker contractions in DCM patients compared to ICM patients. This result suggests that increased levels of heterotrimeric $G_{i\alpha}$ proteins and reduced basal adenylate cyclase activity give rise to the abnormal regulation of contractility in dilated hearts. Other authors have used both neural networks and fuzzy methods to classify different heart diseases, including ischemic and dilated cardiomyopathies [1].

1.3 Objectives

The main objective of this thesis was to study and characterize the variability of the cardiac, respiratory and vascular systems using the electrocardiographic, respiratory flow and blood pressure signals from patients with idiopathic, dilated, or ischemic disease. The aim of this work was to introduce new indices that can contribute to understanding, describing and characterizing these diseases and their classification. This new information could offer insight into the underlying physiological processes involved in cardiovascular regulation. Finally, these processes could improve the diagnosis and risk stratification of heart failure patients.

New indices are proposed to describe cardiovascular and cardiorespiratory interactions under pathological conditions. More specifically, these analyses focus on the study of ischemic and dilated cardiomyopathy patients associated with sudden cardiac risk stratification. Additionally, a new tool is proposed as a means to reconstruct artifacts in biomedical signals whenever possible. This process allows information unrelated to the clinical study to be removed, to prevent it from potentially distorting the results.

1.4 Outline

This thesis is organized as follows:

Chapter 2: ***Cardiac, respiratory and vascular systems.*** This chapter consists of a brief description of the physiology of these systems, their interaction, and their regulation mechanisms.

Chapter 3: ***Databases.*** Here the databases used in this research are described, including clinical information, types of registered signals, and the preprocessing applied. In addition, the statistical methods applied for treatment of indices is presented.

Chapter 4: ***Artifact reconstruction in biomedical signals.*** In this chapter, an artifact reconstruction method for quasi-periodic signals is proposed. The method consists of the reconstruction of corrupted segments of the signal using information from neighboring cycles. This method is tested using both synthetic and real signals.

Chapter 5: ***Classification of heart failure patients through Poincaré plot analysis.*** The Poincaré plot analysis was used to characterize cardiovascular variability in cardiomyopathy patients. This analysis was applied to the stratification of patients considering different levels of sudden cardiac death risk based on their left ventricular ejection fraction.

Chapter 6: ***Cardiovascular coupling analysis applied to cardiomyopathy patients.*** Cardiovascular coupling analysis is proposed as a means of studying of heart rate and blood pressure variabilities. New indices for noninvasive sudden cardiac death risk stratification in idiopathic cardiomyopathy patients are introduced.

Chapter 7: ***Cardiorespiratory and cardiovascular variability analysis.*** Vascular activity and baroreflex behavior were characterized according to cardiorespiratory response. New indices related to the variability of these systems were extracted to classify ischemic and dilated cardiomyopathy patients.

Chapter 8: ***Discussion and conclusions.*** The results and contributions of this thesis are summarized in this chapter. Additionally, some possible future extensions of this research are presented.

Chapter 1 bibliography

[1] R. Acharya, A. Kumar, A. Bhat, C. Lim, S. Lyengar, N. Kannathal, and S. Krishnan. "Classification of cardiac abnormalities using heart rate signals." In: *Med. Biol. Eng. Comput.* (2004).

[2] A. L. Aro, O. Anttonen, J. T. Tikkanen, M. J. Junttila, T. Kerola, H. A. Rissanen, A. Reunanen, and H. V. Huikuri. "Intraventricular conduction delay in a standard 12-lead electrocardiogram as a predictor of mortality in the general population". In: *Circ Arrhythm Electrophysiol* 4.5 (2011), pp. 704–10. ISSN: 1941-3084 (Electronic) 1941-3084 (Linking). DOI: `10.1161/CIRCEP.111.963561`. URL: `https://www.ncbi.nlm.nih.gov/pubmed/21841194`.

[3] B. Azzerboni, M. Carpentieri, F. La Foresta, and F. C. Morabito. "Neural-ICA and wavelet transform for artifacts removal in surface EMG". In: *2004 IEEE International Joint Conference on Neural Networks (IEEE Cat. No.04CH37541).* Vol. 4, 3223–3228 vol.4. DOI: `10.1109/IJCNN.2004.1381194`.

[4] M. Bertini, M. J. Schalij, J. J. Bax, and V. Delgado. "Emerging role of multimodality imaging to evaluate patients at risk for sudden cardiac death". In: *Circ Cardiovasc Imaging* 5.4 (2012), pp. 525–35. ISSN: 1942-0080 (Electronic) 1941-9651 (Linking). DOI: `10.1161/CIRCIMAGING.110.961532`. URL: `https://www.ncbi.nlm.nih.gov/pubmed/22811416`.

[5] M. Bohm, P. Gierschik, K. Jakobs, B. Pieske, P. Schnabel, M. Ungerer, and E. Erdmann. "Increase of $G_{i\alpha}$. in Human Hearts With Dilated but Not Ischemic Cardiomyopathy." In: *Circulation* (1990).

[6] A. Brillantes, P. Allen, T. Takahashi, S. Izumo, and A. Marks. "Differences in cardiac calcium release channel (ryanodine receptor) expression in myocardium from patients with end-stage heart failure caused by ischemic versus dilated cardiomyopathy." In: *Circulation Research* (1992).

[7] M. Bristow, F. Anderson, D. Port, L. Skerl, R. Hershberger, P. Larrabee, J. O'Connell, D. Renlund, K. Volkman, J. Murray, and A. Fledman. "Differences in β-adrenergic neuroeffector mechanisms in ischemic versus idiopathic dilated cardiomyopathy." In: *Circulation* (1991).

[8] W. De Clercq, A. Vergult, B. Vanrumste, W. Van Paesschen, and S. Van Huffel. "Canonical Correlation Analysis Applied to Remove Muscle Artifacts From the Electroencephalogram". In: *IEEE Transactions on Biomedical Engineering* 53.12 (2006), pp. 2583–2587. ISSN: 0018-9294. DOI: `10.1109/TBME.2006.879459`.

[9] M. A. Cohen and J. A. Taylor. "Short-term cardiovascular oscillations in man: measuring and modelling the physiologies". In: *J Physiol* 542.Pt 3 (2002), pp. 669–83. ISSN: 0022-3751 (Print) 0022-3751 (Linking). URL: `https://www.ncbi.nlm.nih.gov/pubmed/12154170`.

[10] E. Ebrahimzadeh, M. Pooyan, and A. Bijar. "A novel approach to predict sudden cardiac death (SCD) using nonlinear and time-frequency analyses from HRV signals". In: *PLoS One* 9.2 (2014), e81896. ISSN: 1932-6203 (Electronic) 1932-6203 (Linking). DOI: `10.1371/journal.pone.0081896`. URL: `https://www.ncbi.nlm.nih.gov/pubmed/24504331`.

[11] A. Fanelli and T. Heldt. "Signal quality quantification and waveform reconstruction of arterial blood pressure recordings". In: *Conf Proc IEEE Eng Med Biol Soc* 2014 (2014), pp. 2233–6. ISSN: 1557-170X. DOI: `10.1109/EMBC.2014.6944063`. URL: `https://www.ncbi.nlm.nih.gov/pubmed/25570431`.

[12] Gregg C. Fonarow. "Refining Classification of Heart Failure Based on Ejection Fraction". In: *JACC: Heart Failure* 5.11 (2017), pp. 808–809. ISSN: 2213-1779. DOI: `10.1016/j.jchf.2017.08.011`. eprint: `https://heartfailure.onlinejacc.org/content/5/11/808.full.pdf`. URL: `https://heartfailure.onlinejacc.org/content/5/11/808`.

[13] V. Fox, J. Hightower, Liao Lin, D. Schulz, and G. Borriello. "Bayesian filtering for location estimation". In: *IEEE Pervasive Computing* 2.3 (2003), pp. 24–33. ISSN: 1536-1268. DOI: `10.1109/MPRV.2003.1228524`.

[14] H. Fujita, R. Acharya, V. Sudarshan, D. Ghista, V. Sree, L. Lim Wei Jie, and J. Koh. "Sudden cardiac death (SDC) prediction based on nonlinear heart rate variability features and SCD index". In: *Applied Soft Computing* 43 (2016), pp. 210–519.

[15] G. Ganeshapillai, J. F. Liu, and J. Guttag. "Reconstruction of ECG signals in presence of corruption". In: *2011 Annual International Conference of the IEEE Engineering in Medicine and Biology Society*, pp. 3764–3767. DOI: `10.1109/IEMBS.2011.6090642`.

[16] Gartheeban Ganeshapillai and John Guttag. "Real time reconstruction of quasiperiodic multi parameter physiological signals". In: *EURASIP Journal on Advances in Signal Processing* 2012.1 (2012), p. 173. ISSN: 1687-6180. DOI: `10.1186/1687-6180-2012-173`. URL: `https://doi.org/10.1186/1687-6180-2012-173`.

[17] Taigang He, Gari Clifford, and Lionel Tarassenko. "Application of independent component analysis in removing artefacts from the electrocardiogram". In: *Neural Computing & Applications* 15.2 (2006), pp. 105–116. ISSN: 1433-3058. DOI: 10.1007/s00521-005-0013-y. URL: https://doi.org/10.1007/s00521-005-0013-y.

[18] J. Holmes, S. Kubo, R. Cody, and P. Kligfield. "Arrhythmias in ischemic and nonischemic dilated cardiomyopathy: Prediction of mortality by ambulatory electrocardiography." In: *The american journal of cardiology* (1985).

[19] C. Israel. "Mechanisms of sudden cardiac death." In: *Indian Heart J* (2014).

[20] Christopher J. James and David Lowe. "Extracting multisource brain activity from a single electromagnetic channel". In: *Artificial Intelligence in Medicine* 28.1 (2003), pp. 89–104. ISSN: 0933-3657. DOI: https://doi.org/10.1016/S0933-3657(03)00037-X. URL: http://www.sciencedirect.com/science/article/pii/S093336570300037X.

[21] "Kalman Filter Based Adaptive Reduction of Motion Artifact from Photoplethysmographic Signal". In: *International Journal of Electrical, Computer, Energetic, Electronic and Communication Engineering* 2 (2008), pp. 12–16. ISSN: 1307-6892. URL: http://waset.org/publications/7359.

[22] R. E. Kalman. "A New Approach to Linear Filtering and Prediction Problems". In: *Journal of Basic Engineering* 82.1 (1960), pp. 35–45. ISSN: 0098-2202. DOI: 10.1115/1.3662552. URL: http://dx.doi.org/10.1115/1.3662552.

[23] A. La Barck, J. Akers, and T. Merrill. "Tissue oxygen transfer during reperfusion and post-conditioning." In: *American society of mechanical engineers* (2013).

[24] M. T. La Rovere, Jr. Bigger J. T., F. I. Marcus, A. Mortara, and P. J. Schwartz. "Baroreflex sensitivity and heart-rate variability in prediction of total cardiac mortality after myocardial infarction. ATRAMI (Autonomic Tone and Reflexes After Myocardial Infarction) Investigators". In: *Lancet* 351.9101 (1998), pp. 478–84. ISSN: 0140-6736 (Print) 0140-6736 (Linking). URL: https://www.ncbi.nlm.nih.gov/pubmed/9482439.

[25] M. T. La Rovere, G. D. Pinna, R. Maestri, A. Mortara, S. Capomolla, O. Febo, R. Ferrari, M. Franchini, M. Gnemmi, C. Opasich, P. G. Riccardi, E. Traversi, and F. Cobelli. "Short-term heart rate variability strongly predicts sudden cardiac death in chronic heart failure patients". In: *Circulation* 107.4 (2003), pp. 565–70. ISSN: 1524-4539 (Electronic) 0009-7322 (Linking). URL: https://www.ncbi.nlm.nih.gov/pubmed/12566367.

[26] J. Lee, D. D. McManus, S. Merchant, and K. H. Chon. "Automatic motion and noise artifact detection in Holter ECG data using empirical mode decomposition and statistical approaches". In: *IEEE Trans Biomed Eng* 59.6 (2012), pp. 1499–506. ISSN: 1558-2531. DOI: 10.1109/TBME.2011.2175729. URL: https://www.ncbi.nlm.nih.gov/pubmed/22086485.

[27] S. Liu, Q. He, R. X. Gao, and P. Freedson. "Empirical mode decomposition applied to tissue artifact removal from respiratory signal". In: *Conf Proc IEEE Eng Med Biol Soc* 2008 (2008), pp. 3624–7. ISSN: 1557-170X. DOI: 10.1109/IEMBS.2008.4649991. URL: https://www.ncbi.nlm.nih.gov/pubmed/19163494.

[28] J. McBride, A. Sullivan, H. Xia, A. Petrie, and X. Zhao. "Reconstruction of physiological signals using iterative retraining and accumulated averaging of neural network models". In: *Physiol Meas* 32.6 (2011), pp. 661–75. ISSN: 1361-6579. DOI: 10.1088/0967-3334/32/6/004. URL: https://www.ncbi.nlm.nih.gov/pubmed/21566268.

[29] F. Morbidi, A. Garulli, D. Prattichizzo, C. Rizzo, and S. Rossi. "Application of Kalman Filter to Remove TMS-Induced Artifacts from EEG Recordings". In: *IEEE Transactions on Control Systems Technology* 16.6 (2008), pp. 1360–1366. ISSN: 1063-6536. DOI: 10.1109/TCST.2008.921814.

[30] R. Muthiah. "Left Ventricular Myxoma—A Case Report." In: *Scientific research* (2016).

[31] World Health Organization. *World Health Statistics 2019*. Geneva: World Health Organization, 2019.

[32] R. Panikkath, K. Reinier, A. Uy-Evanado, C. Teodorescu, J. Hattenhauer, R. Mariani, K. Gunson, J. Jui, and S. S. Chugh. "Prolonged Tpeak-to-tend interval on the resting ECG is associated with increased risk of sudden cardiac death". In: *Circ Arrhythm Electrophysiol* 4.4 (2011), pp. 441–7. ISSN: 1941-3084 (Electronic) 1941-3084 (Linking). DOI: 10.1161/CIRCEP.110.960658. URL: https://www.ncbi.nlm.nih.gov/pubmed/21593198.

[33] G. Piccirillo, D. Magri, S. Matera, M. Magnanti, A. Torrini, E. Pasquazzi, E. Schifano, S. Velitti, V. Marigliano, and R. Quaglione. "QT variability strongly predicts sudden cardiac death in asymptomatic subjects with mild or moderate left ventricular systolic dysfunction: a prospective study." In: *European heart journal* (2006).

[34] Piotr Ponikowski, Stefan D. Anker, Tuan Peng Chua, Roman Szelemej, Massimo Piepoli, Stamatis Adamopoulos, Katharine Webb-Peploe, Derek Harrington, Waldemar Banasiak, Krzysztof Wrabec, and Andrew J. S. Coats. "Depressed Heart Rate Variability as an Independent Predictor of Death in Chronic Congestive Heart Failure Secondary to Ischemic or Idiopathic Dilated Cardiomyopathy". In: *American Journal of Cardiology* 79.12 (1997), pp. 1645–1650. ISSN: 0002-9149. DOI: 10.1016/S0002-9149(97)00215-4. URL: https://doi.org/10.1016/S0002-9149(97)00215-4.

[35] S. D. Roes, C. J. Borleffs, R. J. van der Geest, J. J. Westenberg, N. A. Marsan, T. A. Kaandorp, J. H. Reiber, K. Zeppenfeld, H. J. Lamb, A. de Roos, M. J. Schalij, and J. J. Bax. "Infarct tissue heterogeneity assessed with contrast-enhanced MRI predicts spontaneous ventricular arrhythmia

in patients with ischemic cardiomyopathy and implantable cardioverter-defibrillator". In: *Circ Cardiovasc Imaging* 2.3 (2009), pp. 183–90. ISSN: 1942-0080 (Electronic) 1941-9651 (Linking). URL: https://www.ncbi.nlm.nih.gov/pubmed/19808591.

[36] Seyed M. A. Salehizadeh, Duy Dao, Jeffrey Bolkhovsky, Chae Cho, Yitzhak Mendelson, and Ki H. Chon. "A Novel Time-Varying Spectral Filtering Algorithm for Reconstruction of Motion Artifact Corrupted Heart Rate Signals During Intense Physical Activities Using a Wearable Photoplethysmogram Sensor". In: *Sensors (Basel, Switzerland)* 16.1 (2015), p. 10. ISSN: 1424-8220. DOI: 10.3390/s16010010. URL: https://www.ncbi.nlm.nih.gov/pmc/PMC4732043/.

[37] L. Saxon. *Sudden cardiac death: epidemiology and temporal trends.* Reviews in cardiovascular medicine, 2019.

[38] A. Schmidt, C. F. Azevedo, A. Cheng, S. N. Gupta, D. A. Bluemke, T. K. Foo, G. Gerstenblith, R. G. Weiss, E. Marban, G. F. Tomaselli, J. A. Lima, and K. C. Wu. "Infarct tissue heterogeneity by magnetic resonance imaging identifies enhanced cardiac arrhythmia susceptibility in patients with left ventricular dysfunction". In: *Circulation* 115.15 (2007), pp. 2006–14. ISSN: 1524-4539 (Electronic) 0009-7322 (Linking). URL: https://www.ncbi.nlm.nih.gov/pubmed/17389270.

[39] G. Schmidt, M. Malik, P. Barthel, R. Schneider, K. Ulm, L. Rolnitzky, A. J. Camm, Jr. Bigger J. T., and A. Schomig. "Heart-rate turbulence after ventricular premature beats as a predictor of mortality after acute myocardial infarction". In: *Lancet* 353.9162 (1999), pp. 1390–6. ISSN: 0140-6736 (Print) 0140-6736 (Linking). DOI: 10.1016/S0140-6736(98)08428-1. URL: https://www.ncbi.nlm.nih.gov/pubmed/10227219.

[40] P. J. Schwartz, M. T. La Rovere, and E. Vanoli. "Autonomic nervous system and sudden cardiac death. Experimental basis and clinical observations for post-myocardial infarction risk stratification". In: *Circulation* 85.1 Suppl (1992), pp. I77–91. ISSN: 0009-7322 (Print) 0009-7322 (Linking). URL: https://www.ncbi.nlm.nih.gov/pubmed/1728509.

[41] L. Smital, M. Vítek, J. Kozumplík, and I. Provazník. "Adaptive Wavelet Wiener Filtering of ECG Signals". In: *IEEE Transactions on Biomedical Engineering* 60.2 (2013), pp. 437–445. ISSN: 0018-9294. DOI: 10.1109/TBME.2012.2228482.

[42] A. Stelken, L Younis, S. Jennison, D Miller, L Miller, L Shaw, D. Kargl, and B. Chaitman. "Prognostic value of cardiopulmonary exercise testing using percent achieved of predicted peak oxygen uptake for patients with ischemic and dilated cardiomyopathy." In: *Journal of the American College of Cardiology* (1995).

[43] Task-Force-of-the-European-Society-of-Cardiology-the-North-American-Society-of-Pacing-Electrophysiology. "Heart rate variability: standards of measurement, physiological interpretation and clinical use. Task Force of the European Society of Cardiology and the North American Society of Pacing and Electrophysiology". In: *Circulation* 93.5 (1996), pp. 1043–65. ISSN: 0009-7322 (Print) 0009-7322 (Linking). URL: https://www.ncbi.nlm.nih.gov/pubmed/8598068.

[44] A. R. Teixeira, A. M. Tomé, E. W. Lang, P. Gruber, and A. Martins da Silva. "Automatic removal of high-amplitude artefacts from single-channel electroencephalograms". In: *Computer Methods and Programs in Biomedicine* 83.2 (2006), pp. 125–138. ISSN: 0169-2607. DOI: https://doi.org/10.1016/j.cmpb.2006.06.003. URL: http://www.sciencedirect.com/science/article/pii/S0169260706001283.

[45] A. Voss, S. Schulz, R. Schroeder, M. Baumert, and P. Caminal. "Methods derived from nonlinear dynamics for analysing heart rate variability". In: *Philos Trans A Math Phys Eng Sci* 367.1887 (2009), pp. 277–96. ISSN: 1364-503X (Print) 1364-503X (Linking). DOI: 10.1098/rsta.2008.0232. URL: https://www.ncbi.nlm.nih.gov/pubmed/18977726.

[46] Q. Wang, P. Yang, and Y. Zhang. "Artifact reduction based on Empirical Mode Decomposition (EMD) in photoplethysmography for pulse rate detection". In: *Conf Proc IEEE Eng Med Biol Soc* 2010 (2010), pp. 959–62. ISSN: 1557-170X. DOI: 10.1109/IEMBS.2010.5627581. URL: https://www.ncbi.nlm.nih.gov/pubmed/21096980.

[47] M. M. Wolf, G. A. Varigos, D. Hunt, and J. G. Sloman. "Sinus arrhythmia in acute myocardial infarction". In: *Med J Aust* 2.2 (1978), pp. 52–3. ISSN: 0025-729X (Print) 0025-729X (Linking). URL: https://www.ncbi.nlm.nih.gov/pubmed/713911.

[48] K. C. Wu, G. Gerstenblith, E. Guallar, J. E. Marine, D. Dalal, A. Cheng, E. Marban, J. A. Lima, G. F. Tomaselli, and R. G. Weiss. "Combined cardiac magnetic resonance imaging and C-reactive protein levels identify a cohort at low risk for defibrillator firings and death". In: *Circ Cardiovasc Imaging* 5.2 (2012), pp. 178–86. ISSN: 1942-0080 (Electronic) 1941-9651 (Linking). DOI: 10.1161/CIRCIMAGING.111.968024. URL: https://www.ncbi.nlm.nih.gov/pubmed/22267750.

[49] L. Wu, Z. Jiang, C. Li, and M. Shu. "Prediction of heart rate variability on cardiac sudden death in heart failure patients: a systematic review". In: *Int J Cardiol* 174.3 (2014), pp. 857–860. ISSN: 1874-1754 (Electronic) 0167-5273 (Linking). DOI: 10.1016/j.ijcard.2014.04.176. URL: https://www.ncbi.nlm.nih.gov/pubmed/24804906.

[50] X. Yong, R. K. Ward, and G. E. Birch. "Artifact removal in EEG using Morphological Component Analysis". In: *2009 IEEE International Conference on Acoustics, Speech and Signal Processing*, pp. 345–348. DOI: 10.1109/ICASSP.2009.4959591.

[51] Hong Zeng, Aiguo Song, Ruqiang Yan, and Hongyun Qin. "EOG Artifact Correction from EEG Recording Using Stationary Subspace Analysis and Empirical Mode Decomposition". In: *Sensors* 13.11 (2013). ISSN: 1424-8220. DOI: 10.3390/s131114839.

2

Cardiac, respiratory and vascular systems

In this chapter, we present a brief description of the human cardiac, vascular and respiratory systems. Their interactions and autonomic regulation are described, considering normal conditions and cardiovascular pathologies, associated with heart failure and cardiomyopathy diseases.

2.1 The human body

The human body can be described in terms of chemical, cellular, tissue, organ, systemic and/or organism behavior [26]. The chemical environment of the human body includes the interaction of organic and inorganic compounds. These interactions are a product of the expression of the smallest living units, known as cells. A group of cells can share similar functions and form structures called tissues. There are four types of tissues: epithelial, connective, muscle, and nerve [26]. The organs are made up of different types of tissues that interact with each other to achieve a common function, forming organ systems.

All of the systems work to maintain a balanced environment in which the cells can properly function, and this process is known as homeostasis. For these systems to function correctly, they must maintain low variability. Diseases and the effects of ageing can disrupt the homeostatic process, exposing cells into unviable environments and leading to cell death, thereby endangering the organism [27].

The homeostatic mechanism consists of three components: receptors, which monitor whether the variables are within homeostasis values; the control center, which manages the information received from the receptors; and effectors, which execute changes that contribute to maintaining homeostatic balance [27]. As humans age, their homeostatic balance sometimes diminishes.

2.2 Cardiovascular system

The cardiovascular system is responsible for cardiac and vascular activity. Anatomically, it comprises the heart, the blood and the blood vessels [27].

2.2.1 Cardiac system

The heart is the organ that controls the cardiac system. The primary function of the heart is to pump blood through the arteries, capillaries and veins [26]. Cardiac cells are autorhythmic, and spontaneously generate their own electrical activity.

Blood circulation is achieved through the coordinated action of the four chambers of the heart: the right and left atria, and the right and left ventricles. The atria receive the blood from both the body and the lungs, and the ventricles pump that blood back to the lungs and the rest of the body (Figure 2.1). These chambers are connected by different valves. The mitral and tricuspid valves control the blood flow from the atria to the ventricles; the aortic and pulmonary valves control the blood flow out of the ventricles. One of the functions of the atria is to produce atrial natriuretic peptide (ANP), a hormone related to blood pressure maintenance [26].

Electrical activity of the heart

The electrical activity of the heart is directly related to the biochemical activity of the cardiac myocytes through the sodium-potassium pump mechanism. Cardiac action potentials are products of the movement of calcium, potassium and sodium ions through protein channels, inside and outside of the cardiac membrane. This movement produces depolarization by means of a fast exchange of sodium ions, and repolarization, through the exchange of potassium and by stopping calcium from entering the membrane, which produces the action potential. Heart contractions occur between each depolarization and repolarization (Figure 2.2).

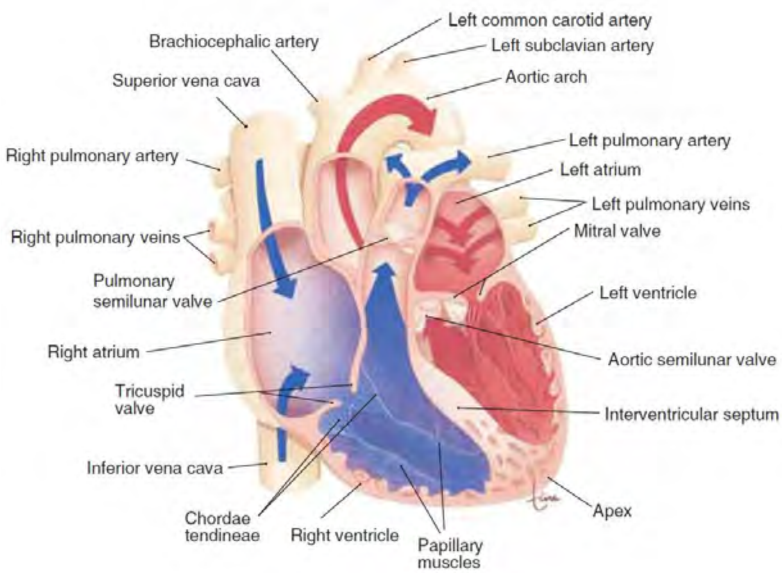

Figure 2.1. Frontal section of the heart's anatomy (the arrows indicate the directions of the blood flow into and out of the heart). Reproduced from [26]

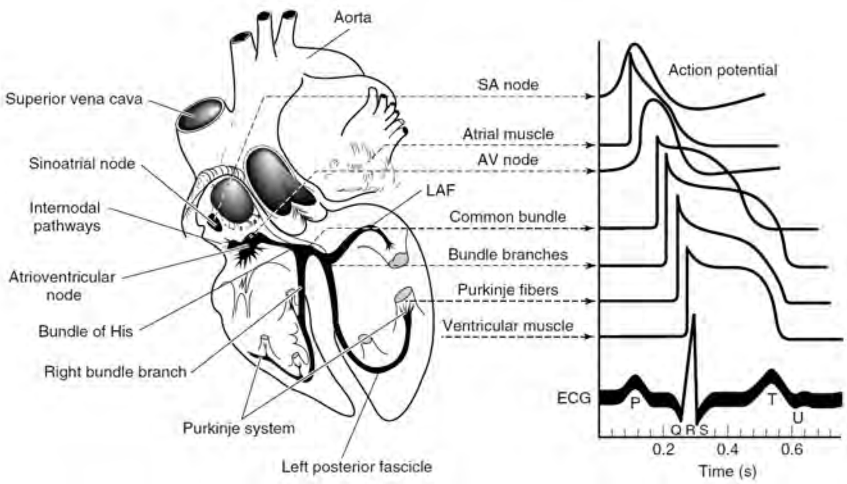

Figure 2.2. Schematic illustration of the morphology and timing of action potentials from different regions of the heart and the related cardiac cycle of the ECG as measured on the body surface. Reproduced from [17]

Action potentials are generated automatically by a group of pacemaker cells comprising the sinoatrial (SA) node, the internodal atrial pathways, the atrioventricular (AV) node, and the Purkinje fibers [11]. The SA node determines the rate at which the heart beats, defined as the cardiac pacemaker.

The electrocardiographic signal (ECG) represents the electrical activity of the heart, and is described considering different waves. The P wave is related to atrial depolarization, the Q, R, and S waves, called the QRS complex, represent ventricular depolarization, and the ST segment and T wave show ventricular repolarization. The U wave represents the repolarization of the Purkinje fibers. Figure 2.3 shows the ECG waves, segments and intervals.

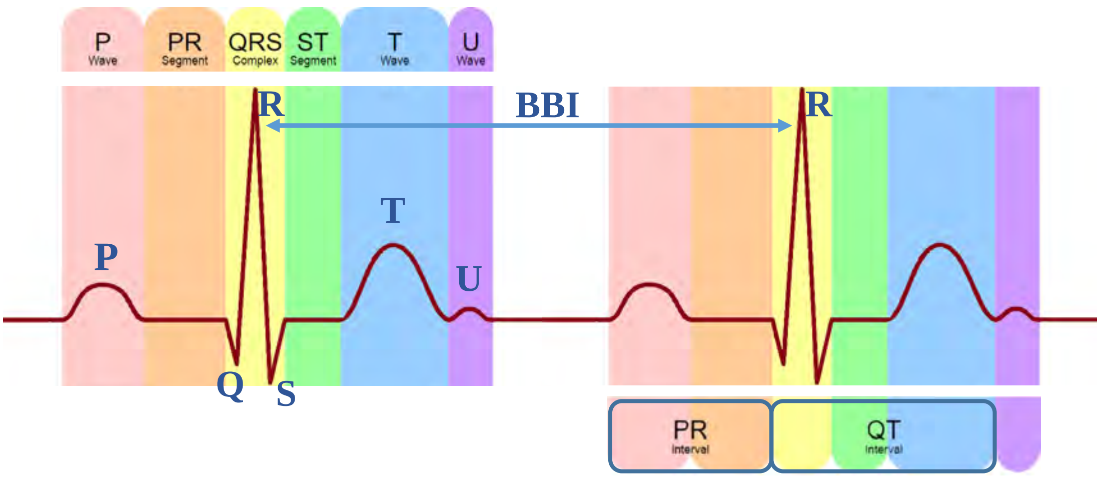

Figure 2.3. Wave definitions of the cardiac cycle and wave durations and intervals. BBI: beat-to-beat interval.

The ECG signal is recorded according to standard configurations. The standard 12-lead ECG is the most widely used lead system in clinical routine, and is defined by a combination of three different lead configurations: the bipolar limb leads, the augmented unipolar limb leads, and the unipolar precordial leads [30]. This 12-lead ECG is recorded by placing 10 electrodes at standardized positions on the body surface.

The three bipolar limb leads, denoted as I, II and III, are obtained by measuring the voltage difference between the left and right arm and left leg (Figure 2.4a). The position of these three electrodes can be viewed as the corners of an equiangular triangle, called Einthoven's triangle, with the heart at its center. The resulting limb leads describe the cardiac electrical activity in three different directions of the frontal plane.

The augmented unipolar limb leads, aVR, aVL, and aVF, use the same electrodes as the bipolar limb leads, but are defined as voltage differences between one corner of the triangle and the average of the remaining two corners.

The precordial leads, V_1, V_2, V_3, V_4, V_5, and V_6, are positioned in succession on the front and left side of the chest, in order to provide a more detailed view of the heart than the limb leads (Figure 2.4b). These leads are unipolar and related to a central terminal, defined by the average of the voltages measured on the right and left arms and left leg.

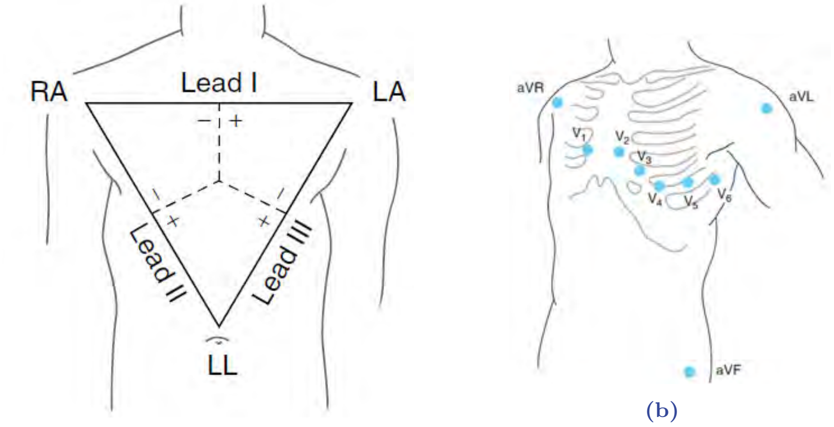

(b)

(a)

Figure 2.4. a) Unipolar electrocardiographic leads I, II, and III, and b) augmented unipolar limb leads, aVR, aVL, and aVF, precordial leads, V_1, V_2, V_3, V_4, V_5, and V_6, and the Einthoven's triangle. Reproduced from [17]

The orthogonal leads reflect the electrical activity in the three perpendicular directions: X, Y, an Z. These leads, known as the *Frank lead system*, are obtained as the linear combination of seven electrodes positioned on the chest, back, neck, and left foot. The resulting leads, X, Y, and Z, view the heart from the left side, from below, and from the front.

2.2.2 Vascular system

The vascular system contributes to homeostasis by controlling blood pressure in conjunction with heart regulation. It also participates in the the exchange of nutrients, waste products, gases and tissues, and hormone transport. This system is formed by two sets of blood vessels: the pulmonary and the systemic vessels. The pulmonary vessels transport blood from the right ventricle, through the lungs, and back to the left atrium. The systemic vessels transport blood through all parts of the body from the left ventricle, and back to the right atrium (Figure 2.5).

The blood vessels can be categorized into three types: arteries, capillaries and veins. The arteries transport blood away from the heart into the large arteries, which progressively branch out into smaller arteries. Then, the blood flows into the capillaries, where the exchange of blood happens. Afterwards, the blood flows into the veins carrying deoxygenated blood back into the heart to be oxygenated again. The veins are classified as venules, small veins, and large veins.

The steady exchange of nutrients and oxygen is vital for maintaining homeostasis. Consequently, any alterations in the circulatory system directly threatens homeostasis. The baroreflex mechanism is capable of regulating blood pressure by increasing or decreasing blood flow to meet homeostatic demands.

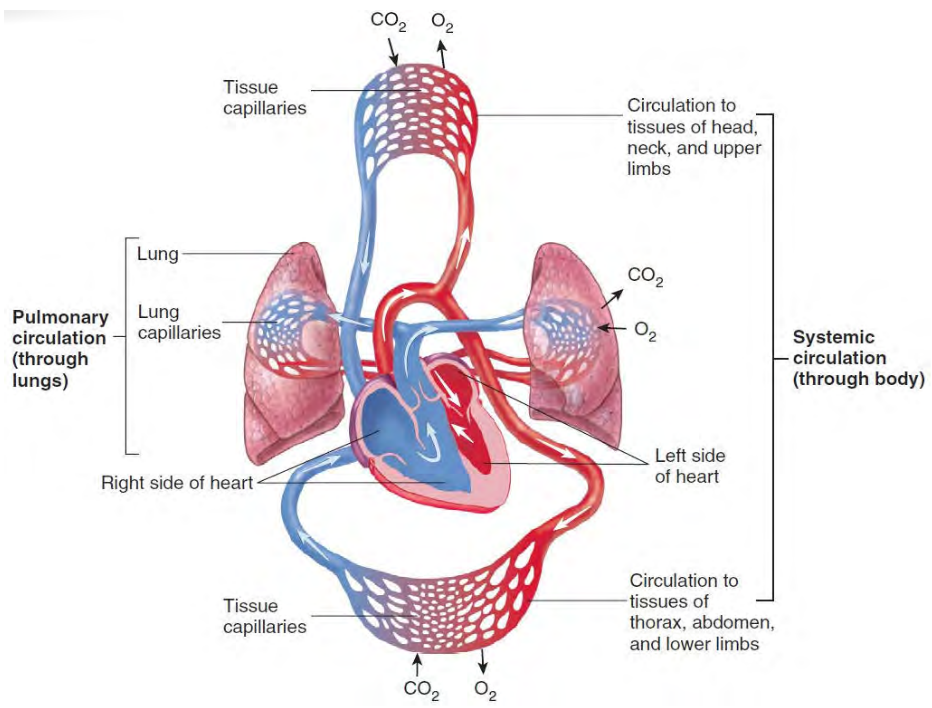

Figure 2.5. Systemic and pulmonary circulation. Reproduced from [27]

The blood pressure signal (BP) registers changes from the proximal aorta to the peripheral arteries and monitors those changes to provide information about the hemodynamic status of the body [3]. Figure 2.6 shows an example of a BP signal.

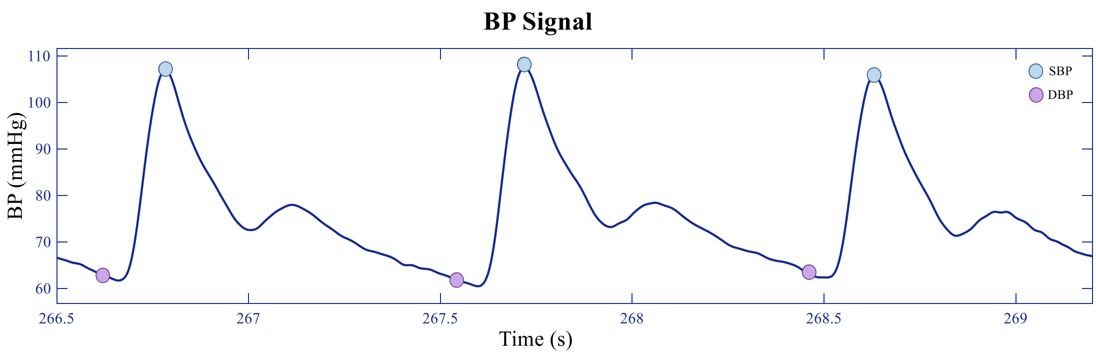

Figure 2.6. Blood pressure signal with systolic (SBP) and diastolic (DBP) blood pressure marks.

2.3 Respiratory system

The respiratory system is responsible for the exchange of oxygen and carbon dioxide during the breathing process inspiration and expiration. It contributes to homeostasis by allowing the circulation of oxygen and carbon dioxide between the circulatory system and the organism [33]. Anatomically, it comprises the upper respiratory tract including the nose, the nasal cavity, the pharynx and the larynx, and the lower respiratory tract including the trachea, the bronchi, and the lungs (Figure 2.7). Additionally, the diaphragm and the muscles of the thoracic and abdominal walls are responsible for respiratory movements.

The lungs are the principal organs of the respiratory system [33]. They are made up of lobes, two in the right lung and three in the left lung. These lobes are formed by bronchopulmonary segments, nine in the left lung and ten in the right lung. At the same time, the bronchopulmonary segments are subdivided into lobules supplied by bronchioles.

Gas exchange occurs in the capillaries, which are wrapped around small air sacs called alveoli. The blood carried by the blood vessels interacts with the gas brought by the airways, consisting of a series of branching tubes, which become narrower and shorter. In addition, the respiratory system performs functions like the regulation of blood pH, the production of chemical mediators, voice production, olfaction, and protection against microorganisms [27].

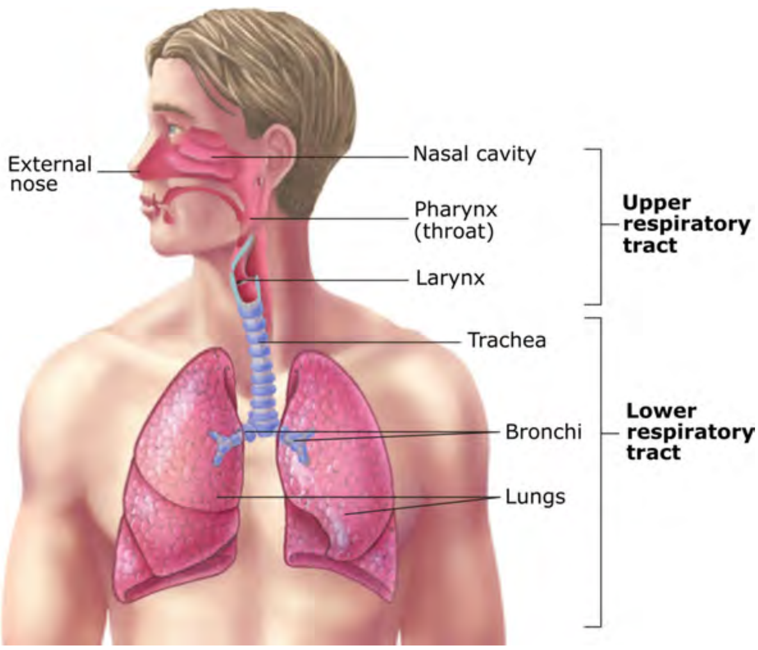

Figure 2.7. Respiratory system. Reproduced from [27]

Respiration takes place in sequential cycles of inspiration and expiration. During inspiration, on every diaphragmatic contraction, the abdominal contents are forced downward and forward, and the chest cavity expands. Other muscles involved in inspiration are the scalene muscles and the sternomastoid muscles, which also contribute to the regulation of this process.

Expiration is a passive process that takes place during breathing due to the elastic nature of the lungs and chest walls. They tend to return to their initial positions after being actively expanded during inspiration [33]. The intercostal muscles assists active expiration by pulling the ribs downward and inwards, decreasing thoracic volume.

The dynamics of the respiratory system can be modeled in terms of air volumes and pulmonary capacities, defined by (Figure 2.8):

- **Tidal volume:** the volume of air inhaled or exhaled during one respiratory cycle
- **Inspiratory reserve volume:** the amount of air that can be forcibly inhaled after a normal tidal volume
- **Expiratory reserve volume:** the amount of air that can be forcibly exhaled after exhalation of the tidal volume
- **Residual volume:** the volume of air still remaining in the lungs after maximal exhalation

Based on these volumes, four pulmonary capacities can be defined according to (Figure 2.8):

- **Inspiratory capacity:** the maximum volume of air that can be inhaled following a resting state
- **Functional residual capacity:** the amount of air remaining in the lungs at the end of a normal exhalation
- **Vital capacity:** the total amount of air exhaled after maximal inhalation
- **Total lung capacity:** the maximum volume of air that the lungs can accommodate

2.3.1 Respiratory volume and flow signals

The respiratory volume signal represents the circulating air flow in the airway of the subject. In normal conditions, inspiratory volume can reach up to 3.5 l and

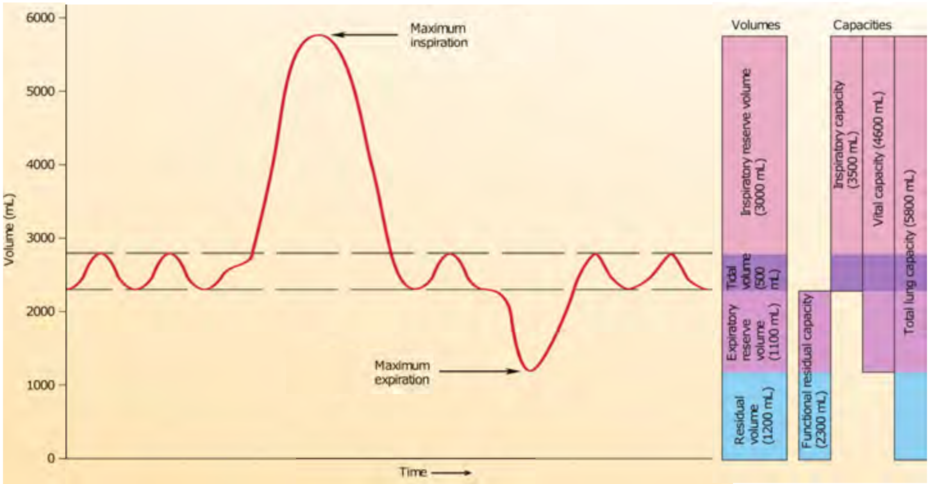

Figure 2.8. Lung volumes and capacities. Reproduced from [27]

expiratory volumes can reach 1 l during regular deep breathing. Respiratory flow occurs by convection, as a result of the pressure difference between the chest and the atmosphere. It is a measure of the circulating air volume over time. Respiratory flow can be estimated through a time derivative of the volume signal. Figure 2.9 is an example of a record of the respiratory flow signal.

The aforementioned signals can be obtained through different recording methods. With a pneumotachograph device, the flow signal is derived from the pressure difference over a fixed resistance. A linear relationship between pressure drop and flow is assumed to exist in accordance with the law of Poiseuille. Respiratory inductive plethysmography is a widely accepted method for quantitative and qualitative noninvasive respiratory measurements [23]. Additionally, a pressure transducer connected to a nasal oxygen cannula can detect fluctuations of about 0.1 kPa during nose breathing [13].

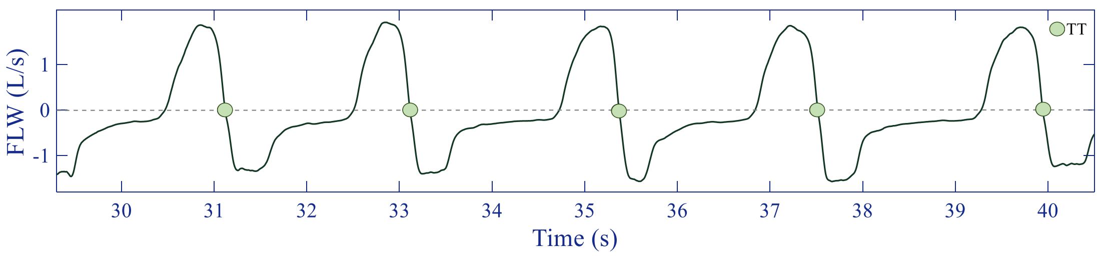

Figure 2.9. Respiratory flow signal with breath duration (TT) marks.

2.4 Autonomic nervous system

The autonomic nervous system (ANS) contributes to regulating of the complex actions involved in maintaining homeostasis. It is involved in the control of body temperature, digestion, heart rate and blood pressure, among other processes. The ANS includes the sympathetic and parasympathetic processes and the enteric nervous system. The enteric nervous system is a complex network of neuron cell bodies and axons within the wall of the digestive tract.

The sympathetic preganglionic neurons are located in the lateral horns of the spinal cord grey matter. These nerves project towards the sympathetic ganglia. The axons of the parasympathetic preganglionic neurons project from the brain in the cranial nerves, and from the spinal cord in the pelvic splanchnic nerves. These axons course through the nerves to the terminal ganglia, where they synapse with postganglionic neurons (Figure 2.10).

The sympathetic and parasympathetic divisions of the autonomous nervous system maintain homeostasis by adjusting the body functions to match levels of physical activity [27]. The autonomous nervous system innervates most organs through sympathetic and parasympathetic fibers. In general, the sympathetic division has increased influence under conditions of physical activity or stress, by stimulating blood and nutrients to structures that are physically active, and by decreasing activity in nonessential organs. The parasympathetic division is active during resting conditions, playing a major role in maintaining blood pressure and body temperature during rest. Increased parasympathetic activity stimulation lowers heart rate, which lowers blood pressure.

Nervous system activity gradually declines as a person ages due to the decrease in the number of neurons. The function of the sensory neurons that monitor blood pressure declines with age, resulting in a higher prevalence of high blood pressure among the elderly.

2.4.1 Cardiovascular autonomic regulation

Blood pressure in the systemic vessels must be high enough in order to maintain homeostasis. The heart has a primary influence over blood pressure and plays an important role in maintaining homeostasis. Heart activity can also vary depending of the demands of the body, for example, in situations of exercise and rest. Regulation is achieved by the action of two mechanisms: the baroreflex and the chemoreflex [27].

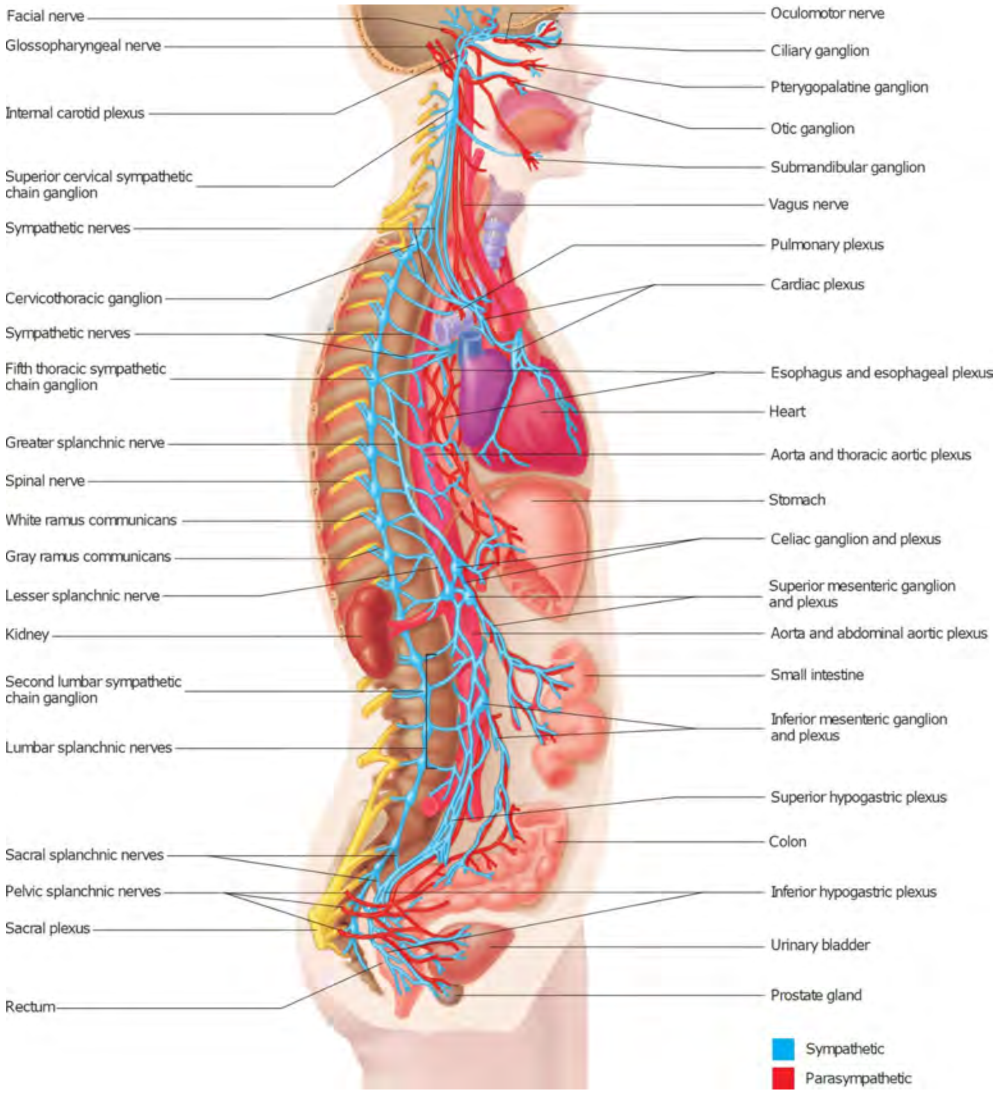

Figure 2.10. Distribution of autonomic nerve fibers. Reproduced from [27]

- Baroreflex mechanism

The main function of the baroreceptors is to detect changes in blood pressure. These stretch receptors are located within the walls of certain large arteries like the carotid and the aorta. Pressure changes in these walls are projected through the glossopharyngeal and vagus nerves from the baroreceptors to an area of the medulla known as the cardioregulatory center, where the action potentials are analyzed. This center acts through the cardioacceleratory center, which increases heart rate, and the cardioinhibitory center, which decreases heart rate. These centers communicate stimulating or inhibitory actions to the heart through both, the sympathetic and parasympathetic divisions of the autonomic nervous system.

High blood pressure in the internal carotid arteries and aorta causes an incremental stretch that stimulates an increase in action potential frequency in the baroreceptors. This effect produces a reduction in sympathetic stimulation and an increase in the parasympathetic stimulation of the heart, causing the heart rate to slow. When blood pressure decreases, the walls are stretched to a lesser extent, and the afferent action potential frequency decreases, causing decreased parasympathetic activity and increased sympathetic stimulation of the heart, and resulting in an increase in heart rate. Several authors have studied the functionality of this baroreflex mechanism associating it with the analysis of changes between the heart rate and blood pressure, the relationship between the systolic blood pressure and pulse intervals, the peripheral sympathetic nerve activity to muscle, or the baroreflex sensitivity [20, 28, 24].

- Cardiopulmonary baroreflex

Stretch receptors are located in the walls of the atria and pulmonary arteries, and respond to changes in blood volume. These receptors are activated by the distension of the vessel walls. The function of the cardiopulmonary baroreceptors is to minimize changes in arterial blood pressure in response to changes in blood volume [33]. This mechanism contributes to the regulation of cardiac and arterial output. Furthermore, prolonged expiration may increase the vagal tone, thereby decreasing the heart rate, and decreasing venous return, vascular resistance and cardiac work [33]. The respiratory-sympathetic coupling could reverse paroxysmal supraventricular tachycardia [4].

- Chemoreceptor reflexes

The chemoreceptors contribute to balancing the levels of carbon dioxide in blood by sensing changes in pH. A drop in pH and a rise in carbon dioxide levels stimulates the chemoreceptors to decrease parasympathetic stimulation and increase sympathetic stimulation. Hence, the heart rate speeds up, causing increased blood flow through the lungs, and eliminating carbon dioxide from the body in the process. The lower carbon dioxide level in the blood helps to increase blood pH, and thus maintain homeostasis.

In the event of a significant decrease in blood oxygen levels, chemoreceptor reflexes force the heart rate to decrease and vasoconstriction to increase. Vasoconstriction causes the blood pressure to rise, which allows the blood to keep flowing despite the decrease in heart rate. Chemoreceptors are primarily located in the carotid and aortic arteries, and close to the brain and heart.

2.5 Cardiorespiratory interaction

Several studies related to cardiorespiratory interaction have analyzed the interdependent response of these systems. Some authors have assessed the suitability of using respiratory sinus arrhythmia to differentiate between ischemic and dilated cardiomyopathy patients through fractal dimension and entropy-based methods. They found that respiratory sinus arrhythmia is lower in chronic heart failure patients, especially in those with ischemic cardiomyopathy [12]. Cardiorespiratory coupling was explored by exposing healthy patients to five different levels of mental stimulation [29]. They found that mental stimulation could enhance cardiorespiratory coupling as an alternative to aerobic exercise.

Other authors have presented different results on the behavior of heart rate variability in relation to the interaction between the cardiac and respiratory systems and variation with age [7, 15]. The influence of respiration on heart mechanics may decrease as a person ages, in a manner similar to respiratory modulation of the heart rate. Different respiratory indices have been estimated from the ECG signal in [6, 21] and the beat-to-beat heart rate have been associated with the sleep disordered breathing using statistical methods in [25]. On the other hand, the respiratory-related components of the heart rate variability have been extracted using a coupled oscillators model [32]. They suggest that these components could be an indicator of vagal tone behavior and the non-respiratory components represents the sympathetic activity.

The heart is sensitive to changes in intrapleural pressure and these can induce physiological responses on both the left and right ventricles [7]. Moreover, the pericardium is directly related to cardiovascular hemodynamic modulations. Under normal conditions, it limits the cardiac preload and attenuates the left ventricular afterload during respiration [22].

2.6 Cardiovascular pathologies

The dysfunction of heart activity and the cardiovascular system is associated with different cardiac pathologies. In this research, we focus on the study of heart failure and heart diseases like idiopathic, ischemic and dilated cardiomyopathies.

2.6.1 Heart failure

Heart failure (HF) is one of the most common pathologies in modern society. It is defined by the incapacity of the heart to provide enough blood pressure to supply the metabolic requirements of the body, or to ensure the venous return. There are multiple causes for the development of this pathology, such as diabetes, cardiac arrest and hypertension, which often lead to the deterioration of the myocardial tissue [18]. Other authors have studied heart failure patients through the characterization of the blood pressure signal. They were able to stratify these patients into high and low cardiovascular risk, using a combination of indices for blood pressure characterization and the left ventricular ejection fraction index [1].

When heart failure occurs, the body compensates by means of a rage of mechanisms, such as increasing output volume, further increasing the thickness and volume of the ventricular walls, and activating the neurohormonal systems to maintain average arterial pressure [18].

Congestive heart failure takes place when the heart becomes weak or stiff and is unable to properly pump blood around the body, so the blood flows through the heart and body at a slower rate. Therefore, the pressure in the heart increases, and the cardiovascular system can no longer maintain homeostasis. The chambers of the heart respond by stretching to hold more blood to pump through the body, or by becoming stiff and thickening their walls. In time, this causes the walls of the heart to weaken and become unable to pump blood efficiently. The kidneys respond by causing the body to retain fluid and salt, and the body becomes congested.

2.6.2 Sudden cardiac death

Sudden cardiac death (SCD) is unexpected death caused by the loss of heart function. The electrical system of the heart malfunctions and suddenly becomes irregular, starting to beat dangerously fast, which may lead to ventricular fibrillation, followed by cardiac arrest. SCD is responsible for half of all heart disease related deaths, and affects men twice as often as it does women, and occurs most frequently in adults between 30 - 50 years of age [16].

2.6.3 Cardiomyopathies

Cardiomyopathies are one of the most common causes of heart failure and occurs when the heart muscle becomes enlarged, thick, or rigid, causing the heart to malfunction. The most prevalent of these afflictions are ischemic and dilated cardiomyopathies.

- Ischemic cardiomyopathy

Ischemic cardiomyopathy (ICM) manifests when a region of the myocardial tissue stops receiving sufficient blood flow, in most cases occasioned by arteriosclerosis. This condition can lead to a heart infarction, which can in turn lead to permanent heart tissue damage [10, 8]. Figure 2.11 shows an illustration of a heart with ICM.

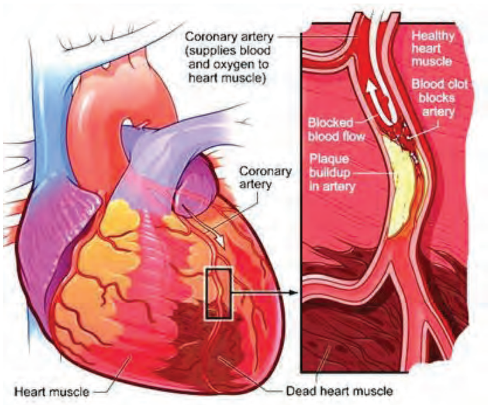

Figure 2.11. Heart with ischemic cardiomyopathy. Reproduced from [14]

- Idiopathic dilated cardiomyopathy

Patients with dilated cardiomyopathy (DCM) have dilated, weakened, elongated hearts that are incapable of ejecting enough blood to sustain homeostasis, occasioning heart disease. Most of the causes of this pathology are idiopathic, i.e. its origins are unknown. Nevertheless, it has some indicators, as it has been associated with genetic heritage, diabetes, viruses, alcoholism, drug abuse and thyroid related diseases. Figure 2.12 shows a comparison between a healthy and a DCM heart. Patients affected by this pathology commonly do not manifest any symptoms or may be affected by minor symptoms such as fatigue, weight gain, dizziness or fainting.

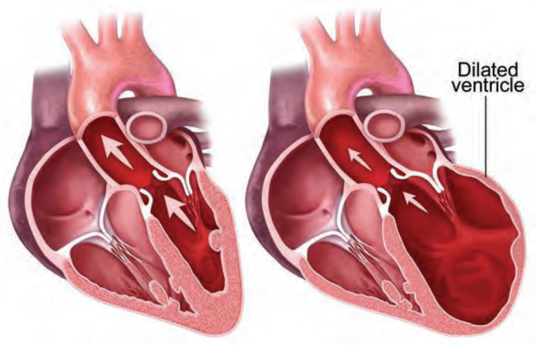

Figure 2.12. Heart with dilated cardiomyopathy. Reproduced from [31]

2.7 Clinical indices

Clinical practice presents several indices to describing the cardiac function contributing to the stratification according to different levels of severity through biomarkers, cardiac mechanical response, and physiological activity, among others. In this section, we describe the most relevant indices associated with the clinical diagnosis of cardiomyopathy patients.

- Left ventricular ejection fraction

The left ventricular ejection fraction (LVEF) is one of the most common indices for heart failure. This parameter is calculated based on the blood volume at the end of the diastole (FDV), and the volume at the end of the systole, also known as final systolic volume (FSV), presented in percentages.

$$LVEF = (FDV - FSV)/FDV. \tag{2.1}$$

A patient with a LVEF above 55% is considered normal, between 35% and 55% is considered below normal, and below 35% is considered pathological [2].

- Left ventricular diameter

The diameter of the left ventricle is analyzed during both, the end-systolic and end-diastolic instances in order to assess the dimensions of the heart during the systole and the diastole, respectively. The left ventricle end-diastolic diameter is measured during the end-diastole, and corresponds to the largest cardiac dimension. The left ventricle end-systolic diameter is measured during the end-systole, and corresponds to the shortest cardiac dimension. These measurements are often associated with cardiovascular death risk.

- New York heart association index

The purpose of the New York heart association index (NYHA) is to stratify the cardiac risk of heart failure patients. Risk is stratified into four classes depending on the severity of the limitations and symptoms experienced by the patient, according to [9]:

- **NYHA I:** No limiting symptoms
- **NYHA II:** Minor limitations
- **NYHA III:** Limitations in workout conditions
- **NYHA IV:** Limitations in rest conditions

- Brain natriuretic peptide

Brain natriuretic peptide (BNP) is a polypeptide of 32 amino acids secreted by the heart ventricles in response to the excessive enlargement of the cardiac muscle. BNP ranges can help in the prediction of heart failure. BNP ranges and their interpretation are shown in Table 2.1

Table 2.1. BNP interpretation

BNP	Heart failure stratification
< 100 ρg/mL	unlikely
100-400 ρg/mL	Use clinical judgement
> 400 ρg/mL	likely

According to clinical criteria, high levels of BNP are evidence of left ventricular symptomatic failure. The N-terminal pro-brain natriuretic peptide (NT-proBNP) is a 76 amino acid N-terminal inactive protein, that releases BNP when it breaks from the molecule [5]. Table 2.2 presents the ranges and interpretation for NT-proBNP.

Table 2.2. NT-proBNP interpretation

Age range	NT-proBNP	Heart failure stratification
	< 300 ηg/mL	unlikely
Age < 50 years	NT-proBNP > 450 ρg/mL	likely
Age 50 - 75 years	NT-proBNP > 900 ρg/mL	likely
Age > 75 years	NT-proBNP > 1800 ρg/mL	likely

- Heart failure survival score

The heart failure survival score (HFSS) is calculated through the combination of several clinical predictors in a mathematical model, including blood pressure, left ventricular ejection fraction, oxygen peak volume, and intraventricular conduction delay [19]. Patients with HFSS values lower than 7.19 are considered at high risk of cardiac infarction, while patients with values higher than 8.10 are considered low risk.

- Body mass index

Body mass index (BMI) is calculated as the ratio between the patient's weight and the square of his or her height. This indicator is used to estimate the patient's degree of obesity (Table 2.3).

Table 2.3. BMI interpretation

BMI	
$< 18.5\frac{Kg}{m^2}$	Underweight
$18.5\frac{Kg}{m^2}$ and $24.9\frac{Kg}{m^2}$	Normal
$25\frac{Kg}{m^2}$ and $29.9\frac{Kg}{m^2}$	Overweight
$> 30\frac{Kg}{m^2}$	Obese

These indices are used to diagnosing heart failure patients and associated with information obtained using other methods can contribute to extract new information about these pathologies.

Chapter 2 bibliography

[1] A. Arcentales, A. Voss, P. Caminal, A. Bayés-Genís, M. T. Domingo, and B. F. Giraldo. "Characterization of patients with different ventricular ejection fractions using blood pressure signal analysis". In: *Computing in Cardiology 2013*, pp. 795–798.

[2] American Heart Association. *Ejection Fraction Heart Failure Measurement.* URL: http://www.heart.org/HEARTORG/Conditions%20/HeartFailure/SymptomsDiag-%20nosisof%20Heart%20Failure/Ejection-Fraction-Heart-Fail%20ure-Measurement_UCM_306339_Article.jsp.

[3] J. Augusto, J. Teboul, P. Radermacher, and P. Asfar. "Interpretation of blood pressure signal: physiological bases, clinical relevance, and objectives during shock states." In: *Intensive Care Med.* (2010).

[4] D. Baekey, Y. Molkov, J. Paton, I. Rybak, and T Dick. "Effect of baroreceptor stimulation on the respiratory pattern: Insights into respiratory-sympathetic interactions". In: *Respir Physiol Neurobiol* (2010), pp. 135–145.

[5] M Bay, Kirk V Parner J, Hassager C, Nielsen H, Krogsgaard K, Trawinski J, Boesgaard S, and Aldershvile J. "NT-proBNP: a new diagnostic screening tool to differentiate between patients with normal and reduced left ventricular systolic function". In: *Heart* (2003), pp. 150–154.

[6] Peter H Charlton, Timothy Bonnici, Lionel Tarassenko, Jordi Alastruey, David A Clifton, Richard Beale, and Peter J Watkinson. "Extraction of respiratory signals from the electrocardiogram and photoplethysmogram: technical and physiological determinants". In: *Physiological Measurement* 38.5 (2017), pp. 669–690. DOI: 10.1088/1361-6579/aa670e. URL: https://doi.org/10.1088%5C%2F1361-6579%5C%2Faa670e.

[7] Ira M Cheifetz. "Cardiorespiratory Interactions: The Relationship Between Mechanical Ventilation and Hemodynamics." In: *Respiratory Care* (2014), pp. 1937–1945.

[8] Cleveland Clinic. *Ischemic Cardiomyopathy.* URL: https://my.clevel%20andclinic.org/services/heart/disorders/hic_What_is_Cardiomyopathy/%20ischemic_cardiomyopathy.

[9] Task force committee. *The Criteria Committee of the New York Heart Association Nomenclature and criteria for diagnosis of diseases of the heart and blood vessels.* 1964.

[10] Science Daily. *Ischemic heart disease.* URL: `http://www.sciencedaily.com/articles/i/ischaemic_heart_disease.htm`.

[11] W.F. Ganong, K. Barrett, M. Barman, S. Boitano, and H. Brooks. *Review of medical physiology,* McGraw Hill, 2005.

[12] BF. Giraldo, M. Pericàs, R. Schröeder, and A. Voss. "Respiratory sinus arrhythmia quantified with linear and non-linear techniques to classify dilated and ischemic cardiomyopathy." In: *Conf Proc IEEE Eng Med Biol Soc* (2018).

[13] AR. Guyatt, SP. Parker, and MJ. McBride. "Measurement of human nasal ventilation using an oxygen cannula as a pitot tube." In: *Am Rev Respir Dis.* (1982).

[14] Danielle Haak. *ischemia.* URL: `http://study.com/academy/lesson/what-is-ischemia-definition-causes-symptoms.html`.

[15] D. Iatsenko, Bernjak A, Stankovski T, Shiogai Y, Owen-Lynch PJ, Clarkson PB, McClintock PV, and Stefanovska A. "Evolution of cardiorespiratory interactions with age." In: *Philosophical Transactions of the royal society.* (2013).

[16] C. Israel. "Mechanisms of sudden cardiac death." In: *Indian Heart J* (2014).

[17] S.A. Jones. *ECG notes: Interpretation and management guide.* FA Davis Company, 2009.

[18] Clinton D. Kemp and Conte JV. "The pathophysiology of heart failure". In: *Cardiovascular Pathology* 21.5 (2011), pp. 365–371.

[19] Todd M. Koelling, Joseph S, and Aaronson KD. "Heart Failure Survival Score Continues to Predict Clinical Outcomes in Patients With Heart Failure Receiving Beta-Blockers". In: *The Journal of Heart and Lung Transplantation* (2004), pp. 1414–1422.

[20] Paola A. Lanfranchi and Virend K Somers. "Arterial baroreflex function and cardiovascular variability: interactions and implications". In: *American Journal of Physiology-Regulatory, Integrative and Comparative Physiology* 283.4 (2002). PMID: 12228049, R815–R826. DOI: `10.1152/ajpregu.00051.2002`.

[21] Jesús Lázaro, Alejandro Alcaine, Daniel Romero, Eduardo Gil, Pablo Laguna, Esther Pueyo, and Raquel Bailón. "Electrocardiogram Derived Respiratory Rate from QRS Slopes and R-Wave Angle". In: *Springer Link* (2014), pp. 2072–2083. DOI: `10.1007/s10439-014-1073-x`.

[22] Sheldon Magder. *Respiratory-Circulatory Interactions in Health and Disease.* Lung Biology in Health and decease. CRC Press, 2001. ISBN: 9780824741747.

[23] P. Neumann, J. Zinserling, C. Haase, M. Sydow, and H. Burchardi. “Evaluation of Respiratory Inductive Plethysmography in Controlled Ventilation”. In: *Chest* (1998).

[24] Jeanie Park, Paul J. Marvar, Peizhou Liao, Melanie L. Kankam, Seth D. Norrholm, Ryan M. Downey, S. Ashley McCullough, Ngoc-Anh Le, and Barbara O. Rothbaum. “Baroreflex dysfunction and augmented sympathetic nerve responses during mental stress in veterans with post-traumatic stress disorder”. In: *The Journal of Physiology* 595.14 (2017), pp. 4893–4908. DOI: `10.1113/JP274269`. URL: `https://physoc.onlinelibrary.wiley.com/doi/abs/10.1113/JP274269`.

[25] Thomas Penzel, Jan W. Kantelhardt, Ronny P. Bartsch, Maik Riedl, Jan F. Kraemer, Niels Wessel, Carmen Garcia, Martin Glos, Ingo Fietze, and Christoph Schöbel. “Modulations of Heart Rate, ECG, and Cardio-Respiratory Coupling Observed in Polysomnography”. In: *Frontiers in Physiology* (2016), p. 460.

[26] V. Scanlon and T. Sanders. *Essentials of anatomy and physiology.* F. A. Davis., 2007.

[27] R. Seely, A. Russo, J. Regan, and C. VanPutte. *Seeley’s Anatomy & physiology.* Mc Graw Hill., 2014.

[28] James E Sharman, Pierre Boutouyrie, Marie-Cécile Perier, Frédérique Thomas, Catherine Guibout, Hakim Khettab, Bruno Pannier, Stéphane Laurent, Xavier Jouven, and Jean-Philippe Empana. “Impaired baroreflex sensitivity, carotid stiffness, and exaggerated exercise blood pressure: a community-based analysis from the Paris Prospective Study III”. In: *European Heart Journal* 39.7 (Dec. 2017), pp. 599–606. ISSN: 0195-668X. DOI: `10.1093/eurheartj/ehx714`.

[29] J. Solà-Soler, A. Cuadros, and BF. Giraldo. “Cardiorespiratory Phase Synchronization increases during certain mental stimuli in healthy subjects.” In: *Conf Proc IEEE Eng Med Biol Soc* (2018).

[30] L. Sörnmo and P. Laguna. “Bioelectrical Signal Processing in Cardiac and Neurological Applications.” In: *Elsevier: Academic Press.* (2005).

[31] Vanessa Stewart. *Cardiomyopathy.* URL: `http://www.accaq.org.au/category/health/`.

[32] Çağdaş Topçu, Matthias Frühwirth, Maximilian Moser, Michael Rosenblum, and Arkady Pikovsky. “Disentangling respiratory sinus arrhythmia in heart rate variability records”. In: *Physiological Measurement* 39.5 (2018), p. 054002. DOI: `10.1088/1361-6579/aabea4`. URL: `https://doi.org/10.1088%2F1361-6579%2Faabea4`.

[33] J. West and A. Luks. *Respiratory physiology: The Essentials,* Wolters Kluwer, 2015.

3

Databases

Four databases were explored to analyze the behavior of cardiovascular and cardiorespiratory dynamics. The Heris, WeanDB and Healthy databases were used to test an artifact reconstruction technique. The Heris database was explored using the Poincaré plot analysis, the ART database was used in the coupling analysis section, and the Healthy database was used as a reference.

3.1 Heris database

The Heris database is composed of synchronized recordings of the electrocardiogram, blood pressure, and respiratory volume and flow signals of 52 patients diagnosed with either ischemic (ICM) or dilated (DCM) cardiomyopathy disease.

The signals were recorded at Santa Creu i Sant Pau Hospital, Barcelona, Spain. This work was developed in collaboration with the Technical University of Catalonia (UPC), Barcelona, Spain, and the University of Applied Sciences of Jena, Department of Medical Engineering and Biotechnology, Jena, Germany. All patients were studied according to the protocol previously approved by the ethics committee of Santa Creu i Sant Pau Hospital, with the patient's prior consent.

The signals were acquired with the Portapres-System (TNO Applied Physics

Institute, Amsterdam, the Netherlands), and the Porti 16-biosignal amplifier (TMS BV International, Enschede, the Netherlands). All signals were recorded in high resolution at a 1600 Hz sample frequency for 30 minutes. Orthogonal derivations were recorded from ECG signals X, Y and Z. Atrium diameters were estimated from an echocardiogram obtained a few days prior to the recordings. All patients were recorded under resting conditions in supine position.

The patients were allowed to participate in the study according to the following inclusion criteria:

- New York Heart Association (NYHA) II – IV
- No syncope or life-threatening ventricular arrhythmias to date
- 45-80 years of age
- No secondary disease that influences the prognosis
- Medication: besides anti-arrhythmic drugs, all drugs necessary for standard drug therapy were allowed

And the following exclusion criteria:

- New York Heart Association (NYHA) < II
- < 45 years of age
- Atrial fibrillation / flutter
- Ventricular premature contractions (VPC) > 10%
- Active cardiac pacemaker or active implantable cardioverter defibrillator

Additionally, the following clinical indices were recorded: weight, height, sex, birth date, the medications the patient takes, systolic pressure, diastolic pressure, New York heart association index (NYHA), left ventricular ejection fraction (LVEF), left ventricular diastolic dimension (LVDD), brain natriuretic peptide (ProBNP), hemoglobin levels, smoker status, hypercholesterolemia, coronary artery disease, and information about the myocardial infarction sustained (Table 3.1).

3.2 ART database

The signals contained in the Autonomic Regulation Trial (ART) database are part of a study that aimed to evaluate the risk predictors of sudden cardiac death (SCD) and to improve risk stratification in idiopathic dilated cardiomyopathy (IDC) patients.

Table 3.1. Clinical parameters of the Heris database (mean and standard deviation).

	DCM	ICM
Patients	22	28
Age [years]	64.5 ± 11.5	65.8 ± 10.0
Weight [Kg]	74.2 ± 22.6	77.8 ± 21.1
BMI [Kg/m^2]	27.0 ± 7.8	27.2 ± 6.6
NYHA	2.0 ± 0.6	2.1 ± 0.3
LVDD [mm]	61.5 ± 5.0	60.9 ± 8.1
AD [mm]	41.3 ± 13.9	46.7 ± 6.9
ProBNP	2119.4 ± 4051.8	1537.5 ± 1395.7
LVEF [%]	35.4 ± 9.9	32.6 ± 8.7

BMI: body mass index; **NYHA**: New York Heart Association functional classification; **LVDD**: left ventricular diastolic dimension; **AD**: auricular diameter; **ProBNP**: brain natriuretic peptide; **LVEF**: left ventricular ejection fraction.

Signals from 220 IDC patients were recorded in two hospitals: Friedrich-Schiller University Hospital in Jena (44 patients) and Franz-Volhard Clinic in Berlin, Germany (176 patients). All participants provided written informed consent for the protocol approved by the local ethics committee of the two hospitals (No. 0986-11/02). This study complies with the Declaration of Helsinki.

In the acquisition protocol, the ECG signals (32 bit resolution, 1600 Hz sampling frequency) and blood pressure (32 bit, 500 Hz) were synchronously recorded for 30 minutes. The ECG recordings were taken with a Porti system (TMSi BV, the Netherlands), and the blood pressure recordings with the Portapres NIBP monitor (TNO Biomedical Instrumentation, Amsterdam, the Netherlands). All patients were recorded under resting conditions in supine position.

The inclusion criteria for the IDC patients were LVEF $< 45\%$ and/or fractional shortening $< 25\%$, and the left ventricle end-diastolic diameter (LVEDD) $> 117\%$. The New York heart association index (NYHA) for each patient was also included. The exclusion criteria were systemic hypertension at rest, coronary artery disease, congenital heart disease, pericardial diseases, valvular heart diseases, systemic disease known to cause dilated cardiomyopathy, chronic alcoholism, sustained ventricular tachycardia, atrial fibrillation, diabetes mellitus, renal failure, and an active permanent cardiac pacemaker, as well as patients without sinus rhythm [11, 12].

Afterwards, an additional exclusion criterion was applied to rule out patients with comorbidities and confounding factors influencing the autonomic regulation system. 129 of the 220 patients were excluded for the following reasons: 36 for paced rhythm, 34 for coronary artery disease, 32 for a high ($> 5\%$) percentage of ectopic beats or artifacts, 19 for atrial fibrillation, 4 due to technical problems, 2 for hypertrophic non-obstructive cardiomyopathy, 1 for arrhythmogenic right ventricular cardiomyopathy, and 1 patient who was clinically unstable due to acute decompensation [12].

After a median follow-up period of 28 months (range: 17–38 months), the patients were classified into two groups according to their SCD risk. The group of patients that remained in stable physical condition were considered at low risk for cardiovascular sudden death (IDC_{LR}). The remaining patients, who either died of SCD or needed resuscitation because of a life-threatening tachyarrhythmia, were categorized as high risk for cardiac sudden death (IDC_{HR}). None of these patients died from a non-cardiac disease. Table 3.2 presents the clinical parameters of the patients from the ART database selected for this research.

Table 3.2. Clinical parameters of the ART database (median and interquartile range).

	IDC_{LR} N = 77 (59 ♂, 18 ♀)	IDC_{HR} N = 14 (11 ♂, 3 ♀)
Follow-up [months]	27 [17 ; 37]	30 [21; 38]
Age [years]	55 [50 ; 60]	56 [50 ; 63]
LVEF [%])	29 [27 ; 37]	35 [27 ; 46]
LVEDD [mm]	69 [61 ; 79]	61 [58 ; 68]
LVESD [mm]	60 [53 ; 69]	49 [44 ; 56]
NYHA	3 [2 ; 4]	2 [2 ; 3]

IDC_{HR} and IDC_{LR}, high risk and low risk group of patients with dilated cardiomyopathy; **N**, number of patients within the groups (♂= Male; ♀= Female); **LVEF**, left ventricular ejection fraction; **LVEDD**, left ventricular end-diastolic diameter; **LVESD**, left ventricular end-systolic diameter; **NYHA**, New York heart association index.

3.3 WeanDB database

Electrocardiographic (ECG) and respiratory flow signals were recorded in 154 patients on weaning trials from mechanical ventilation (WeanDB database). These patients were recorded in the Department of Intensive Care Medicine at Santa Creu i Sant Pau Hospital, Barcelona, Spain, and Getafe Hospital, Getafe, Spain, according to the protocols approved by the local ethics committees. The patients gave their informed consent to participate, and were recorded under resting conditions in supine position.

The patients underwent a spontaneous breathing test prior to disconnection from mechanical ventilation during which they had to maintain spontaneous respiration through an endotracheal tube for 30 minutes. The patients who were able to maintain spontaneous breathing were extubated, while the others were reconnected. Patients who were able to maintain spontaneous breathing after 48 hours were considered to have passed the weaning test, while those who were not able to were reintubated.

Based on the weaning test, the patients were classified into three groups: 94 patients (61 male, 33 female, 65 ± 17 years) who passed the test and could maintain spontaneous breathing after 48 hours (GS); 39 patients (24 male, 15 female, 67 ± 15 years) who failed to maintain spontaneous breathing and were reconnected to a mechanical ventilator (GF); and 21 patients (11 male, 10 female, 68 ± 14 years) who successfully passed the spontaneous breathing test, but were reintubated before the 48 hours were reached (GR).

The ECG signal was obtained using a SpaceLabs Medical monitor. The respiratory flow signal was recorded using a pneumotachograph connected to an endotracheal tube. The pneumotachograph consists of a Datex-Ohmeda monitor with a variable reluctance transducer (Validyne Model MP45-1-871). Both signals were recorded synchronously with a sampling frequency of 250 Hz and 12-bit resolution for 30 minutes.

3.4 Healthy databases

The Healthy1 and Healthy2 databases are compilations of records from healthy subjects. The Healthy1 database contains electrocardiographic (ECG), respiratory flow signals from 35 healthy volunteers (23 female, 27 ± 7 years, respiratory frequency 15.5 ± 3.7 breaths/min). The signals were recorded at Santa Creu i Sant Pau Hospital, Barcelona, Spain. All subjects were studied according to the protocol approved by the local ethics committee. The ECG signals were recorded using a BIOPAC Pro system with a single lead for 30 minutes. The respiratory flow signals were acquired using a pneumotachograph consisting of a Datex-Ohmeda monitor with a Validyne Model MP45-1-871 variable-reluctance transducer. The pneumotachograph was connected to a mask. All subjects were recorded under resting conditions in sitting position. All signals were sampled at 250 Hz and with 12 bit resolution.

Prior to data acquisition, an adaptation period of a few minutes was provided to ensure that the subjects felt comfortable with the mask. Respiratory flow signals were recorded for 30 minutes. All subjects were seated and remained awake throughout the data acquisition. For the 35 subjects, respiratory frequency was found to range from 0.2 to 0.4 Hz, and the modulation frequency from 0.01 to 0.04 Hz [8]. The flow signals were decimated from 250 to 2 Hz, using null-phase anti-aliasing filtering to account for the fact that the frequencies of interest only range up to about 0.5 Hz.

The Healthy2 database contains ECG leads I, II, III, as well as blood pressure and respiratory flow signals of 44 healthy subjects, recorded under resting conditions (quiet environment, same place), using BIOPAC Systems Inc. MP150. This database was recorded at the Institute for Bioengineering of Catalonia (IBEC) according to the protocol approved by the local ethics committee. The subjects were recorded for 30 min in supine position, and after 5 min at rest, for 15 min in sitting position. All signals were sampled at 500 Hz with 12 bit resolution.

Additionally, another database also related to healthy subjects was analyzed to compare the cardiovascular interactions through coupling analysis. It contains ECG and blood pressure records from 49 elderly subjects, who did not suffer from any cardiovascular disease at the time the recordings were taken. The age range of these subjects is 46 ± 14 years, 30 of them were male and 19 female.

3.5 Signal characterization

For the mathematical analysis of the signals included in all databases presented before, we obtained time series containing information about the physiological dynamics of the systems.

3.5.1 Electrocardiographic signal characterization

One way to characterize electrocardiographic signals is by means of time series that determine the behavior of the heart. The beat to beat interval (BBI) represents the time interval between two consecutive heart beats (in ms). Linear methods (both in time and in frequency domain) and non-linear methods of recording BBI can be used to estimate the behavior of the heart rate. Heart rate, also known as cardiac pulse, is calculated as the number of times a heart beats per minute. The normal range is between 60 to 100 beats per minute.

BBI time series were extracted automatically from the ECG signal using an algorithm based on wavelet analysis [6]. These series were then filtered by applying an adaptive variance estimation algorithm, to remove artifacts (e.g. movements, electrode noises, spikes or outliers).

Heart rate variability (HRV) represents the variability between cardiac beats over time. HRV is regulated by the autonomic nervous system, by both the sympathetic and parasympathetic branches. The sympathetic branch increases cardiac output and the heart's contraction rate while decreasing HRV. Under stress conditions, the parasympathetic branch decreases cardiac output, increasing HRV to maintain the homeostatic process. Under normal conditions, HRV is high. On the other hand, low HRV would be a predictor of some types of cardiac disease [10].

HRV can be mathematically transformed to measure sympathetic and parasympathetic activity, along with the activity of the autonomic nervous system. HRV frequency components were obtained using Welch's method and classified into the following frequency bands:

- Very low frequency (VLF): 0.003 - 0.04 Hz
- Low frequency (LF): 0.04 - 0.15 Hz
- High frequency (HF): 0.15 - 0.4 Hz.

3.5.2 Blood pressure signal characterization

To analyze vascular function, we obtained time series related to systolic and diastolic blood pressure (in mmHg). Blood pressure fluctuates between a minimum diastolic blood pressure (DBP) and a maximum systolic blood pressure (SBP). The degree of these fluctuations is reflected in the pulse pressure (PP), which depends on the ventricular ejection volume and rate, peripheral resistance, and the viscoelastic properties of the arterial walls. PP is defined by the difference between SBP and DBP (PP = SBP − DBP) [1].

The DBP value depends on the duration of the diastole. Tachycardic events in which the diastoles are normally short, may be associated with high DBP. On the other hand, in bradycardic episodes, in which the diastoles are normally prolonged, the DBP may have lower values. In general, low DBP is observed in cases of vasodilatation, bradycardia, or increased arterial compliance. Like the heart rate, the blood pressure oscillates due to the interplay among different neurohumoral systems [7]. Blood pressure variability (BPV) can be analyzed in the short-term (minutes-hours) or in the long-term (days-months), reflecting different characteristics of vascular activity.

Due to its interaction with different mechanisms like the baroreflex, BP varies between beats, known as ultra-short term BP variability. Blood pressure variability can be analyzed through frequency features. At a very low frequency band (VLF: 0.02 Hz - 0.07 Hz), BPV activity is influenced by the myogenic vascular function and the renin angiotensin system. At a low frequency band (LF: 0.07 Hz - 0.15 Hz), this variability is modulated by the sympathetic modulation of vascular tone. At a high frequency band (HF: 0.15 Hz - 0.40 Hz), the variability is mainly affected by changes in cardiac output [5].

Short-term variability analyses study fluctuations in BP in periods of up to 24 hours. BP fluctuations in the minutes to hours range reflect central and autonomic modulation and the elastic properties of the arteries. 24 hour BPV assessments are used to predict cardiovascular risk in hypertensive patients.

Long-term BPV has been associated with increased risk of cardiovascular disease. Pronounced variation in BP could also indicate the poor reaction of a patient to a specific treatment.

Using the BP signal, we calculated time series consisting of the maximum successive end-systolic blood pressure amplitude values (systogram, SBP - mmHg). Time series consisting of the minimum successive end-diastolic blood pressure amplitude values (diastogram, DBP - mmHg) were also extracted.

3.5.3 Respiratory flow signal characterization

Respiratory function is commonly analyzed in terms of inspiration and expiration time series. The most common of these are inspiratory time ($\mathrm{T_I}$), expiratory time ($\mathrm{T_E}$), breath duration (TT), tidal volume ($\mathrm{V_T}$), fractional inspiratory time ($\mathrm{T_I}$/TT), mean inspiratory flow ($\mathrm{V_T}/\mathrm{T_I}$), and frequency-tidal volume ratio ($f/\mathrm{V_T}$), where f is the respiratory frequency.

Similar to heart rate, respiratory flow oscillates from breath to breath, with a higher variance under normal conditions. A lower respiratory flow variability is associated with pathological conditions. The loss of a system's variability usually reflects a loss of degrees of freedom of the system, leading to poor adaptation to internal or external disturbances [2].

The time series (in s) of breath duration (TT) were extracted automatically using an algorithm based on the zero-crossing of the respiratory flow signal. They were then visually inspected and edited if necessary.

3.5.4 Baroreflex mechanism characterization

To characterize the baroreflex mechanism, different actions involved in the regulation of blood pressure activity were considered. Measures related to changes in stroke volume (SV), heart rate (HR), and vascular resistance (R) allow BP variability to be analyzed, according to:

$$\Delta BP = SV * HR * R. \tag{3.1}$$

The sympathetic response increases blood pressure by stimulating an increase in the heart rate and stroke volume and by promoting vasoconstriction. On the other hand, the parasympathetic response decreases blood pressure by decreasing the heart rate and stroke volume and by promoting vasodilatation.

3.6 Statistical test

Statistical analyses make it possible to obtain descriptive information about the signals studied. Several indices have allowed us to describe the characteristics and behavior of the systems analyzed. These indices are extracted directly from the samples through the application of different statistical procedures. The indices and tests used in this work are introduced below.

3.6.1 Probability of an event

Being $X = x_1, \ldots, x_n$ a random vector, the likelihood of the occurrence of an event resulting from a statistical experiment is evaluated by means of weights or probabilities, ranging from 0 to 1. The sum of all probabilities is 1. If a certain sample point is quite likely to occur when the experiment is conducted, the probability assigned should be close to 1. On the other hand, a probability closer to 0 is assigned to a sample point that is not likely to occur.

The probability of an event X is the sum of the weights of all sample points in X, denoted by $P(X)$. If an experiment can result in any one of N different equally likely outcomes, and if exactly n of these outcomes corresponds to event X, then the probability of event X is:

$$P(X) = \frac{n}{N}\,. \tag{3.2}$$

The cumulative distribution function $F(x_i)$ of discrete random variable X with probability distribution $f(x_i)$ is:

$$F(X_i) = P(X \leq x_i) = \sum_{t \leq x_i} f(t), \text{ for } -\infty < x_i < \infty\,. \tag{3.3}$$

The cumulative distribution function $F(x_i)$ of a continuous random variable X with density function $f(x_i)$ is [4]:

$$F(x_i) = P(X \leq x_i) = \int_{-\infty}^{\infty} f(t)dt, \text{ for } -\infty < x_i < \infty\,. \tag{3.4}$$

3.6.2 Descriptive indices

The most commonly used statistics for measuring the location, dispersion, variability and morphology of a set of data, arranged in order of magnitude are:

- *Mean*: Represents the central value of a set of numbers, it corresponds to the average value of a dataset and is given by [3]:

$$\overline{X} = \frac{1}{n} \sum_{i=1}^{n} x_i \; , \tag{3.5}$$

where X_i is the i^{th} sample of a set of samples X of length n

- *Median*: It is also a location measure that shows the middle value after the sample is sorted, given by [3]:

$$\tilde{X} = \begin{cases} x_{(n+1)/2} \; , & \text{if } n \text{ is odd} \; , \\ \frac{1}{2}(x_{n/2} + x_{n/2+1}) \; , & \text{if } n \text{ is even} \; . \end{cases} \tag{3.6}$$

- *Standard deviation*: it is a measure of the dispersion of a set of values and given by:

$$sd = \sqrt{\frac{1}{n} \sum_{i=1}^{n} (x_i - \overline{X})^2} \; , \tag{3.7}$$

where x_i is the i^{th} sample of a set of values X of length n and $\overline{X}$ the mean value of X [3].

- *Coefficient of variation*: It is also known as relative standard deviation and is a standardized measure of dispersion of a probability distribution or frequency distribution. It is often expressed as a percentage, and defined by:

$$Cv = \frac{sd}{\overline{X}} \; . \tag{3.8}$$

- *Skewness*: It is the third standardized moment, defined as:

$$Sk(X) = E\left[\left(\frac{X - \overline{X}}{sd}\right)^3\right] = \frac{E[(X - \overline{X})^3]}{(E[(X - \overline{X})^2])^{3/2}} = \frac{\overline{X}_3}{sd^3} \; , \tag{3.9}$$

where $\overline{X}$ is the mean, sd is the standard deviation, E is the expectation operator, and $\overline{X}_3$ is the third central moment. The skewness values can be positive, zero, negative or undefined. For an unimodal distribution, in negative skew the left tail is longer, and in positive skew the right tail is longer [3].

- *Kurtosis*: It is the fourth standardized moment, defined as:

$$K(X) = E\left[\left(\frac{X-\overline{X}}{sd}\right)^4\right] = \frac{E[(X-\overline{X})^4]}{(E[(X-\overline{X})^2])^2} = \frac{\overline{X}_4}{sd^4}\,, \tag{3.10}$$

where $\overline{X}$ is the mean, sd is the standard deviation, E is the expectation operator, and $\overline{X}_4$ is the fourth central moment. Kurtosis evaluates morphology considering three different cases: mesokurtic, when the distribution presents zero excess kurtosis; leptokurtic, when the distribution has positive excess kurtosis; and platykurtic, when the distribution has negative excess kurtosis [3].

- *Interquartile range*: It is also a measure of statistical dispersion, being equal to the difference between 75^{th} (Q_3) and 25^{th} (Q_1) percentiles, represented by [3]:

$$IQR = Q_3 - Q_1\,. \tag{3.11}$$

Each quartile is a median calculated as follows: given an even $2n$ or odd $2n+1$ number of values,

$$\begin{aligned} Q_1 &= \text{median of the } n \text{ smallest values,} \\ Q_3 &= \text{median of the } n \text{ largest values.} \end{aligned}$$

The second quartile is the same as the ordinary median.

3.6.3 Tests of hypotheses

A major area of statistical inference is based on the procedures that lead to acceptance or rejection of statistical hypotheses. For this, a parametric or non-parametric statistical test is applied in function of the behavior of the samples. When the samples are independent, follows a normal distribution and are homoscedastic a parametric statistical test is applied, otherwise, when one of these conditions is not fulfilled a non-parametric statistical test is applied. The tests used in this study are briefly described below.

Normality test

A normality test determines if a data set can be modeled by a normal distribution and computes how likely it is for a random variable underlying the data set to be normally distributed. In hypothesis testing, the dataset are tested against the null hypothesis that samples are normally distributed [9].

Levene's test

Levene's test is an inferential statistic used to assess the equality of variances for a variable calculated for two or more groups. The homoscedasticity (equality of variances) is tested as the null hypothesis [9]. If the resulting value of Levene's test is lower than a previously set significance level, the null hypothesis of equal variances is rejected.

Kolmogorov–Smirnov test

The Kolmogorov-Smirnov test (KS test) is a non-parametric test of the equality of continuous one-dimensional probability distributions to compare a sample with a reference probability distribution. It quantifies a distance between the empirical distribution function of the sample and the cumulative distribution function of the reference distribution (one - sample KS test) or between the empirical distribution functions of two samples (two - sample KS test). The null distribution of this statistic is calculated under the null hypothesis that the sample is drawn from the reference distribution (in the one sample case) or that the samples are drawn from the same distribution (in the two sample case) [9]. This test is used with smaller datasets.

Mann-Whitney U test

The Mann-Whitney U test is a non-parametric statistical test that makes it possible to determine if the means of two data sets present statistically significant differences. The test assumes that the observations of both groups are independent [9]. The null hypothesis states that all data comes from the same population.

3.6.4 Classification performance indices

The following indices are statistical measures of the performance of a classification test:

- *Accuracy (Acc)*: This measure is the proportion of correct predictions (true positives and true negatives) among the total number of cases examined and given by:

$$Acc = \frac{TP + TN}{TP + FP + TN + FN}\ , \tag{3.12}$$

  being TP the true positive, TN the true negative, FP the false positive, and FN the false negative.

- *Sensitivity (Sn)*: It is also called true positive rate and measures the proportion of actual positives that are correctly identified, given by:

$$Sn = \frac{TP}{TP + FN} \,, \tag{3.13}$$

where TP is the true positive, and FN the false negative.

- *Specificity (Sp)*: It is also called true negative rate and measures the proportion of actual negatives that are correctly identified, given by:

$$Sp = \frac{TN}{TN + FP} \,, \tag{3.14}$$

where TN is the true negative, and FP is the false positive.

- *Area under the curve (AUC)*: This measure estimates how capable a model is at distinguishing between classes. A receiver operating characteristic curve, or ROC curve, is a graphical plot created by plotting the true positive rate against the false positive rate. The true positive rate is also known as sensitivity or probability of detection, and the false positive rate is also known as probability of false detection, calculated as $1 - Sp$. The AUC is the area under the curve of the ROC curve. A higher AUC indicates that the model is better at predicting than a model with lower AUC.

3.6.5 Covariance and correlation

Covariance

Covariance establishes the extent to which two variables vary together, defined by:

$$Cov(X, Y) = \frac{\sum_{i=1}^{N} \left(x_i - \overline{X}\right)\left(y_i - \overline{Y}\right)}{N} \,. \tag{3.15}$$

Covariance values are positive when high magnitudes of one variable correspond to high magnitudes of the other. On the other hand, covariance values are negative if high magnitudes of one variable correspond to low magnitudes of the other [4].

Correlation

Correlation represents the statistical dependency between two variables. The correlation between variables is typically measured by means of the correlation coefficient obtained by calculating the ratio of the covariance between the product of its standard deviations:

$$r = \frac{\sum_{i=1}^{n} \left(x_i - \overline{X}\right)\left(y_i - \overline{Y}\right)}{\sqrt{\sum_{i=1}^{n} \left(x_i - \overline{X}\right)^2} \sqrt{\sum_{i=1}^{n} \left(y_i - \overline{Y}\right)^2}} \,. \tag{3.16}$$

The ranges of the correlation coefficient are between -1 and 1. The extreme values indicate a clear marked linear relationship between the variables. Negative values indicate that one variable increases while the other decreases. On the other hand, positive values indicate that if one variable increases the other increases too. Small or close to zero values of the index indicate that there is no linear correlation between the variables [4].

Chapter 3 bibliography

[1] J. Augusto, J. Teboul, P. Radermacher, and P. Asfar. "Interpretation of blood pressure signal: physiological bases, clinical relevance, and objectives during shock states." In: *Intensive Care Med.* (2010).

[2] F. Baudin, H. Wu, A. Bordessoule, J. Beck, P. Jouvet, M. Frasch, and G. Emeriaud. "Impact of Ventilatory Modes on the Breathing Variability in Mechanically Ventilated Infants." In: *Frontiers in Pediatrics.* (2014).

[3] J Martin Bland and Douglas G Altman. "Statistics notes: Measurement error". In: *BMJ* 312.7047 (1996), p. 1654. DOI: `10.1136/bmj.312.7047.1654`. eprint: `https://www.bmj.com/content/312/7047/1654`. URL: `https://www.bmj.com/content/312/7047/1654`.

[4] B. Everitt. "The Cambridge dictionary of statistics." In: *Cambridge University Press* (2006).

[5] C. Höcht. "Blood Pressure Variability: Prognostic Value and Therapeutic Implications." In: *ISRN Hypertension.* (2013).

[6] J. Martinez, R. Almeida, S. Olmos, A. Rocha, and P. Laguna. "A wavelet-based ECG delineator: evaluation on standard databases." In: *IEEE Trans. Biomed.* (2004).

[7] G. Parati, G. Bilo, and M. Valentini. "Blood pressure variability: methodological aspects, pathophysiological and clinical implications." In: *Informa Healthcare.* (2008).

[8] G. Pinna, R. Maestri, A. Mortara, M. La Rovere, F. Fanfulla, and P. Sleight. "Periodic breathing in heart failure patients: testing the hypothesis of instability of the chemoreflex loop." In: *J. Appl. Physiol.* (2000).

[9] S. Siegal. "Non-parametric statistics for the behavioral sciences." In: *McGraw-Hill* (1988).

[10] Task Force of The European Society of Cardiology, The North American Society of Pacing, and Electrophysiology. "Heart rate variability - Standards of measurement, physiological interpretation, and clinical use." In: *European Heart Journal.* (1996).

[11] A. Voss, C. Fischer, R. Schroeder, H. R. Figulla, and M. Goernig. “Segmented Poincare plot analysis for risk stratification in patients with dilated cardiomyopathy”. In: *Methods Inf Med* 49.5 (2010), pp. 511–5. ISSN: 2511-705X (Electronic) 0026-1270 (Linking). DOI: 10.3414/ME09-02-0050. URL: https://www.ncbi.nlm.nih.gov/pubmed/20526525.

[12] A. Voss, M. Goernig, R. Schroeder, S. Truebner, A. Schirdewan, and H. R. Figulla. “Blood pressure variability as sign of autonomic imbalance in patients with idiopathic dilated cardiomyopathy”. In: *Pacing Clin Electrophysiol* 35.4 (2012), pp. 471–9. ISSN: 1540-8159 (Electronic) 0147-8389 (Linking). DOI: 10.1111/j.1540-8159.2011.03312.x. URL: https://www.ncbi.nlm.nih.gov/pubmed/22268614.

4

Artifact reconstruction in biomedical signals

4.1 Introduction

Biomedical signals can yield useful information about the physiological condition of the patient. The analysis of these signals has become a powerful tool in both clinical diagnosis and health research. However, signals can be corrupted by noise, artifacts, or missing data during the acquisition stage. Signal corruption can hinder the application of processing techniques, and consequently, the further analysis and interpretation of the signal.

A quasi-periodic signal exhibits an irregular periodic behavior with recurring patterns. Several physiological processes can be studied through the analysis of these types of signals. Some examples of biomedical quasi-periodic signals are electrocardiographic (ECG), blood pressure (BP), and respiratory flow (FLW) signals.

The implementation of an artifact reconstruction step prior to analyzing the signal can minimize the presence of information unrelated to the physiological process, thereby improving the quality of the signal under study. The original dynamics of the signal, and thus of the physiological process, must be preserved.

Therefore, the reconstructed segments should resemble their corresponding physiological recordings.

A range of reconstruction methods have been reported for use on different types of signals and applications. Bayesian and wavelet filters have been used to eliminate different types of artifacts in ECG, electroencephalographic (EEG) and photoplethysmographic (PPG) signals [6, 12, 18]. Independent component analysis (ICA) has also been explored as an artifact detection and signal reconstruction technique [14, 2, 11]. Other authors have achieved reconstruction by means of the characterization of a signal divided into segments and the application of template-based methods [7, 8].

The aforementioned methods are optimized to work on one type of signal or to remove a specific type of artifact, but are not generalizable. Moreover, some methods require additional resources in order to work, like additional sensors, signal models or templates. However, these resources are not always available, sometimes require multiple channels to function, and cannot operate automatically.

In this chapter, we propose a novel artifact reconstruction method for application to the physiological pseudo-cycles in biomedical signals corrupted by artifacts. This method is applicable to any quasi-periodic signal, regardless of the morphology of its cycles. The reconstruction process is based on the information of neighboring events, while maintaining the dynamics of the original signal. The method has been tested using ECG, BP and FLW signals.

4.2 Artifact reconstruction in pseudo-periodic signals

Due to their quasi-periodic nature, the behavior of biomedical signals can be analyzed based on pseudo-periods related to physiological cycles and their activity. During the acquisition process, some of these signals can be affected by events related to artifacts or interruptions. To reconstruct these events, we propose the following procedure:

- *Cycle detection:* To identify and characterize each physiological cycle

- *Artifact detection:* To identify and characterize each artifact event

- *Artifact reconstruction:* To replace each artifact event with the corresponding physiological cycles, generated from neighboring cycles

4.2.1 Cycle detection

A quasi-periodic biomedical signal can be broken down into consecutive pseudo-periods. For each signal $X(t)$, we defined a vector $E(n)$ with each initial time of each pseudo-period, as:

$$E(n) = E_1, ..., E_N, \quad \text{where } n = 1, \ \ldots, \ N, \tag{4.1}$$

being N the number of cycles detected. The initial position of these quasi-periods was detected by analyzing local windows defined based on the length of each cycle. This process adapts to the shape and duration of the cycles depending on each type of signal.

In this work, we propose a method for reconstructing the physiological cycles of ECG, BP and FLW signals. We therefore needed to identify the initial position of each cycle. To reconstruct an ECG signal, its cycles were detected according to the maximum value of each pseudo-period. An adaptive window was defined, and afterwards, the first maximum value corresponding to the position of the R-peak was obtained, through the derivative signal. From this peak position, a new window was defined to determine the position of the P wave, and in the same way, through the derivative signal, the initial position of this wave was obtained and defined as the onset of the cycle. In BP signal reconstruction, the diastolic value was defined as the initial position of each blood pressure cycle, using wavelet decomposition method. For the reconstruction of FLW signals, an algorithm based on a zero-crossing was used to define the initial position of the cycles. In all cases, the cycle detection step was applied after the baseline of the signals was eliminated. Figure 4.1 illustrates an example of the ECG, BP, and FLW signals with their physiological cycles detected.

4.2.2 Artifact detection

To identify an artifact segment, the area under the curve of different cycles was analyzed using the Θ_E parameter, determined by:

$$\Theta_E = \sum_{j=1}^{M} |A_i - A_{i+j}|, \quad \forall i = 1, ..., N, \tag{4.2}$$

where A_i is the area under the curve of cycle i, N is the total number of cycles of the signal, and M is the number of neighboring cycles. The area of each cycle A_i is compared with the cumulative areas A_{i+j}. The result of each $\Theta_{E_{(i)}}$ is related to the number of neighbors used, and thus, the M value must be optimized considering that $M \leq \frac{N-1}{2}$. To define the optimal M value, Θ_E was evaluated using different numbers of neighboring cycles.

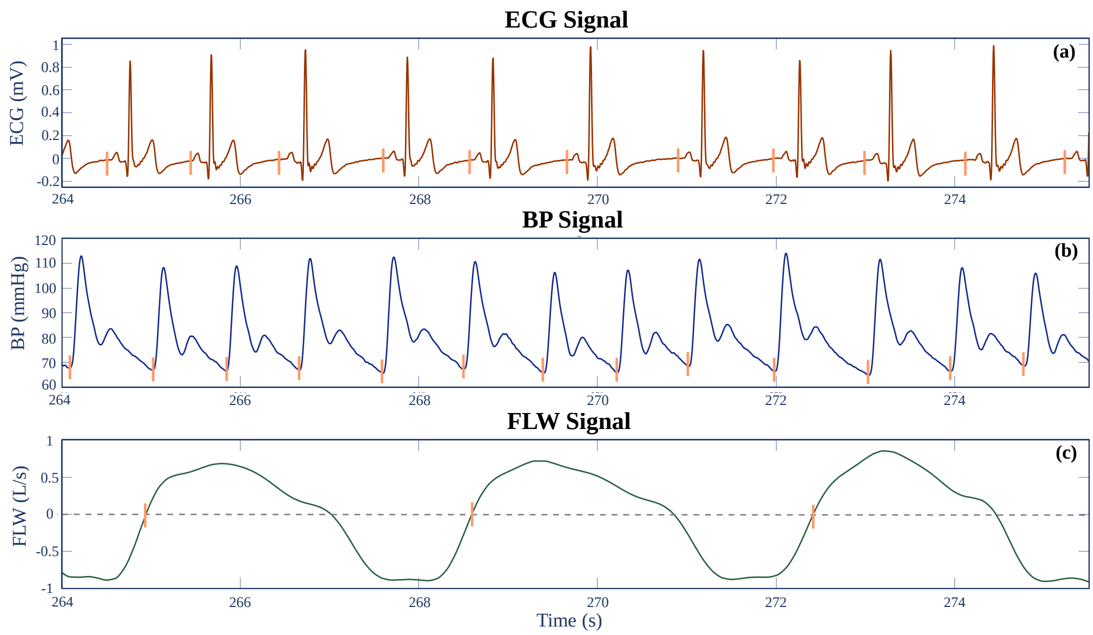

Figure 4.1. Physiological cycle detection in a) electrocardiographic (ECG), b) blood pressure (BP), and c) respiratory flow (FLW) signals.

The morphological similarity or dissimilarity of the physiological cycle was defined based on the result of Θ_E as:

- *low value*: events with similar morphology (Figure 4.2.a)
- *high value*: events with dissimilar morphology (Figure 4.2.b)

The difference between a physiological cycle and an artifact was determined by comparing each $\Theta_{E_{(i)}}$. An adaptive threshold (Th_{Θ_E}) was defined as $Th_{\Theta_E} = \overline{\Theta_E} \pm 3\sigma_{\Theta_E}$, where $\overline{\Theta_E}$ and σ_{Θ_E} are the mean and standard deviation of Θ_E. Figure 4.3 is an example of the behavior of Θ_E for different values of M evaluated in a blood pressure signal. In this case, M values of less than 10 caused some physiological cycles to be considered artifacts.

In order to begin the reconstruction process the first physiological cycle must be correctly identified. To this end, the first 10 cycles were analyzed and the areas between each event and its neighbors were compared. This first cycle was selected if the difference of these areas was less than or equal to Th_{Θ_E}, and it constituted the pattern used to reconstruct the other cycles. Table 4.1 summarizes the artifact detection process, and Figure 4.4 shows an example of these processes applied to a BP signal with different artifact segments.

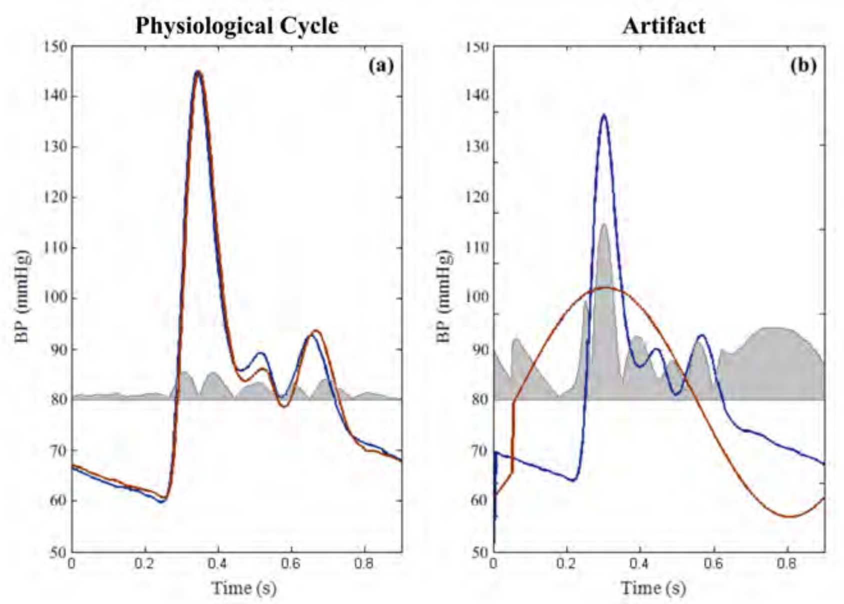

Figure 4.2. An example of the areas superposition of a) a physiological event and a neighboring cycle, and b) a physiological event and an artifact. The result is the difference between the areas under the curve (grey area).

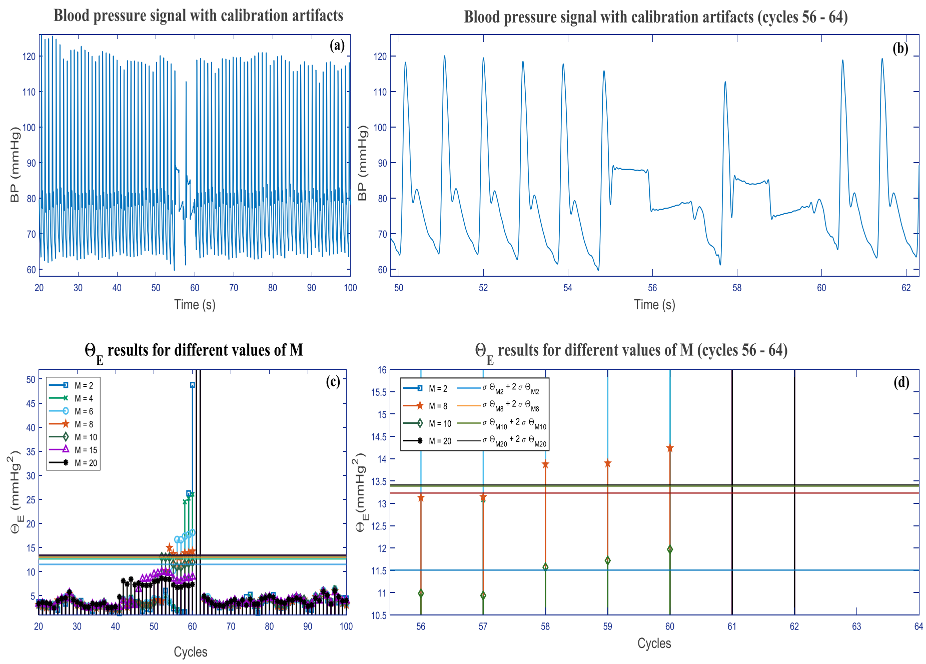

Figure 4.3. Behavior of different M values evaluated in a blood pressure signal. a) An excerpt of a blood pressure signal with some artifacts, b) a zoom of the area with artifacts in the signal, c) results of Θ_E considering different M values, and d) representation of different M values in the artifact segment with different thresholds. In this example, the optimal threshold is obtained when $M = 10$.

Table 4.1. Pseudocode of the artifact detection process.

Artifact detection process
$\boldsymbol{A} = [\boldsymbol{A_1} \quad ... \quad \boldsymbol{A_N}]$ (area under the curve of each cycle)
$\boldsymbol{Av} = [\boldsymbol{Av_1} \quad ... \quad \boldsymbol{Av_N}]$ (each event identification, 1: artifact, 0:cycle)
$\boldsymbol{k}$ number of current iteration (initial value: 1)
$\boldsymbol{a}$ number of artifacts detected in current iteration (initial value: 0)
while $\boldsymbol{k} = 1 \quad \vert\vert \quad \boldsymbol{a} \neq 0$
$\boldsymbol{\Theta_{E_{(i)}}} = \sum_{j=1}^{M} \vert A_i - A_{i+j}\vert, \forall \boldsymbol{i} = 1, ..., N \in \boldsymbol{Av}, \quad [\boldsymbol{Av} = 0]$
(calculate $\Theta_{E_{(i)}}$ parameter, leaving out artifacts already detected)
$\boldsymbol{Th_{\Theta_E}} = \boldsymbol{\overline{\Theta_E} + 3\sigma_{\Theta_E}}$ (calculate the artifact detection threshold)
$\boldsymbol{a} = 0$
for $\boldsymbol{i} \in \boldsymbol{\Theta_E}$
if $\boldsymbol{\Theta_{E_i}} \geq \boldsymbol{Th_{\Theta_E}}$ (Θ_E determines if the event is a cycle or an artifact)
$A_{v_i} = 1$ (current event is marked as an artifact)
$\boldsymbol{a} = \boldsymbol{a} + 1$
else
$A_{v_i} = 0$ (current event is marked as a physiological cycle)
end
end (process stops when no more artifacts are detected)
$k = k + 1$
end

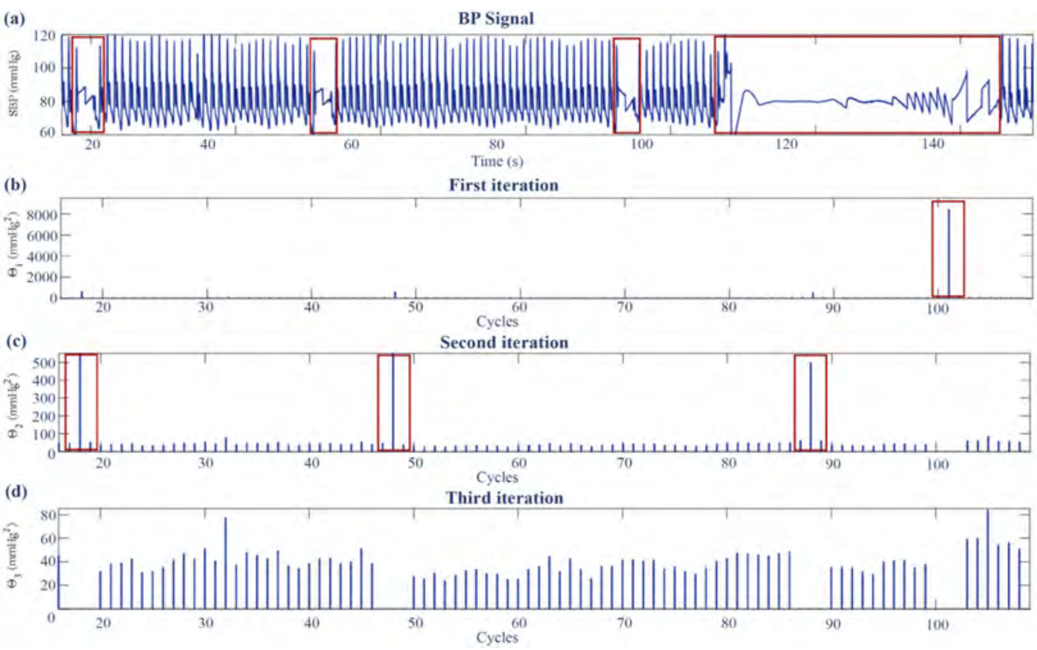

Figure 4.4. An example of the number of iterations necessary to detect the artifacts segments: a) an excerpt of a BP signal with different artifact segments; b) result of Θ_E in the first iteration, where the largest artifact segments were detected; c) result of Θ_E in the second iteration, where the next artifacts segments were detected, in accordance with their length; d) results of the Θ_E in the third iteration, where no artifact segments were detected. With this last result the process was finished.

4.2.3 Reconstruction process

The artifact segments were reconstructed using information from the neighboring cycles of the original signal through the following steps:

- *First step*: determine the length of the event (le) to reconstruct, and the necessary number of cycles for this segment, calculated based on the average number of neighboring cycles that would fit in the segment to be reconstructed.

- *Second step*: generate the reconstruction cycles using a same number of physiological cycles to the left and right of the artifact segment.

The artifact was then replaced by crossfading the two extrapolated values using the following window [1]:

$$w(n) = \begin{cases} 1 - \frac{1}{2}(2u(n))^{\alpha}, & u(n) \leq \frac{1}{2} \\ \frac{1}{2}(2 - 2u(n))^{\alpha}, & u(n) > \frac{1}{2} \end{cases}, \tag{4.3}$$

where $u(n) = \frac{n+1}{le}, n = 1, ..., le$. Crossfading was carried out by multiplying the forward extrapolated sequence by $w(n)$ and the backward extrapolated sequence by $1 - w(n)$. A linear down-slope was attained with $\alpha = 1$, whereas a step-like transition resulted when $\alpha \rightarrow \infty$. The optimal transition window was obtained when $\alpha = 3$. Events with Θ_E values greater than the threshold Th_{Θ_E} were excluded from reconstruction until the next event corresponded to a physiological cycle, and it was used instead. The process was repeated twice, and finally, the most similar reconstructed event to the physiological cycle was selected. The whole reconstruction process is represented in Figure 4.5.

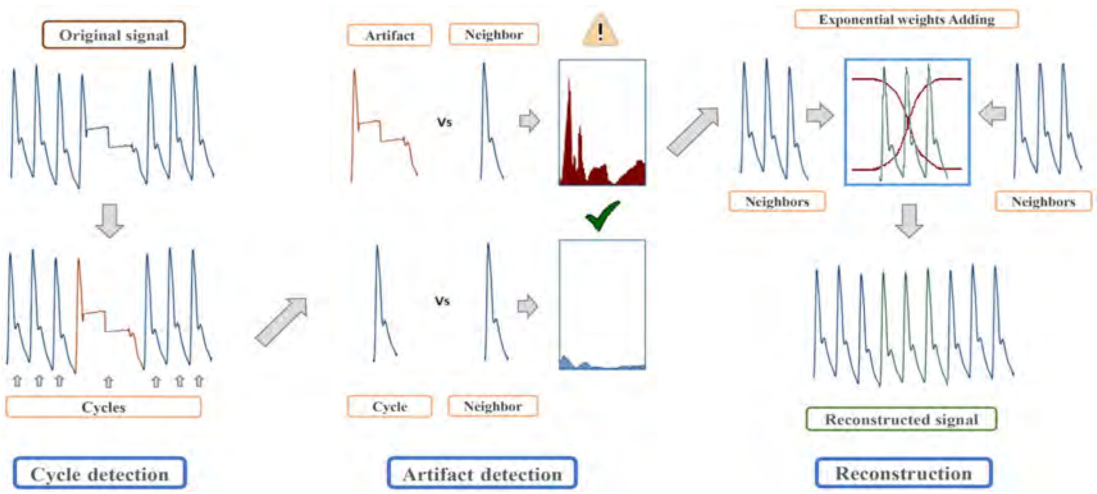

Figure 4.5. Method description of the cycle and artifact detection and reconstruction steps.

4.2.4 Validation

To evaluate the quality of the reconstruction process, each reconstructed cycle was compared with its original segment. To quantify the goodness of the process, three different quality measures were considered:

- *Detc*: number of artifacts present in the reconstructed signal, as undetected artifacts
- *Rwr*: number of reconstructed artifacts, that because of their difference from the original event were still considered artifact
- *Cwr*: number of physiological cycles incorrectly treated as artifacts

Finally, each area under the curve of the original signal (A_i) was compared to its corresponding pair in the reconstructed signal (A_{R_i}). This process is described in Table 4.2.

Table 4.2. Pseudocode for the automatic validation process.

Automatic validation process

$\boldsymbol{A} = [\boldsymbol{A_1} \ \ldots \ \boldsymbol{A_N}]$ (area under the curve of cycles in the signal)
$\boldsymbol{A_R} = [\boldsymbol{A_1} \ \ldots \ \boldsymbol{A_N}]$ (area under the curve of cycles in the reconstructed signal)
$\alpha = \frac{A_i}{A_{R_i}}$ if $A_i < A_{R_i}$ or $\frac{A_{R_i}}{A_i}$ otherwise
Detc: number of artifacts missed (initial value: 0)
Rwr: number of poor-quality reconstructions (initial value: 0)
Cwr: number of cycles wrongly detected as artifacts (initial value: 0)
$\Theta_{E_{(i)}} X = \sum_{j=1}^{M} |A_i - A_{i+j}|, \forall i = 1, ..., N$ ($\boldsymbol{\Theta_E}$ for the original signal)
$\Theta_{E_{(i)}} X_R = \sum_{j=1}^{M} |A_{Ri} - A_{R(i+j)}|, \forall i = 1, ..., N$ ($\boldsymbol{\Theta_E}$ for the reconstructed signal)
$\boldsymbol{Th_{\Theta_E}} = \overline{\Theta_E} + 3\sigma_{\Theta_E}$ (artifact detection threshold is calculated)

```
for i ∈ Θ_E
    if  α < 0.95
        if Θ_E X < Th_Θ_E
            Cwr = Cwr + 1
        else
            if Θ_E X_R ≥ Th_Θ_E
                Rwr = Rwr + 1
            end
        end
    else
        if Θ_E X ≥ Th_Θ_E
            Detc = Detc + 1
        end
    end
end
```

4.3 Illustration of the method

The performance of the artifact reconstruction method proposed was analyzed using both simulated and real signals.

4.3.1 Simulated and real signals

The behavior of physiological signals like ECG, blood pressure and respiratory flow often resemble a periodic signal subjected to amplitude modulation. In order to illustrate the method's performance, the following signals were studied:

$$\textit{Sinusoidal wave: } S_1(t) = sin(2\pi f t) \tag{4.4}$$

$$\textit{Rectangular pulse wave: } S_2(t) = \begin{cases} 1 & \text{if} \quad ||t|| \text{ is odd} \\ -1 & \text{if} \quad ||t|| \text{ is even} \end{cases} \tag{4.5}$$

$$\textit{Saw-tooth wave: } S_3(t) = \frac{1}{2} - \frac{1}{\pi} \sum_k \frac{sin(2kft)}{k} \tag{4.6}$$

$$\textit{Mixed wave: } S_4(t) = S_1(t) + S_2(t) + S_3(t) \tag{4.7}$$

where f is the sample frequency, and k is the number of truncated ramp functions. Figure 4.6 shows an example of the simulated signals used to illustrate the method.

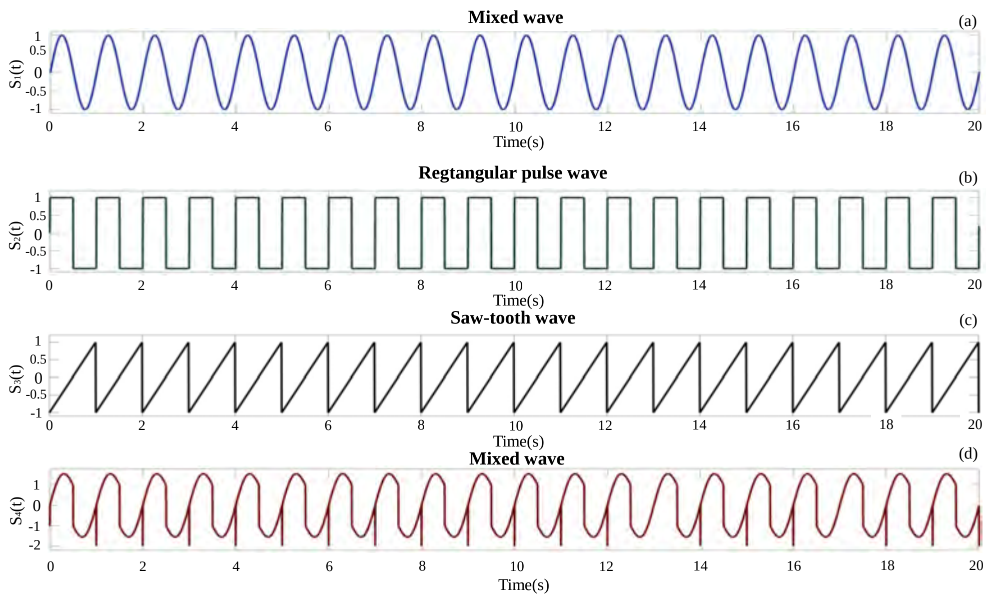

Figure 4.6. Example of the a) sinusoidal, b) rectangular pulse, c) saw-tooth, and d) mixed simulated signals.

Additionally, real signals like ECG, blood pressure and respiratory flow from the HERIS, Weandb and Healthy datasets (Chapter 3) were used to evaluate the goodness of the method. Figure 4.7 shows an example of the real signals with artifact segments.

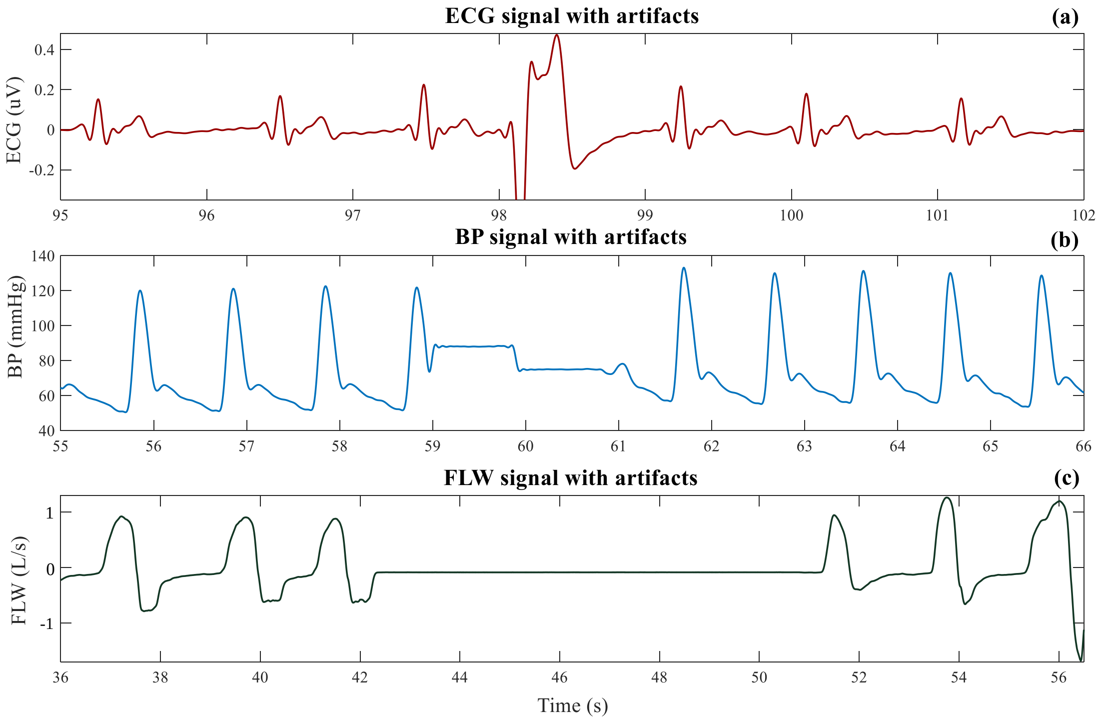

Figure 4.7. Example of the original signals with an artifact segment in: a) ECG, b) BP, and c) FLW.

The method was tested using simulated and real signals. In addition, events related to different levels of Gaussian noise, interruptions or different periodic waves were introduced in parts of the signals. Figure 4.8 is an example of the reconstruction process applied to simulated signals with different forced artifact segments. Forced artifacts were also introduced in the real signals. Figure 4.9 is an example of the process applied to an ECG signal with a forced artifact and its reconstruction.

Real signals were also modified by introducing different levels of Gaussian noise (5, 20 and 40 dB) into a segment. Figure 4.10 is an example of this process applied to a BP signal. The results showed that successful reconstruction is possible as long as the signal-noise ratio (SNR) is high enough.

This study was undertaken because blood pressure signals are often contaminated by the calibration episodes necessary for signal sensing. The following example (Figure 4.11) shows the artifact reconstruction process applied to a BP signal with a calibration segment. The results verify the good reconstruction of

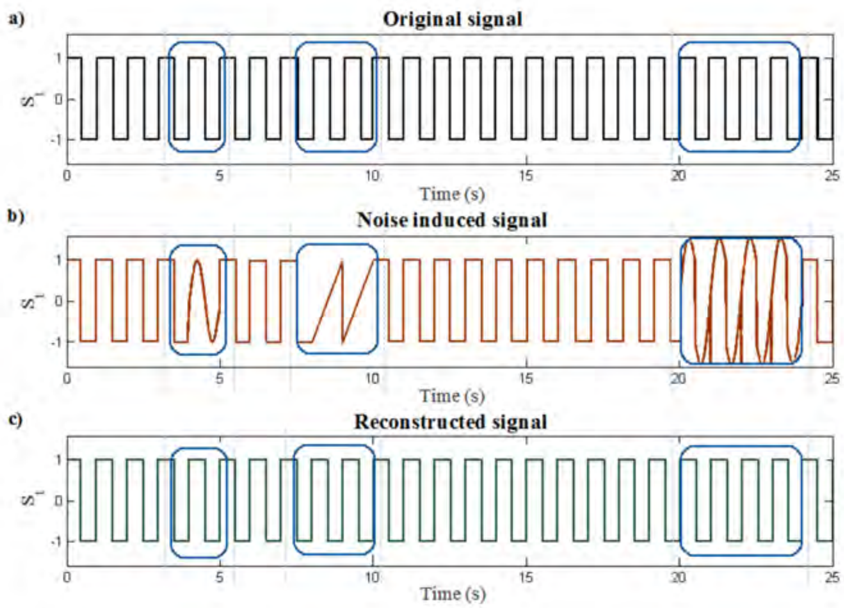

Figure 4.8. Reconstruction of simulated artifacts in a rectangular pulse wave: a) original signal, b) original signal with simulated artifacts, and c) reconstructed signal.

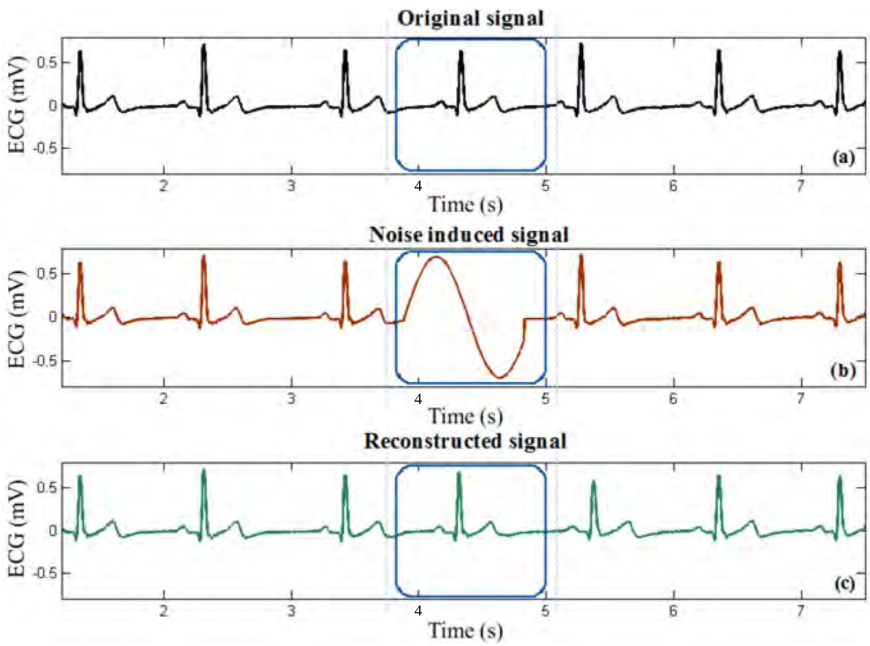

Figure 4.9. Reconstruction process applied to an ECG signal with simulated artifacts: a) original signal, b) ECG signal with simulated artifacts, and c) reconstructed signal.

these events, which maintain the dynamic of the signal.

Figure 4.12 is an example of the reconstruction process applied to an ECG signal when some physiological cycles were marked as artifacts. As the figure

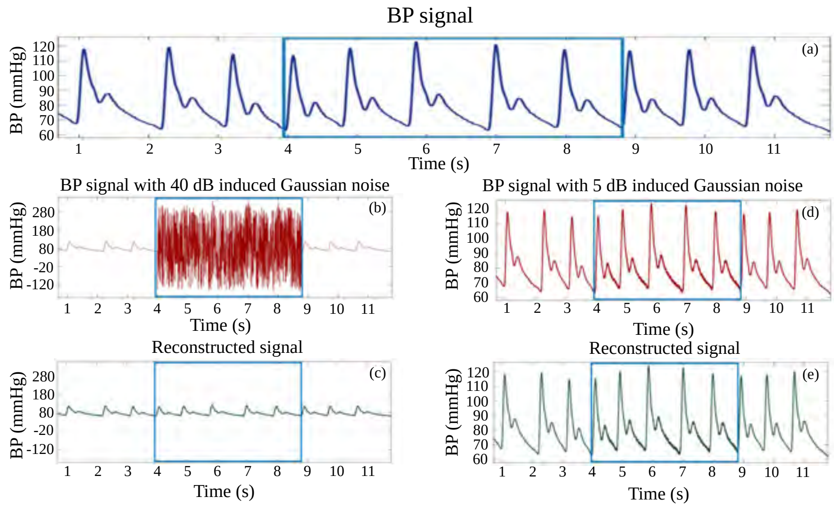

Figure 4.10. Reconstruction process applied to a BP signal with a segment contaminated with either 40 dB or 5 dB Gaussian noise. a) Real BP signal, b) signal with a segment contaminated with 40 dB Gaussian noise, c) reconstructed signal (40 dB Gaussian noise), d) signal with a segment contaminated with 5 dB Gaussian noise, e) reconstructed signal (5 dB Gaussian noise).

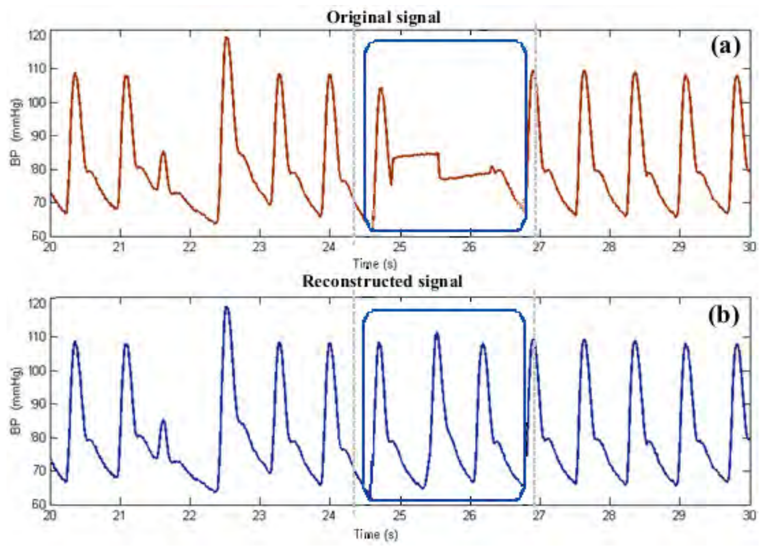

Figure 4.11. Example of the reconstruction of a BP signal affected by calibration artifacts. a) original signal, and b) reconstructed signal.

shows, the reconstructed events are very similar to the original signal. Another test was applied in which interruptions were forced into the signal, simulating a possible disconnection in the acquisition process. Figure 4.13 shows an example of an interruption forced into a respiratory flow signal, which also presents a periodic breathing pattern. Our proposed method was able to reconstruct the signal, while maintaining its pseudo-periodic pattern.

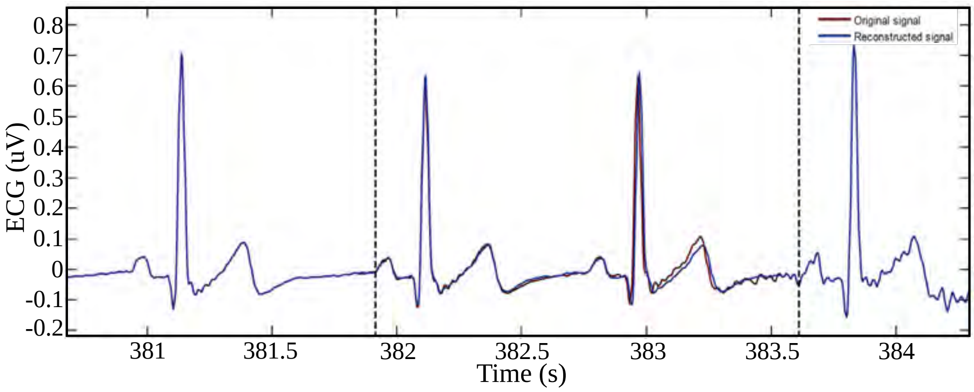

Figure 4.12. Reconstruction process applied to an ECG signal, with two physiological cycles marked as an artifact segment.

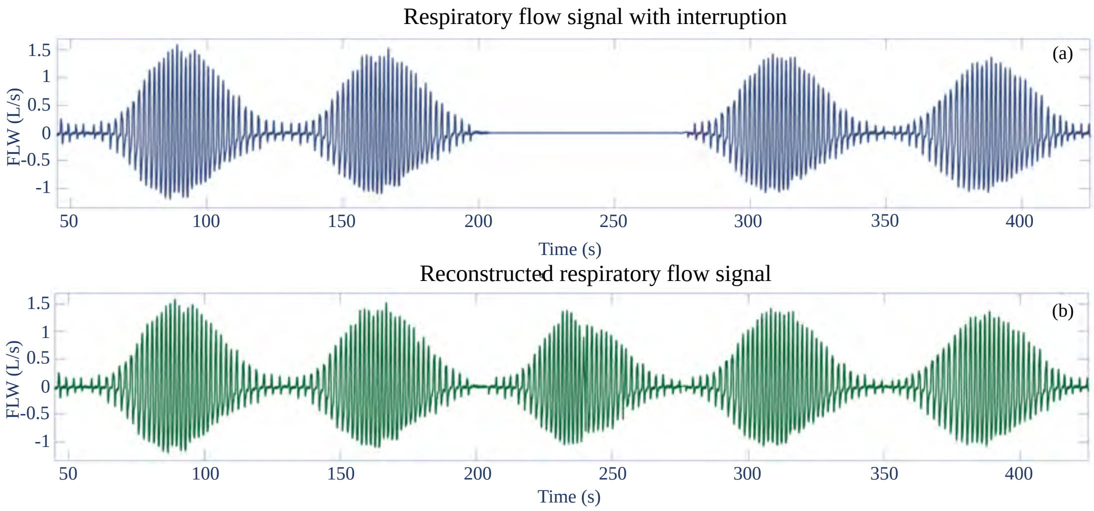

Figure 4.13. Results of the reconstruction of a FLW signal with induced interruption. a) A respiratory flow signal with induced interruption, and b) a reconstructed signal.

4.3.2 Validation

To analyze the effectiveness of the reconstruction process, the response of the signal-noise ratio was evaluated in the different tests. Table 4.3 presents the results of these tests in terms of SNR before and after the reconstruction process. The table shows that in all cases, for all tested signals, the ratio increased after the process. Similar results were obtained when the BP signal was contaminated with different Gaussian noise levels, unless the noise was low.

In order to evaluate the goodness of the method, a random sample of 10 signals from each database used in this study was selected, to quantify the performance of the method. Table 4.4 present the results obtained with the visual inspection, and automatic process.

Table 4.3. Signal noise ratio (SNR) of the simulated signals before and after the reconstruction process.

Signal	SNR(dB) Before	SNR(dB) After
BP - real, with calibration marks	10.38	16.86
Sinusoidal wave	6.56	21.68
Rectangular pulse wave	8.57	28.59
Saw-tooth wave	-0.87	21.45
Mixed wave	7.06	23.67
ECG - real, simulated artifacts	-5.92	6.42
BP - real, simulated artifacts	-1.35	5.81
FLW - real, simulated artifacts	1.78	4.08
BP Gaussian noise (40 dB)	-8.98	6.8
BP Gaussian noise (20 dB)	5.4	11.07
BP Gaussian noise (5 dB)	25.3	25.3

SNR: signal noise ratio; BP: blood pressure signal; ECG: electrocardiographic signal; FLW: respiratory flow signal

Table 4.4. Mean values of *Detc*, *Cwr* and *Rwr* of the visual inspection (V) of an automatic process (A) of the reconstruction method, applied to different types of signals.

Dataset	*A.Detc(%)*	*V.Detc(%)*	*A.Cwr(%)*	*V.Cwr(%)*	*A.Rwr(%)*	*V.Rwr(%)*
Dset1	97	99.5	0.39	0.69	0.7	0.7
Dset2	99	97	0.44	0.49	0.7	0.29
Dset3	98.5	98	2.4	2	0	0

A.Dect: percentage of artifacts detected (automatic); *V.Dect:* percentage of artifacts detected (visual inspection); *A.Cwr:* percentage of cycles wrongly detected as artifacts (automatic); *V.Cwr:* percentage of cycles wrongly detected as artifacts (visual inspection); *A.Rwr:* percentage of poor quality reconstruction of artifacts detected (automatic); *A.Rwr:* percentage of poor quality reconstruction of artifacts detected (visual inspection)

According to the validation results, most of the artifacts were correctly detected and successfully reconstructed. Additionally, physiological cycles were only incorrectly detected as artifacts in less than 1% of the cases.

4.4 Discussion and conclusions

4.4.1 Discussion

We propose an automatic and iterative method with which to reconstruct artifact events in pseudo-periodic physiological signals. The method has been applied to ECG, blood pressure and respiratory flow signals. The simulated events used to replace the artifacts segments were generated using the neighboring physiological cycles. This process has been shown to maintain the original signal dynamics.

Given the variability in the length and shape of the artifact segments, this method allows an adaptive threshold to be defined so that large and small events present in the same signal can be detected. The second iteration makes it possible to process potentially undetected artifacts in signals with high numbers of corrupted segments. An attractive result of this method is its robustness, as it can reconstruct signals containing a periodic breathing pattern in the respiratory flow signal, as shown in Figure 4.13. The method has been able to adapt to the slow modulation of the physiological process in addition to the frequency of each cycle.

The method was successful in all the proposed tests, except with signals simulated with low level Gaussian noise. Both the simulation and validation process yielded positive results. The algorithm was able to reconstruct all the artifact containing segments in most of the simulated cases, improving their SNR. In all the databases tested, the *Detc* was higher than 97%, and the *Cwr* and *Rwr* were lower than 1%.

In contrast with the most common advanced filtering techniques, this method does not require the calculation of any additional parameters previous to its application [6, 17, 9, 16]. Complementary information, like an accurate model of the signal or an additional reference signal, is not always available. In addition, no extra hardware is necessary in order to reconstruct the signal, which is an advantage when the methodology is applied in a clinical or m-health setting.

The execution of the method is completely automatic, which constitutes an advantage over the currently used ICA-based methods [3, 5, 13, 15]. These methods rely on the use of external information in addition to the original signal to perform properly. This may be a problem because of the specific assumptions that must be fulfilled in relation of the nature of the external input used. As an example, in multichannel ICA, the independent sources must be non-Gaussian, in order to obtain an estimate of the original source [10].

Additionally, this method processes each channel individually, using only the information from the original signal. Several currently used reconstruction methods require additional channels [11, 4]. Additional channels with the required criteria are not usually available, and often increase the complexity of the implementation.

The performance of the method heavily relies on the morphological differences between cycles and artifacts. So, its use is recommended in applications where the physiological pseudo-cycles are similar to one another, but significantly different from the artifacts. As an example, the algorithm will perform successfully on blood pressure signals with calibration events but will not work properly on signals with local low power Gaussian noise artifacts. Additionally, it is relevant to mention that the performance of the reconstruction is significantly improved with the precision in the cycle detection. This is due to the influence of the analysis of the cycles in both the artifact detection and reconstruction process. An incorrectly detected cycle will negatively influence the reconstruction process, leading to the incorrect detection of cycles as artifacts, thereby increasing the probability of missing the detection of a true artifact, and lowering the quality of the overall reconstruction.

The method does have some limitations worth mentioning. The quality of the reconstruction is directly dependent on the similarity of the cycles and their morphological differences from artifacts. The method would not work on signals with dissimilar cycles, or on signals in which the artifacts and the cycles are similar in terms of their areas under the curve. Despite the efficacy of the area under the curve-based artifact detection, there is some probability that an artifact might have its area under the curve in the same magnitude range as its neighboring cycles by chance, even though their shapes differ. Based on our tests, in real data the likelihood of this happening is quite low given the high variability in the shapes and frequencies of the artifacts. On the other hand, despite being an automatic method independent of external data, in contrast with template-based methods, the algorithm is by nature iterative, and by extension, not a real time process.

4.4.2 Conclusion

The analysis of the morphology of the pseudo cycles of physiological signals and their posterior processing allows artifact segments within it to be detected and reconstructed. The method described in this chapter is automatic and does not require additional signals or information in order to function, in contrast to existing reconstruction techniques. It is capable of reconstructing signals tainted by artifacts and other interruptions, while preserving the dynamics of the original signal and improving the SNR ratio. The method may be useful in applications in which the signals involved are affected by frequent local artifacts, and the variability of the signal is valuable. We developed this method to reconstruct artifact segments in blood pressure and respiratory flow signals from the Heris and Healthy databases, mostly affected by calibration episodes.

The performance of the method is dependent on the precision in the cycle detection step, the adequate identification of the number of cycles to be reconstructed, and the quality of the prediction of the cycles used to reconstruct the missing segments. The method is capable of dealing with a large variety of situations and different types of pseudo-periodic signals, given that the pseudo-periods can be distinguished and properly differentiated from one another. It is important to mention that the results are not ideal when reconstructing artifacts whose morphology, more specifically the sum of their areas, is similar to the physiological cycles. The application of a reconstruction step before signal processing can potentiate the information that can be extracted from the signals analyzed, and therefore, the results of the studies in which they are involved.

Chapter 4 bibliography

[1] A. Arcentales, A. Voss, P. Caminal, A. Bayés-Genís, M. T. Domingo, and B. F. Giraldo. "Characterization of patients with different ventricular ejection fractions using blood pressure signal analysis". In: *Computing in Cardiology 2013*, pp. 795–798.

[2] B. Azzerboni, M. Carpentieri, F. La Foresta, and F. C. Morabito. "Neural-ICA and wavelet transform for artifacts removal in surface EMG". In: *2004 IEEE International Joint Conference on Neural Networks (IEEE Cat. No.04CH37541).* Vol. 4, 3223–3228 vol.4. DOI: 10.1109/IJCNN.2004.1381194.

[3] W. De Clercq, A. Vergult, B. Vanrumste, W. Van Paesschen, and S. Van Huffel. "Canonical Correlation Analysis Applied to Remove Muscle Artifacts From the Electroencephalogram". In: *IEEE Transactions on Biomedical Engineering* 53.12 (2006), pp. 2583–2587. ISSN: 0018-9294. DOI: 10.1109/TBME.2006.879459.

[4] Pierre Comon. "Independent component analysis, A new concept?" In: *Signal Processing* 36.3 (1994), pp. 287–314. ISSN: 0165-1684. DOI: https://doi.org/10.1016/0165-1684(94)90029-9. URL: http://www.sciencedirect.com/science/article/pii/0165168494900299.

[5] M. E. Davies and C. J. James. "Source separation using single channel ICA". In: *Signal Processing* 87.8 (2007), pp. 1819–1832. ISSN: 0165-1684. DOI: https://doi.org/10.1016/j.sigpro.2007.01.011. URL: http://www.sciencedirect.com/science/article/pii/S0165168407000151.

[6] V. Fox, J. Hightower, Liao Lin, D. Schulz, and G. Borriello. "Bayesian filtering for location estimation". In: *IEEE Pervasive Computing* 2.3 (2003), pp. 24–33. ISSN: 1536-1268. DOI: 10.1109/MPRV.2003.1228524.

[7] G. Ganeshapillai, J. F. Liu, and J. Guttag. "Reconstruction of ECG signals in presence of corruption". In: *2011 Annual International Conference of the IEEE Engineering in Medicine and Biology Society*, pp. 3764–3767. DOI: 10.1109/IEMBS.2011.6090642.

[8] Gartheeban Ganeshapillai and John Guttag. "Real time reconstruction of quasiperiodic multi parameter physiological signals". In: *EURASIP Journal on Advances in Signal Processing* 2012.1 (2012), p. 173. ISSN: 1687-6180.

DOI: 10.1186/1687-6180-2012-173. URL: https://doi.org/10.1186/1687-6180-2012-173.

[9] M. Izzetoglu, A. Devaraj, S. Bunce, and B. Onaral. "Motion artifact cancellation in NIR spectroscopy using Wiener filtering". In: *IEEE Transactions on Biomedical Engineering* 52.5 (2005), pp. 934–938. ISSN: 0018-9294. DOI: 10.1109/TBME.2005.845243.

[10] Christopher J. James and Christian W. Hesse. "Independent component analysis for biomedical signals". In: *Physiological Measurement* 26.1 (2004), R15–R39. ISSN: 0967-3334 1361-6579. DOI: 10.1088/0967-3334/26/1/r02. URL: http://dx.doi.org/10.1088/0967-3334/26/1/R02.

[11] Christopher J. James and David Lowe. "Extracting multisource brain activity from a single electromagnetic channel". In: *Artificial Intelligence in Medicine* 28.1 (2003), pp. 89–104. ISSN: 0933-3657. DOI: https://doi.org/10.1016/S0933-3657(03)00037-X. URL: http://www.sciencedirect.com/science/article/pii/S093336570300037X.

[12] R. E. Kalman. "A New Approach to Linear Filtering and Prediction Problems". In: *Journal of Basic Engineering* 82.1 (1960), pp. 35–45. ISSN: 0098-2202. DOI: 10.1115/1.3662552. URL: http://dx.doi.org/10.1115/1.3662552.

[13] Jing Lin and Aimin Zhang. "Fault feature separation using wavelet-ICA filter". In: *NDT & E International* 38.6 (2005), pp. 421–427. ISSN: 0963-8695. DOI: https://doi.org/10.1016/j.ndteint.2004.11.005. URL: http://www.sciencedirect.com/science/article/pii/S0963869504001525.

[14] J. McBride, A. Sullivan, H. Xia, A. Petrie, and X. Zhao. "Reconstruction of physiological signals using iterative retraining and accumulated averaging of neural network models". In: *Physiol Meas* 32.6 (2011), pp. 661–75. ISSN: 1361-6579. DOI: 10.1088/0967-3334/32/6/004. URL: https://www.ncbi.nlm.nih.gov/pubmed/21566268.

[15] B. Mijovic, M. De Vos, I. Gligorijevic, J. Taelman, and S. Van Huffel. "Source Separation From Single-Channel Recordings by Combining Empirical-Mode Decomposition and Independent Component Analysis". In: *IEEE Transactions on Biomedical Engineering* 57.9 (2010), pp. 2188–2196. ISSN: 0018-9294. DOI: 10.1109/TBME.2010.2051440.

[16] Hongxia Pan and Jifang Men. "De-noising method research on bearing fault signal based on particle filter". In: *2010 Second World Congress on Nature and Biologically Inspired Computing (NaBIC)*, pp. 311–315. DOI: 10.1109/NABIC.2010.5716353.

[17] M. Zia Ur Rahman, R. A. Shaik, and D. V. R. K. Reddy. "Cancellation of artifacts in ECG Signals using sign based normalized adaptive filtering technique". In: *2009 IEEE Symposium on Industrial Electronics & Applications*. Vol. 1, pp. 442–445. DOI: 10.1109/ISIEA.2009.5356413.

[18] L. Smital, M. Vítek, J. Kozumplík, and I. Provazník. “Adaptive Wavelet Wiener Filtering of ECG Signals”. In: *IEEE Transactions on Biomedical Engineering* 60.2 (2013), pp. 437–445. ISSN: 0018-9294. DOI: 10.1109/TBME.2012.2228482.

5

Classification of heart failure patients through Poincaré plot analysis

5.1 Introduction

Heart diseases are one of the most common causes of death, especially in elderly patients [13, 14]; however, the early detection of patients at high risk of sudden cardiac death (SCD) remains a scientific challenge, and identifying cardiomyopathy patients at risk of SCD is still problematic. Analysis based on the left ventricular ejection fraction (LVEF) is one of the indices most widely used in clinical practice today to determine heart function capacity. Patients with LVEF values over 55% are considered to have cardiac activity within the normal ranges, those with values between 35% and 55% are considered to have below normal cardiac activity, and patients with values lower than 35% are classified as pathological [13, 3].

Conventional signal-processing techniques such as time-domain, power spectral density and cross-correlation analysis are often insufficient to characterize the complex dynamics of the systems associated with heart failure.

Several authors have studied different methods to stratify cardiovascular risk through the assessment of different forms of ECG signal characterization. Parameters related to QT intervals, T-wave inversions, wide QRS-T angle, as well as the relationships between autonomic sympathetic dominance and ventricular fibrillation problems have been addressed [15, 4, 18]. The suitability of other parameters like peak oxygen uptake and ventricular arrhythmias has also been researched as means to stratify cardiovascular risk [20, 10].

A Poincaré plot is a graphic method used to evaluate the self-similarity in a given system. It also allows the chaotic and random behaviors of these systems to be identified [9, 6]. The self-similarities are analyzed considering the behavior of the system at a certain point in time and immediately beforehand. In this study, we analyzed the performance of the cardiac, vascular and respiratory systems through the time series that represent their physiological cycles. The method allowed us to quantify the long- and short- term variabilities of these signals [16, 12, 11].

The behavior of cardiorespiratory and cardiovascular interactions in cardiomyopathy patients has been analyzed in previous works using the parameters of time- and frequency- domain or joint symbolic dynamics analysis [3, 8]. In this chapter, we propose new parameters with which to classify patients with ischemic and dilated cardiomyopathies, based on the left ventricular ejection fraction (LVEF). We analyzed the interactions between time series extracted from ECG, respiratory flow and blood pressure signals using the Poincaré plot method. Afterwards, these patients were classified based on their LVEF using the linear discriminant analysis and the support vector machines methods.

5.2 Signal description

A sample of 46 cardiomyopathy patients from the Heris dataset were used to explore the methodology described in this chapter. Information about the cardiomyopathy patient database is presented in [3, 8]. Additionally, 35 healthy subjects from the Healthy database were used as reference. These databases are presented in Chapter 3.

According to clinical diagnoses, the patients were classified based on their LVEF as high-risk (HR: LVEF $\leq 35\%$, 30 patients) or low-risk (LR: LVEF $> 35\%$, 16 patients) patients. Table 5.1 shows the clinical data.

Table 5.1. Clinical parameters (mean and standard deviation)

	LR	HR
Patients	16	30
Age [years]	62.25 ± 13.28	66.56 ± 9.20
Weight [Kg]	75.31 ± 15.10	80.83 ± 15.98
BMI [Kg/m^2]	27.25 ± 3.92	28.46 ± 4.89
NYHA	2.25 ± 0.57	2.03 ± 0.31
LVDD [mm]	56.43 ± 6.67	63.5 ± 6.03
AD [mm]	44.43 ± 5.04	47.43 ± 6.58
ProBNP	137.56 ± 906.09	2298.3 ± 3649.45
LVEF [%]	43.81 ± 8.79	29.23 ± 5.42

BMI: body mass index; **NYHA**: New York Heart Association functional classification; **LVDD**: left ventricular diastolic dimension; **AD**: auricular diameter; **ProBNP**: brain natriuretic peptide; **LVEF**: left ventricular ejection fraction.

All signals were visually inspected, the linear trend removed, and pre-processing tools were used to treat artifacts, spikes, and outliers. From the ECG signal, the cardiac inter-beat interval (BBI) time series were extracted automatically using a custom algorithm based on wavelet analysis. Systolic blood pressure (SBP) time series were obtained from the blood pressure signal as the difference between two consecutive absolute maximums. The time series of the breathing duration (TT) from the respiratory flow signal were extracted using an algorithm based on zero-crossing. Then all of the time series were visually inspected and corrected, if necessary. Figure 5.1 shows an excerpt of ECG, BP and FLW signals with the marks corresponding to the BBI, SBP, and TT time series, respectively.

To apply the Poincaré plot analysis, all of the time series were re-sampled to 1 Hz, scaled, and normalized (mean of zero and standard deviation of 1).These series, which describe the behavior of the physiological cycles of the ECG, vascular and respiratory systems, were used to analyze the interactions between these three systems.

5.3 Poincaré plot method

5.3.1 Mathematical description

The Poincaré plot analysis (PPA) quantifies self-similarity in a process, plotting the data into a higher dimensional state space [9]. To apply this method, given a time series $X(n) = x_1, x_2, x_3, \ldots, x_N$, the Poincaré plot is obtained by plotting $X(n)$ vs $X(n+1)$. This representation have the shape of an elongated scatter

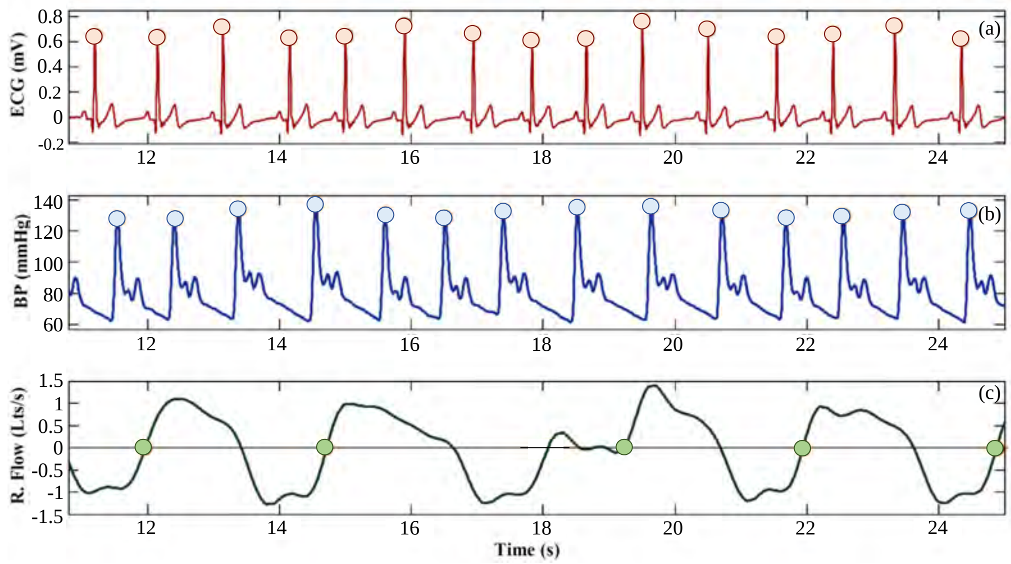

Figure 5.1. Excerpt of (a) ECG signal with BBI time series marks, (b) BP signal with SBP time series marks, and (c) respiratory flow signal with TT time series marks.

of plots through the identity line. The line is the reference used to analyze the scatter.

The short- and long- term variabilities were calculated by fitting an ellipse to the shape of the plot, and measuring the dispersion along the minor (SD1) and major (SD2) axes of the ellipse, around the identity line Id. The values of SD_1 and SD_2 represent the standard deviation of the data in the ellipse around the minor and major axes, respectively, and given by [17],

$$SD_1 = \frac{\sqrt{2}}{2} SD(x_n - x_{n+1}), \tag{5.1}$$

$$SD_2 = \sqrt{2SD(X_n)^2 - \frac{1}{2} SD(X_n - X_{n+1})^2}. \tag{5.2}$$

We considered additional indices such as the ratio between SD_1 and SD_2 and the difference between them (ΔSD). Figure 5.2 is a schematic representation of the Poincaré plot method with the identity line, and short- and long- term variability measures.

The information above the Id line represents an increase in the variability of the system, while the information below the line represents a decrease. This variability is calculated by measuring the distance between each point and the Id line, above (D_{UP_i}) and below (D_{D_i}).

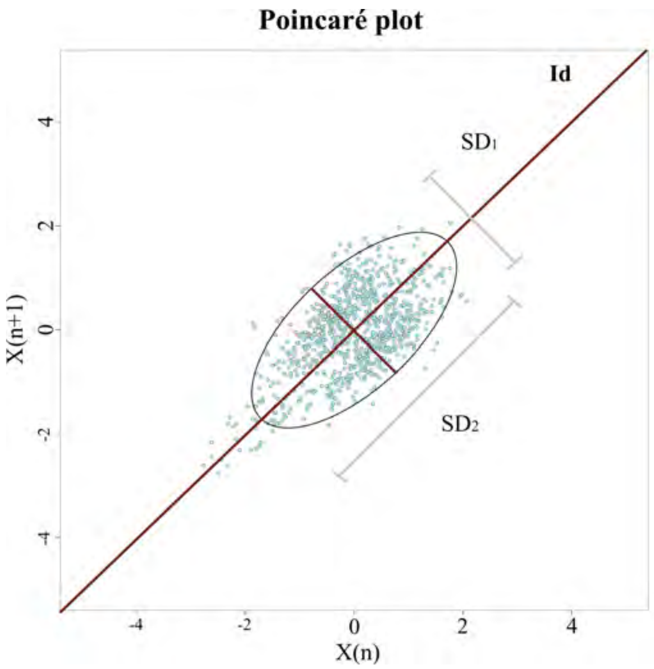

Figure 5.2. Schematic representation of a Poincaré plot characterized by the identity line and short- and long- term variabilities (SD_1, SD_2).

The SD_{UP} and SD_D indices represent the variability of the system around the identity line, with n_{UP} being the number of points above and n_D the number of points below, and defined as:

$$SD_{UP} = \frac{1}{n_{UP}} \sum_{i=1}^{n_{UP}} (D_{UP_i})^2, \tag{5.3}$$

$$SD_D = \frac{1}{n_D} \sum_{i=1}^{n_D} (D_{D_i})^2. \tag{5.4}$$

The acceleration and deceleration of the response of the system is characterized by the C_{UP} and C_D indices, given by:

$$C_{UP} = \frac{SD^2_{UP}}{SD^2_1}\ , \tag{5.5}$$

$$C_D = \frac{SD^2_D}{SD^2_1}\ . \tag{5.6}$$

Likewise, by replacing the Id with a regression line (Lr), the normalized deceleration (LrC_{UP}) and acceleration (LrC_D), based on this linear regression are obtained by:

$$LrC_{UP} = \frac{LrSD^2_{UP}}{LrSD^2_1}\ , \tag{5.7}$$

$$LrC_D = \frac{LrSD_D^2}{LrSD_1^2} \ . \tag{5.8}$$

The complex correlation index (CCI), which represents the time domain changes of the signals, was also calculated [12]. This parameter is based on the measurement of area A_i, defined by every three consecutive points, and a coefficient C_n for area normalization, calculated as $C_n = \pi \cdot SD_1 \cdot SD_2$ [16]. For a Poincaré plot made up of N points, CCI is defined by:

$$CCI = \frac{1}{C_n(N-2)} \sum_{i=1}^{N-2} ||A_i|| \ . \tag{5.9}$$

This method was used to analyze the interaction between different time series of the ECG (c), BP (b), and FLW (r) signals. In addition of these indices, another group were extracted to study the relations between the differences within each time series represented by Δc, Δb and Δr, respectively. Their interactions were analyzed considering the indices extracted from the following bivariate systems: cardio-vascular ($\Delta c \Delta b$), cardio-respiratory ($\Delta c \Delta r$) and vascular-respiratory ($\Delta b \Delta r$). In the end, a total of 81 indices were obtained. Table 5.2 summarizes all of the indices proposed.

Table 5.2. Indices for the analysis of the Poincaré plot

Indices	Description
xSD_1	Short-time standard deviation
xSD_2	Long-time standard deviation
$\frac{xSD_1}{SD_2}$	Short and long deviations ratio
$x\Delta SD$	Standard deviation difference
xC_{UP}	Normalized deceleration
xC_D	Normalized acceleration
$xLrC_{UP}$	Linear regression based normalized deceleration
$xLrC_D$	Linear regression based normalized acceleration
$xCCI$	Complex correlation index

x represents: c for BBI time series, b for SBP time series, and r for TT time series

A Kolmogorov-Smirnov test was used to determine indices with statistically significant differences between different groups (p-value < 0.05). Indices with a high correlation ($\rho \geq 0.7$) were excluded.

5.3.2 Classification and validation

We used the linear discriminant analysis and the support vector machines methods with different kernel functions to classify heart failure patients considering risk stratification based on LVEF. The leave-one-out cross-validation procedure was applied to validate the results. These classification results were presented in terms of accuracy (Acc), sensitivity (Sn), and specificity (Sp).

- Linear discriminant analysis

Linear discriminant analysis (LDA) is used to find a linear combination of predictors that characterize two or more classes. The method is based on maximizing the distance between variances of classes [5]. Given a set of parameters, the linear discrimination is defined as:

$$Y = \mu_0 + \mu_i \cdot x_i, \tag{5.10}$$

where μ_0 and μ_i are the independent term and independent parameters, respectively, and x_i is the discriminant function coefficient. The distances between groups are calculated using Mahalanobis distance method.

- Support vector machines

The support vector machines (SVM) method uses higher dimensional space data transformation to convert a complex classification problem into a simpler one that can be solved by a linear discriminant function, known as a hyperplane. Given a set of data vectors, $X = \{x_1, \ldots, x_L\}$, where $x_i \in \mathbb{R}^n$, and their corresponding labels $Y = \{y_1, \ldots, y_L\}$, where $y_i \in \{1, -1\}$, SVM function is defined by [8],

$$f(x) = wz + b = \sum_{i}^{L} \alpha_i y_i K(x_i y_i) + b, \tag{5.11}$$

where α_i and b define the efficiency of the classifier based on the optimal values, and K represents the kernel function used. From all the possible kernel types, we used the Gaussian, Laplacian and ANOVA kernels.

The Gaussian kernel is commonly used when the data is distributed radially, and is defined by:

$$K(x, y) = e^{-(\frac{||x-y||^2}{2\sigma^2})}, \tag{5.12}$$

being σ the penalty term.

The Laplacian kernel is similar to the Gaussian kernel but less influenced by the σ parameter, and is given by:

$$K(x, y) = e^{-(\frac{||x-y||}{2\sigma})}. \tag{5.13}$$

The ANOVA kernel is defined by:

$$K(x, y) = \sum_{k=1}^{n} e^{(-\sigma(x^k - y^k)^2)^d}, \tag{5.14}$$

where σ and d are the parameters used to optimize the kernel.

5.4 Results

We used the Poincaré plot method to classify heart failure patients in a sample of 46 cardiomyopathy patients (CMP) and 35 healthy subjects (CON). The patients were stratified based on left ventricular ejection fraction, and two groups were defined: low-risk patients (LR: $LVEF > 35\%$), and high-risk patients (HR: $LVEF < 35\%$). Two different comparisons were performed:

- High risk vs low risk patients (HR vs LR)
- Cardiomyopathy patients vs control subjects (CMP vs CON)

To illustrate these results, Figure 5.3 presents an example of the Poincaré plot outcomes for the BBI, SBP, and TT time series in the control subjects and in the low- and high- risk patients.

Our results showed that 11 indices presented statistically significant differences when comparing patients the LR and HR patient groups, A correlation test was then applied to rule out the most highly correlated ones. In the end, 5 indices were selected to compare the two groups (Table 5.3). The same process was applied to compare the CMP and CON groups. Our results are presented in Table 5.4, which lists 13 indices capable of differentiating between these two groups.

In the classification process, multiple combinations of different indices, kernels, and optimized parameters were iterated. The process identified cSD_2, cSD_1/SD_2, and $cCCI$ as the optimal choices to build the SVM and LDA models for the purpose of classifying LR vs HR patients. Likewise, cSD_2, cSD_1/SD_2, and $c\Delta SD$ were deemed the most suitable options for comparing control subjects and patients.

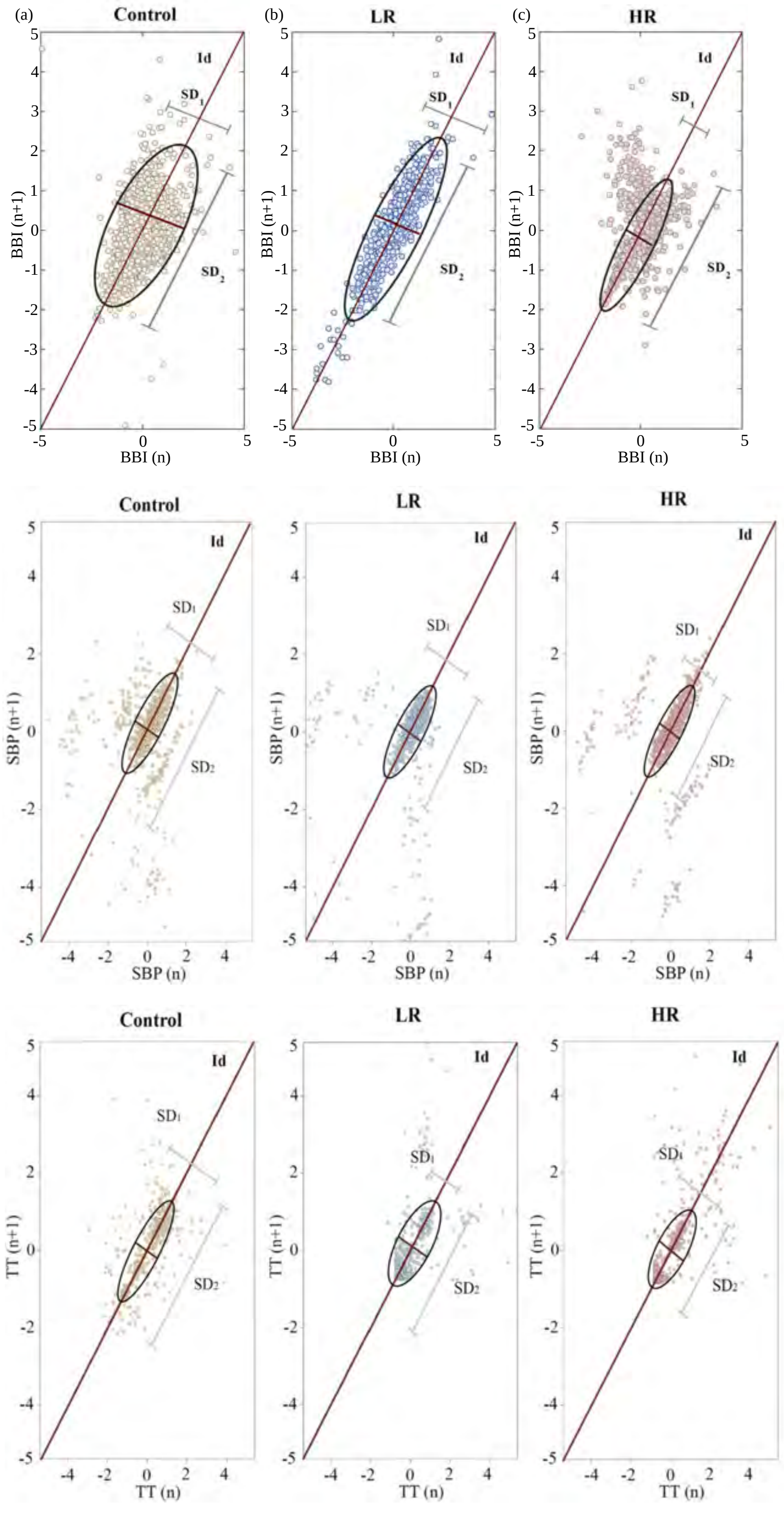

Figure 5.3. Poincaré plot results of cardiac activity (BBI) for (a) a subject from the control group, (b) a patient from the LR group, and (c) a patient from the HR group; vascular activity (SBP) of (d) a subject from the control group, (e) a patient from the LR group, and (f) a patient from the HR group; and respiratory activity (TT) of (g) a subject from the control group, (h) a patient from the LR group, and (i) a patient from the HR group.

All the models tested were optimized in terms of accuracy. For the LR vs HR comparison, the best accuracy (98.12%) was obtained with an SVM model using the ANOVA kernel. When comparing control vs patient groups, the best accuracy (97.01%) was obtained using an SVM model with a Laplacian kernel. The best results for SVM with each kernel tested and for the LDA models are presented in Table 5.5 for the LR vs HR comparison, and in Table 5.6 for CMP vs CON comparison.

5.5 Discussion and conclusions

Poincaré plot analysis is used to characterize the nonlinear dynamics of a system. With this study, we have characterized the nonlinear dynamics of the cardiovascular and cardiorespiratory systems. Our purpose was to obtain new indices for the risk stratification of heart failure patients using LVEF. The left ventricular ejection fraction is a proven independent predictor of cardiovascular mortality [2]. Patients with values lower than 35% are considered at high risk of cardiovascular death. In addition, low HRV has been shown to be independently predictive of increased mortality in post-myocardial infarction and chronic heart failure patients, but this information could be limited when analyzing low risk patients [19]. The statistical analysis of the morphology of the Poincaré plot us to classify these patients into different levels of risk for cardiovascular death, and distinguish between patients and control subjects.

The best differentiation between LR and HR patient groups was achieved by indices associated with cardiac short-term variability (cSD_1), the ratio between long-term and short-term cardiac variabilities (cSD_1/cSD_2), and the cardiac $cCCI$ index. We observed a higher mean value and less disperse cardiac short-term variability (cSD_1) in patients at high risk compared to patients at low risk. According to these results, patients with lower LVEF levels could have a more limited ability to regulate cardiac activity due to slower and less active electrical stimulation. The results of the cSD_1/cSD_2 analysis shown a similar

Table 5.3. Mean, standard deviation, and p-value of the best indices to classify LR vs HR patients

Index	LR (16)	HR (30)	p-value
$\boldsymbol{cSD_1}$	0.66 ± 0.32	0.81 ± 0.22	0.015
$\boldsymbol{cSD_1/SD_2}$	0.35 ± 0.18	0.43 ± 0.13	0.015
$\boldsymbol{cCCI}$	37083 ± 19032	27611 ± 20448	0.009
$\boldsymbol{\Delta c\Delta rSD_1/SD_2}$	0.41 ± 0.04	0.38 ± 0.02	0.003
$\boldsymbol{\Delta c\Delta rC_{UP}}$	0.89 ± 0.98	0.74 ± 1.83	0.041

Table 5.4. Mean, standard deviation, and p-value of the best indices to classify CON subjects vs CMP patients

Index	CON	CMP	p-value
$\boldsymbol{cSD_2}$	150.31 ± 66.52	109.62 ± 61.93	0.010
$\boldsymbol{cSD_1/SD_2}$	0.35 ± 0.07	0.40 ± 0.15	0.017
$\boldsymbol{c\Delta SD}$	0.02 ± 0.04	0.02 ± 0.06	0.015
$\boldsymbol{cCCI}$	22916 ± 8415	30906 ± 20273	0.0017
$\boldsymbol{cLrC_{UP}}$	0.47 ± 0.04	0.52 ± 0.13	0.0002
$\boldsymbol{cLrC_D}$	0.53 ± 0.04	0.48 ± 0.13	0.0002
$\boldsymbol{bSD_1/SD_2}$	0.37 ± 0.05	0.41 ± 0.09	0.0020
$\boldsymbol{bLrC_{UP}}$	0.52 ± 0.04	0.57 ± 0.11	0.0035
$\boldsymbol{bLrC_D}$	0.48 ± 0.04	0.43 ± 0.11	0.0004
$\boldsymbol{rSD_1}$	0.11 ± 0.03	0.21 ± 0.15	0.0004
$\boldsymbol{rLrC_{UP}}$	0.48 ± 0.04	0.50 ± 0.04	0.030
$\Delta\boldsymbol{rCCI}$	7.95 ± 5.02	4.24 ± 4.22	0.00003
$\Delta\boldsymbol{c}\Delta\boldsymbol{rCCI}$	16243 ± 5307	20056 ± 7579	0.019

Table 5.5. Accuracy (Acc), sensitivity (Sn) and specificity (Sp) obtained with LDA and SVM classifiers when comparing LR and HR groups

Method	C	σ	D	Acc	Sn	Sp
SVM - Gaussian	3	0.1	-	76.04	43.44	93.33
SVM - Laplace	3	0.1	-	97.87	93.89	100
SVM - ANOVA	0.3	100	1	98.12	94.57	100
LDA	-	-	-	71.5	25.41	96.08

behavior more extended and less disperse cardiac activity in patients with diminished LVEF.

The CCI index is sensitive to changes in autonomic regulation, especially in parasympathetic activity [12]. Our results suggest that patients at high risk of cardiovascular death have reduced parasympathetic activity compared to patients at lower risk. Impaired parasympathetic activity has been observed in heart failure patients in other studies [7]. Some authors have found that neurohumoral and inflammatory disturbances within the central nervous system stimulate a stronger sympathetic response while dampening parasympathetic outflow in heart failure patients, beginning a positive feedback loop that stimulates further adverse immune responses [21, 1].

Our results also show significant differences in the interactions between the

Table 5.6. Accuracy (Acc), sensitivity (Sn) and specificity (Sp) obtained with LDA and SVM classifiers when comparing CON and CMP groups

Method	C	σ	D	Acc	Sn	Sp
SVM - Gaussian	1	0.1	-	95.06	91.3	100
SVM - Laplace	1	0.3	-	97.01	94.72	100
SVM - ANOVA	0.3	0.3	1	92.7	91.3	94.54
LDA	-	-	-	92.25	91.01	93.89

cardiac and respiratory systems of heart failure patients in accordance with their left ventricular ejection fraction. These dissimilarities were observed in the cardiac and respiratory coupling, specifically in the ratio of short- and long- term variability $\Delta c\Delta rSD_1/SD_2$ and deceleration $\Delta c\Delta rC_{UP}$. These results suggest that low-risk patients have greater cardiorespiratory acceleration than patients at higher risk. We hypothesize that this effect might be caused by the physical impairment of the cardiac and respiratory muscles due to ageing, or a dysfunction of the autonomic mechanisms, or a combination of both. Hence, the cardiorespiratory system of patients at low risk would be able to adapt faster to environmental demands under stress conditions.

On the other hand, the cardiac response is less active (slower acceleration and faster deceleration) and more unstable ($cLrC_D$, $cLrC_{UP}$) in cardiomyopathy patients compared to the control group. This behavior is reflected in the vascular response ($bLrC_D$, $bLrC_{UP}$), in which changes in blood pressure occur at a slower pace in patients than in control subjects. Similarly, the respiratory response ($rLrC_{UP}$) decelerates faster and accelerates significantly slower ($\Delta rCCI$) in these patients. These patterns suggest that control subjects may be able to adapt to homeostatic imbalances faster and more stably.

In conclusion, the analysis of the cardiac, vascular, and respiratory systems through the Poincaré plot analysis has allowed us to assess indices that have proven useful in stratifying patients at cardiovascular risk, based on the left ventricular ejection fraction. Patients with lower levels of left ventricular ejection fraction also show lower heart rate variability. The cardiac, vascular and respiratory responses occur faster and more stably in control subjects, suggesting an impairment of the cardiovascular control mechanisms in chronic heart failure patients. All this suggests reduced parasympathetic activity in patients at high risk, and consequentially, the compensation of the sympathetic autonomic response. However, these results should be validated with a greater number of patients.

Chapter 5 bibliography

[1] F. Abboud, S. Harwani, and M. Chapleau. "Autonomic neural regulation of the immune system: implications for hypertension and cardiovascular disease." In: *Hypertension.* (2012).

[2] A. Aimo, J. Januzzi, G. Vergaro, C. Petersen, E. Pasanisi, S. Molinaro, C. Passino, and M. Emdin. "Left ventricular ejection fraction for risk stratification in chronic systolic heart failure." In: *International Journal of Cardiology* (2018).

[3] A. Arcentales, A. Voss, P. Caminal, A. Bayés-Genís, M. T. Domingo, and B. F. Giraldo. "Characterization of patients with different ventricular ejection fractions using blood pressure signal analysis". In: *Computing in Cardiology 2013*, pp. 795–798.

[4] A. L. Aro, O. Anttonen, J. T. Tikkanen, M. J. Junttila, T. Kerola, H. A. Rissanen, A. Reunanen, and H. V. Huikuri. "Intraventricular conduction delay in a standard 12-lead electrocardiogram as a predictor of mortality in the general population". In: *Circ Arrhythm Electrophysiol* 4.5 (2011), pp. 704–10. ISSN: 1941-3084 (Electronic) 1941-3084 (Linking). DOI: 10.1161/CIRCEP.111.963561. URL: https://www.ncbi.nlm.nih.gov/pubmed/21841194.

[5] Huberty C. "Applied Discriminant Analysis, Whiley Series in Probability and Mathematical Statistics." In: *Editorial John Wiley and Sons Inc* (1994).

[6] A. Drkosova, J. Kozumplík, and Z. Nováková. "Heart Rate Variability Expressed by Poincaré Plot in Metabolic Syndrome." In: *International Congress on Electrocardiology* (2014), pp. 221–224.

[7] J. Floras and P. Ponikowski. "The sympathetic/parasympathetic imbalance in heart failure with reduced ejection fraction." In: *European Heart Journal* (2015).

[8] B. F. Giraldo, J. Rodriguez, P. Caminal, A. Bayes-Genis, and A. Voss. "Cardiorespiratory and cardiovascular interactions in cardiomyopathy patients using joint symbolic dynamic analysis". In: *Conf Proc IEEE Eng Med Biol Soc* 2015 (2015), pp. 306–9. ISSN: 1557-170X (Print) 1557-170X (Linking). DOI: 10.1109/EMBC.2015.7318361. URL: https://www.ncbi.nlm.nih.gov/pubmed/26736261.

[9] Agnieszka Kitlas Golinska. "Poincaré Plots in Analysis of Selected Biomedical Signals." In: *Studies in logic, grammar and rhetoric* (2013), pp. 117–127.

[10] J. Holmes, S. Kubo, R. Cody, and P. Kligfield. "Arrhythmias in ischemic and nonischemic dilated cardiomyopathy: Prediction of mortality by ambulatory electrocardiography." In: *The american journal of cardiology* (1985).

[11] R. A. Hoshi, C. M. Pastre, L. C. M. Vanderlei, and M.F. Godoy. "Poincaré plots indexes of heart rate variability: relationship with other nonlinear variables." In: *Autonomic Neuroscience* (2009), pp. 271–274.

[12] C. Karmakar, A. Khandoker, A Voss, and M. Palaniswami. "Sensitivity of temporal heart rate variability in Poincaré plot to changes in parasympathetic nervous system activity." In: *Biomedical Engineering Online* (2011), pp. 10–17.

[13] RJ. Mentz, S. Broderick, LK. Shaw, M. Fiuzat, and CM. O'Connor. "Heart Failure With Preserved Ejection Fraction." In: *Journal of the American College of Cardiology.* 63 (2014).

[14] M. Nichols, N. Townsend, P. Scarborough, and M. Rayner. "Cardiovascular disease in Europe 2014: epidemiological update." In: *European Heart Journal* (2014), pp. 1–10.

[15] R. Panikkath, K. Reinier, A. Uy-Evanado, C. Teodorescu, J. Hattenhauer, R. Mariani, K. Gunson, J. Jui, and S. S. Chugh. "Prolonged Tpeak-to-tend interval on the resting ECG is associated with increased risk of sudden cardiac death". In: *Circ Arrhythm Electrophysiol* 4.4 (2011), pp. 441–7. ISSN: 1941-3084 (Electronic) 1941-3084 (Linking). DOI: 10.1161/CIRCEP.110.960658. URL: https://www.ncbi.nlm.nih.gov/pubmed/21593198.

[16] J. Piskorski and P. Guzik. "Geometry of the Poincaré plot of RR intervals and its asymmetry in healthy adults." In: *Physiological Measurement* (2007), pp. 287–300.

[17] J. Rodriguez, A. Voss, P. Caminal, A. Bayes-Genis, and B. F. Giraldo. "Characterization and classification of patients with different levels of cardiac death risk by using Poincare plot analysis". In: *Conf Proc IEEE Eng Med Biol Soc* 2017 (2017), pp. 1332–1335. ISSN: 1557-170X (Print) 1557-170X (Linking). DOI: 10.1109/EMBC.2017.8037078. URL: https://www.ncbi.nlm.nih.gov/pubmed/29060122.

[18] P. J. Schwartz, M. T. La Rovere, and E. Vanoli. "Autonomic nervous system and sudden cardiac death. Experimental basis and clinical observations for post-myocardial infarction risk stratification". In: *Circulation* 85.1 Suppl (1992), pp. I77–91. ISSN: 0009-7322 (Print) 0009-7322 (Linking). URL: https://www.ncbi.nlm.nih.gov/pubmed/1728509.

[19] Francesco Sessa, Valenzano Anna, Giovanni Messina, Giuseppe Cibelli, Vincenzo Monda, Gabriella Marsala, Maria Ruberto, Antonio Biondi, Orazio Cascio, Giuseppe Bertozzi, Daniela Pisanelli, Francesca Maglietta, Antonietta Messina, Maria P Mollica, and Monica Salerno. "Heart rate variability as predictive factor for sudden cardiac death". In: *Aging* 10.2 (2018), pp. 166–177. ISSN: 1945-4589. DOI: `10.18632/aging.101386`. URL: `https://europepmc.org/articles/PMC5842851`.

[20] A. Stelken, L Younis, S. Jennison, D Miller, L Miller, L Shaw, D. Kargl, and B. Chaitman. "Prognostic value of cardiopulmonary exercise testing using percent achieved of predicted peak oxygen uptake for patients with ischemic and dilated cardiomyopathy." In: *Journal of the American College of Cardiology* (1995).

[21] I. Zucker. "Novel mechanisms of sympathetic regulation in chronic heart failure." In: *Hypertension.* (2006).

6

Cardiovascular coupling analysis applied to cardiomyopathy patients

6.1 Introduction

According to the 2015 update of the heart disease and stroke statistics of the American Heart Association [42], 325,000 cases of sudden cardiac death (SCD) occurred in the United States in that year, and it is the cause of 15–20% of mortality worldwide [2]. The implantable cardioverter defibrillator (ICD) is commonly recommended in patients that are at high risk of suffering SCD, and the risk of SCD is halved when one is implanted, although the presence or absence of an ICD implant has no significant influence over the rate of death itself [31].

The implantation of an ICD is recommended in patients with an ejection fraction (EF) lower than or equal to 35%. Today, it is difficult to stratify SCD risk in patients with EFs above the risk threshold, who account for at least 70% of the patients who will suffer SCD [10]. In addition, the effectiveness of ICD therapy is time dependent, making a reduction in the duration of the treatment desirable for the purpose of optimizing costs, among other reasons. Therefore, the need persists for additional predictors to identify patients with idiopathic dilated cardiomyopathy (IDC) who have an increased risk of SCD and who have benefited from ICD implantation [15, 8].

Estimating cardiovascular SCD risk remains a challenge in clinical practice. Studies related to linear and non-linear time series analyses have been conducted to quantify the cardiovascular system response. Linear methods can describe the most general behavior of the systems directly related to the response between their time series. However, these linear approaches may not be sufficient to quantify non-linear structures and the complexity of physiological systems. Therefore, approaches based on non-linear methods may be better suited to analyzing the complex interactions between systems. They also make it possible to quantify direct interrelationships, such as the non-linear influence of blood pressure on heart rate. These coupling approaches are used to quantify direct and indirect relationships, as well as causal and non-causal relationships between time series, providing deeper insights into alterations of the cardiovascular system and leading to improved knowledge of the interacting regulatory mechanisms under different physiological and pathophysiological conditions. These approaches represent promising tools for generating multivariate information flows [55].

Several studies are focused on the analysis of these interactions through the application of bivariate coupling methods. For example, the directional cardiovascular interactions in young healthy subjects were assessed by means of bivariate and multivariate coupling measures, and it was found that bivariate measures better quantify the information transferred between indices, while trivariate measures better reflect the existence and delay of directed interactions [28]. Information decomposition measurements for variance or entropy were explored to assess information dynamics in cardiovascular networks through the analysis of the heart period, systolic blood pressure, and respiratory activity [18]. The authors concluded that these measures of information transfer and information modification are better assessed through entropy-based and variance-based methods. Another work explored polysomnographic recordings and finger blood pressure measurements in healthy subjects in order to investigate the differences between the wake-sleep states in the heart period and systolic blood pressure coupling [62]. They found that at low frequencies there are differences between these states in human subjects. In addition, the complexity and causality of the interactions of cardiovascular variability series were assessed through linear model-based and non-linear model free techniques, and it was deduced that model free methods provide additional insights compared to the simpler linear model-based approaches [48].

The behavior of cardiovascular coupling differs based on physiological conditions. Thus, we hypothesize that the relationships between the cardiac and vascular systems will differ between IDC patients at a high and low risk of SCD. Therefore, the aim of this study was to analyze the suitability of cardiovascular couplings for risk stratification in these patients. We propose to characterizing the interactions through features extracted from ECG and blood pressure signals to better describe the complex dynamics of these interactions and identify new indices of cardiovascular risk.

6.2 Signal description

We studied 91 idiopathic dilated cardiomyopathy (IDC) patients (21 female, 70 male) from the ART database to evaluate risk predictors of sudden cardiac death (SCD). In addition, 49 healthy subjects (30 male, 19 female; aged 46 ± 14 years) were used as a control group (CON). These databases are presented in Chapter 3.

After a median follow-up period of 28 months (range: 17–38 months), the patients were classified into two groups, according to their SCD risk. The group of patients that remained in stable physical condition were considered at low risk for cardiovascular sudden death (IDC_{LR}). The remaining patients, who either died of SCD or needed resuscitation because of a life-threatening tachyarrhythmia, were categorized as at high risk for cardiac sudden death (IDC_{HR}). None of these patients died from a non-cardiac disease. Table 6.1 presents the baseline clinical information of the IDC patients, in terms of median and interquartile range.

Table 6.1. Clinical parameters (median and interquartile range).

	IDC_{LR} N = 77 (59 ♂, 18 ♀)	IDC_{HR} N = 14 (11 ♂, 3 ♀)	**p-value**
Follow-up [months]	27 [17 ; 37]	30 [21; 38]	n.s.
Age [years]	55 [50 ; 60]	56 [50 ; 63]	n.s.
LVEF [%])	29 [27 ; 37]	35 [27 ; 46]	n.s.
LVEDD [mm]	69 [61 ; 79]	61 [58 ; 68]	n.s.
LVESD [mm]	60 [53 ; 69]	49 [44 ; 56]	0.0028
NYHA	3 [2 ; 4]	2 [2 ; 3]	0.0024

IDC_{LR} and IDC_{HR}: low- and high- risk patient groups with dilated cardiomyopathy, respectively; N, number of patients within the groups (♂= Male; ♀= Female); LVEF, left ventricular ejection fraction; LVEDD, left ventricular end-diastolic diameter; LVESD, left ventricular end-systolic diameter; NYHA, New York heart association functional classification index.

To characterize the autonomic regulation of the cardiovascular systems, the following time series were extracted using algorithms based on zero crossings and different thresholds:

- Time series related to heart rate, such as beat-to-beat intervals (BBI, ms)

- Time series related to maximum successive end-systolic blood pressure amplitude (SBP, mmHg)
- Time series related to minimum successive end-diastolic blood pressure amplitude (DBP, mmHg)

6.3 Methods

The following methods were employed to quantify the coupling between the cardiac and vascular systems: high resolution joint symbolic dynamics (HRSJD), segmented Poincaré plot analysis (SPPA), normalized short-time partial directed coherence (NSTPDC), and the dual sequence method (DSM) [50].

6.3.1 High resolution joint symbolic dynamics

The joint symbolic dynamics (JSD) method is based on the analysis of dynamic processes by means of symbols [5]. Considering BBI, SBP, and DBP time series, X is defined as a bivariate sample vector that contains two out of the three time series for all the possible combinations (BBI-SBP, BBI-DBP, and SBP-DBP), expressed as,

$$\left.\begin{aligned} \boldsymbol{X^{BBI\_SBP}} &= [x_n^{BBI}, x_n^{SBP}]^T \\ \boldsymbol{X^{BBI\_DBP}} &= [x_n^{BBI}, x_n^{DBP}]^T \\ \boldsymbol{X^{SBP\_DBP}} &= [x_n^{SBP}, x_n^{DBP}]^T \end{aligned}\right\} \quad n = 0, 1\ , \ldots, N \quad \text{with} \quad x \in \mathbb{R}, \tag{6.1}$$

being N the total number of samples.

In JSD, the increments between two successive values of the time series are coded as "1" and the decrements and equilibriums are coded as "0". These increments and decrements are considered in relation to a threshold l. The vector X can be transformed into the symbolic vector S, with the threshold l equal to 0, using the rules given by [5, 24]:

$$\left.\begin{aligned} \boldsymbol{S^{BBI\_SBP}} &= [S_n^{BBI}, S_n^{SBP}]^T \\ \boldsymbol{S^{BBI\_DBP}} &= [S_n^{BBI}, S_n^{DBP}]^T \\ \boldsymbol{S^{SBP\_DBP}} &= [S_n^{SBP}, S_n^{DBP}]^T \end{aligned}\right\} \quad n = 0, 1\ ,\ \ldots\ , N,\ \text{with}\ S \in 0, 1$$

$$S_n^{BBI} = \begin{cases} 0 : (x_{n+1}^{BBI} - x_n^{BBI}) \leq 0 \\ 1 : (x_{n+1}^{BBI} - x_n^{BBI}) > 0 \end{cases}$$

$$S_n^{SBP} = \begin{cases} 0 : (x_{n+1}^{SBP} - x_n^{SBP}) \leq 0 \\ 1 : (x_{n+1}^{SBP} - x_n^{SBP}) > 0 \end{cases} \tag{6.2}$$

$$S_n^{DBP} = \begin{cases} 0 : (x_{n+1}^{DBP} - x_n^{DBP}) \leq 0 \\ 1 : (x_{n+1}^{DBP} - x_n^{DBP}) > 0 \end{cases}$$

A sequence of symbols is considered a word of length k. These words are arranged in a vector matrix W. For this study, we defined words with $k = 3$ (S_n, S_{n+1}, S_{n+2}), and an 8×8 vector matrix was derived, taking values from $(000, 000)^T$ to $(111, 111)^T$.

To obtain JSD indices that are more robust against noise, fluctuations and artifacts, the comparison threshold should be something other than 0. There are several advantages for choosing a non-zero threshold. For instance, a state will be generated that will help to distinguish between small and large changes in the system's variability response. It is also possible to differentiate between equal and decreased values because both states have now different code. Also, the number of word types included in the W matrix is not increased by words with the code "0", and the distribution is based on each code [59, 58]. This method is called high-resolution joint symbolic dynamics (HRJSD), and is implemented using three symbols for JSD, after setting a threshold l. The increment states are coded as "2" the decrements are coded as "1", and the equilibrium states are coded as "0". With this technique, the transformation from X to S varies, as is given by:

$$S_n^{BBI} = \begin{cases} 0 : & (x_{n+1}^{BBI} - x_n^{BBI}) < -l^{BBI} \\ 1 : -l^{BBI} \leq & (x_{n+1}^{BBI} - x_n^{BBI}) \leq l^{BBI} \\ 2 : & (x_{n+1}^{BBI} - x_n^{BBI}) > l^{BBI} \end{cases}$$

$$S_n^{SBP} = \begin{cases} 0 : & (x_{n+1}^{SBP} - x_n^{SBP}) < -l^{SBP} \\ 1 : -l^{SBP} \leq & (x_{n+1}^{SBP} - x_n^{SBP}) \leq l^{SBP} \\ 2 : & (x_{n+1}^{SBP} - x_n^{SBP}) > l^{SBP} \end{cases} \tag{6.3}$$

$$S_n^{DBP} = \begin{cases} 0 : & (x_{n+1}^{DBP} - x_n^{DBP}) < -l^{DBP} \\ 1 : -l^{DBP} \leq & (x_{n+1}^{DBP} - x_n^{DBP}) \leq l^{DBP} \\ 2 : & (x_{n+1}^{DBP} - x_n^{DBP}) > l^{DBP} \end{cases}$$

The new space comprised combinations of 27 different possible types of words (from 000 to 222) and a total of 729 indices. All the word types were grouped into eight pattern families, transforming the vector matrix W into a vector matrix family (W_f). These indices were analyzed by their occurrence probabilities and grouped according to their family description, as shown in Table 6.2. The pattern families represent different interactions between the branches of the autonomic regulation system, leading to the definition of indices that determine occurrence probabilities [58]. In addition, the Shannon entropy was calculated for all the proposed families in order to assess the complexity of the coupling [51].

Table 6.2. Description of pattern families explored in the HRJSD method.

Family	Description
E0	No variation of 3 successive “0” symbols (“000”)
E1	No variation of 3 successive “1” symbols (“111”)
E2	No variation of 3 successive “2” symbols (“222”)
LU1	Low increasing behavior (“122”, “022”, “112”,“221”,“220”,“211”,“121”,“212”)
LD1	Low decreasing behavior (“011”, “001”, “002”,“110”,“100”,“200”,“010”,“101”)
LA1	Fast alternant behavior (“020”,“202”)
P	Alternant peak-like behavior (“120”,“201”,“210”)
V	Alternant valley-like behavior (“021”,“102”,“012”)

Thresholds for cardiac and vascular activity were defined to analyse cardiovascular coupling. For the BBI and blood pressure times series, 5 ms and 1 mmHg thresholds were applied, respectively, as these values were successfully applied in a previous work [59]. The threshold level using spontaneous baroreflex sensitivity, in contrast to other thresholds, is the most suitable for highlighting different specific cardiovascular coupling patterns.

6.3.2 Segmented Poincaré plot analysis

A mathematical description of the Poincaré plot analysis (PPA) is presented in Chapter 5 (Section 5.3). We used this method to obtain the indices related to short- (SD1) and long- (SD2) term variabilities, which represent the dispersion along the minor (SD1) and major (SD2) axes, fitting an ellipse around an elongated scatter on the plots.

Although PPA is a non-linear characterization method, its indices (SD1 and SD2) can be correlated with the linear behavior of the system, which makes it a sub-optimal approach to exploring information about the non-linear part of the process [60, 67].

A segmented Poincaré plot analysis (SPPA) is an enhanced pseudo-phase space quantification method that yields indices that also represent the non-linear information of the system. In SPPA, the SD_1 and SD_2 indices are calculated similarly to PPA, and then the scatter points are rotated α degrees around the main focus of the plot, as defined by:

$$\begin{bmatrix} X'_n \\ X'_{n+1} \\ z' \end{bmatrix} = \begin{bmatrix} \overline{X'_n} \\ \overline{X'_{n+1}} \\ z \end{bmatrix} + \left(\begin{bmatrix} cos\alpha & -sin\alpha & 0 \\ sin\alpha & cos\alpha & 0 \\ 0 & 0 & 1 \end{bmatrix} \times \begin{bmatrix} X'_n - \overline{X'_n} \\ X'_{n+1} - \overline{X'_{n+1}} \\ z \end{bmatrix} \right). \tag{6.4}$$

The x and y axis correspond to $X(t)$ and $X(t+1)$ values, $\overline{X_n}$ and $\overline{X_{n+1}}$ are the mean values of the original and shifted X time series, respectively, and z is the axis of the rotation [68, 67, 60]. In this case, we define $\alpha = 45$ degrees in order to simplify the estimating procedure of the SD_1/SD_2 adapted probability. A 12×12 rectangular grid is drawn for the plot. The size of the rectangles (height, width) is adapted based on the SD_1 (row) and SD_2 (column) values.

Afterwards, for each rectangle in position (i, j) the single probability (ρ_{ij}) is calculated considering the number of points contained by the total number of points in the series. Then, the probabilities of each row (ρ_{ri}) and column (ρ_{cj}) are calculated as the sum of their single probabilities, as shown below:

$$\rho_{ri} = \sum_{j=1}^{12} \rho_{ij}$$

$$\rho_{cj} = \sum_{i=1}^{12} \rho_{ij}. \tag{6.5}$$

6.3.3 Normalized short-time partial directed coherence

The directed coherence method (DC) describes how and if two complex physiological signals are functionally connected [17]. The DC method studies the relative structural relationships between the systems by analyzing their interactions into feedback and feedforward behaviors. The partial directed coherence method (PDC) determines the either, direct or indirect causality between the systems analyzed. The PDC is limited to working on stationary signals and is unable to yield information about the properties of partial correlative short-time interaction [3].

The normalized short-time partial directed coherence (NSTPDC) method is able to manage non-stationary signals by evaluating their dynamic coupling changes, and detecting their level and directions in multivariate and complex dynamic systems [1, 56]. NSTPDC is based on an m-dimensional multichannel auto-regressive model (MAR) process with model order p to determine Granger causality in the frequency domain. To select the optimal model order p_{opt} of the $AR(p)$ model and to estimate its coefficients, the stepwise least squares algorithm [44] and the Schwarz's Bayesian criterion are applied [54]. NSTPDC is based on the time-variant partial directed coherence approach (tvPDC), which provides information about the partial correlative short-time interaction properties of non-stationary signals ($\pi_{xy}(f,n)$), where f is the frequency associated with the behavior of the system in the frequency domain, and n the number of windows [40].

To quantify the coupling direction between two time series, X and Y (e.g., BBI and SBP: with x_{BBI} and y_{SBP}) with the covariate z (e.g., DBP with z_{DBP}), a coupling factor (CF) was introduced. CF is defined as the quotient between the mean value of x coupled with y ($\pi_{xy}(f,n)$) and the mean value of y coupled with x ($\pi_{yx}(f,n)$), given by:

$$CF = \frac{\frac{1}{n}\sum \pi_{x_{BBI}y_{SBP}}(f,n)}{\frac{1}{n}\sum \pi_{y_{SBP}x_{BBI}}(f,n)}, \quad \overline{a} = \frac{1}{n}\sum \pi_{x_{BBI}y_{SBP}}(f,n),$$

$$\overline{b} = \frac{1}{n}\sum \pi_{y_{SBP}x_{BBI}}(f,n). \tag{6.6}$$

A normalized factor (NF) was defined as NF $= \{-2,-1,\ 0,1,2\}$. The NF represents the coupling directions, and the causal connections between the time series under study (x_{BBI} and y_{SBP}) according to f. Therefore, the CF was normalized in function of NF values to analyze the behavior of the couplings according to $\overline{a}$ and $\overline{b}$, based on:

$$NF = \begin{cases} 2, & if\ (max = \overline{a}\ \&\ \frac{\overline{a}}{\overline{b}} > 5) \\ 1, & if\ (max = \overline{a}\ \&\ 2 < \frac{\overline{a}}{\overline{b}} \leq 5) \\ 0, & if\ (max = \overline{a}\ \&\ 0 < \frac{\overline{a}}{\overline{b}} \leq 2) \end{cases}$$

$$NF = \begin{cases} -2, & if\ (max = \overline{b}\ \&\ \frac{\overline{b}}{\overline{a}} > 5) \\ -1, & if\ (max = \overline{b}\ \&\ 2 < \frac{\overline{b}}{\overline{a}} \leq 5) \\ 0, & if\ (max = \overline{b}\ \&\ 0 < \frac{\overline{b}}{\overline{a}} \leq 2) \end{cases}. \tag{6.7}$$

Strong unidirectional coupling is indicated if NF is -2 or 2 (where -2 denotes y_{SBP} as the driver); bidirectional coupling if NF = -1 or 1 (-1 denotes y_{SBP} as the driver); an equal influence in both directions indicates no coupling, if NF = 0 in relation to the coupling strengths.

To determine the coupling strength between two time series, e.g., x_{BBI} and y_{SBP}, with covariate (z_{DBP}), the areas ($A_{BBI\to SBP(DBP)}$, $A_{SBP\to BBI(DBP)}$, [a.u.]) generated in space by CF were estimated, in each window within the frequency band $f = 0-2$ Hz, and averaged. $A_{BBI\to SBP(DBP)}$ and $A_{SBP\to BBI(DBP)}$ were defined between 0 to 1, where 1 indicated that all causal influence originating from time series X was directed toward (arrows: $\rightarrow$) time series Y. If both area indices have equal values and are greater than zero, an equal influence in both directions is present. On the other hand, if both area indices have equal values and are equal to zero, there is no coupling.

In order to take advantage of the stationarity behavior and scale-invariance for NSTPDC analysis, a normalization (zero mean and unit variance) of the time series BBI, SBP, and DBP was performed [56], using

$$x_{norm}(i) = \frac{x(i) - \overline{x}}{std(x)} \quad , \tag{6.8}$$

being x_i each of the time series, and $\overline{x}$ and $std(x)$ the mean value and standard deviation of these series, respectively.

6.3.4 Dual sequence method

A widely used method for the study of spontaneous baroreflex sensitivity (BRS) is the sequence method [7]. Using this method, BRS is obtained by scanning the SBP and BBI time series for sequences of three or more successive heart beats, in which a progressive increase (or decrease) in SBP is followed (with a one-beat delay). In our case, the dual sequence method (DSM) was applied to improve the analysis of baroreflex sensitivity [35, 34]. A fluctuation was defined as variations greater than 1 mmHg (increasing or decreasing) in SBP, and greater than 5 ms in BBI values. The slopes of the regression lines between the SBP and BBI sequences were taken as an index for local BRS [ms/mmHg], and calculated in each recording, and then the highest slope was selected. DSM is based on standard sequence methods, and the enhancement lies in the analysis of two different kinds of BBI response: bradycardic (an increase in SBP causes an increase in BBI), and tachycardic fluctuations (a decrease in SBP causes a decrease in BBI), whereas only the bradycardic fluctuations represented the classical spontaneous baroreflex sensitivity (*bslope*). Analyzing the tachycardic fluctuations (*tslope*) provided additional information about autonomic cardiovascular regulation [45].

6.3.5 Heart rate and blood pressure variability standard indices

Heart rate variability (HRV) and blood pressure variability (BPV) were quantified using the standard indices from the time and frequency domain. The following indices were calculated from the beat-to-beart intervals (BBI), systolic blood pressure (SBP), and diastolic blood pressure (DBP) time series. These time series were analyzed considering the normal-to-normal intervals (NN), defined as the intervals between two consecutive events after artifacts are removed:

- The mean of BBI, SBP, and DBP time series (BBI_meanNN, SBP_meanNN and DBP_meanNN, respectively).
- The standard deviation of BBI, SBP, and DBP time series (BBI_sdNN, SBP_sdNN, and DBP_sdNN, respectively).
- The proportion derived by dividing NN_{50} (number of pairs of adjacent NN intervals differing by more than 50 ms in the entire recording) by the total number of NN intervals (BBI_PNN_{50}, SBP_PNN_{50}, and DBP_PNN_{50}. respectively).
- The square root of the mean squared differences of BBI, SBP, and DBP time series (BBI_rmssd, SBP_rmssd, and DBP_rmssd, respectively).
- The power of the low frequency (LF) components (0.04-0.15 Hz) of BBI, SBP, and DBP time series (BBI_LF, SBP_LF, and DBP_LF, respectively).
- The power of the high frequency (HF) components (0.15-0.4 Hz) of BBI, SBP, and DBP time series (BBI_HF, SBP_HF, and DBP_HF, respectively).
- The ratio between the low and high frequency power components of BBI, SBP, and DBP time series (BBI_LF/HF, SBP_LF/HF, and DBP_LF/HF, respectively.)

6.3.6 Feature extraction

A total of 621 indices were extracted to analyze the coupling between the cardiac and vascular systems, using ECG and blood pressure signals. The "cd" label represents the cardiac and diastolic coupling, the "cs" label indicates the cardiac and systolic coupling, and the "ds" label the diastolic and systolic coupling. The distribution of these indices was as follows: 264 indices from the HRJSD, 216 from the SPPA, 97 from the JSD, 12 from the PPA, 9 from the NSTPDC, 21 from the standard HRV and BPV indices, and 2 from the DSM. Summary descriptions of the indices are shown in Table 6.3.

6.3.7 Statistical analysis

In order to reduce dataset dimensionality, a Mann Whitney non-parametric statistical test was used to determine the statistical significance of the indices obtained in the characterization process. The results were analyzed for different levels of significance, including the Bonferroni criterion, considering:

n.s	$\rho > 0.01$
*	$\rho \leq 0.01$ significant
**	$\rho \leq 0.001$ highly significant
***	$\rho \leq 0.0000167$ Bonferroni criterion
	n = 621 indices

Table 6.3. Coupling indices extracted from high-resolution joint symbolic dynamics (HRJSD), segmented Poincaré plot analysis (SPPA), joint symbolic dynamics (JSD), Poincaré plot analysis (PPA), and normalized short-time partial directed coherence (NSTPDC).

Index	**Description**
HRJSD$_{xy}$_F$_x$-F$_y$	Probability of occurrence of F$_x$ and F$_y$ word families from the x-y coupling
HRJSDSh$_{xy}$	Shannon entropy of all the word families from the x-y coupling
HRJSD$_{xy}$_F$_x$	Summation of the occurrences of F$_x$ on all the families from the x-y coupling
SPPA$_{xy}$_row_n-m	Probability of occurrence of row n-m from the x-y coupling
SPPA$_{xy}$_column_n-m	Probability of occurrence of column n-m from the x-y coupling
JSD$_{xy}$-n	Probability of occurrence of the word n from the x-y coupling
PPA$_{xy}$SD1	Short-time standard deviation from the x-y coupling
PPA$_{xy}$SD2	Long-time standard deviation from the x-y coupling
PPA$_{xy}$SD1/SD2	Short and long deviation ratio from the x-y coupling
NSTPDC$_{xy}$NF	Normalized coupling factor from the x-y coupling
NSTPDC$_{xy}$Ax $\rightarrow$ y	Coupling strength of x-y from x to y
NSTPDC$_{xy}$Ay $\rightarrow$ x	Coupling strength of x-y from y to x

x and y represent the couplings cd, cs, and ds; F represents the word families: E0, E1, E2, LU1, LD1, LA1, P and V; n and m represent the number of row and column in the PPA based indices, respectively.

Additionally, a correlation analysis was performed on the statistically significant indices. The ones with high correlation ($p \geq 0.7$) and relative lower significance were discarded.

The leave-one-out cross-validation procedure was used to validate the results. The classification results are presented in terms of accuracy (Acc), sensitivity (Sn), specificity (Sp), and area under the curve (AUC).

6.3.8 Classification

We used the SVM method to classifying patients by their SCD risk. Several models were built based on the most significant indices found, and a novel cascade model was developed.

- Support vector machines classification

A mathematical description of the support vector machines classification method (SVM) is presented in Chapter 5 (Section 5.3.2). This method allowed us to solve a complex non-linear problem in a higher dimensional space using linear classifiers. The classification problem was solved by maximizing the margin while minimizing the training error. Using the Lagrange multiplier method, a dual formulation can be obtained by [11]:

$$minP(w,b) = \frac{1}{2}||w_m z||^2 + C\sum_i K_i[y_i f(x_i)] \ , \tag{6.9}$$

where w is the normal vector that defines the hyperplane, b defines the efficiency of the classifier for the optimal values, K_i relates to the kernel function, and C is a penalty parameter. Besides the scale of C having no direct meaning, as its value increases, the penalty assigned to errors becomes stronger, narrowing the decision boundary [6]. For this study, we considered the Gaussian, Laplacian and ANOVA kernels.

Each feature was scaled and normalized (zero mean and unit variance) in order to avoid scaling biases. For each iteration of features, the model was built by optimizing the value of C for each of the kernels considered. This consisted by iterating different values of the kernel optimization indices, σ and d. The indices with statistical differences and low correlations were used in pairs to build several SVM models. The accuracy of each model was then calculated and the one with the highest value was chosen as optimal for each type of kernel.

- Cascade model

In order to consider the typical clinical case in which the original condition of the subject is unknown, a cascade model was developed to classify this new subject using the label SDC risk and comparing the IDC vs CON and IDC_{HR} vs IDC_{LR} models (Figure 6.1). The general aim of this model was to classify the subject as either CON, LR or HR without any prior labeling. The first step was to decide if a subject was an IDC patient or not using the IDC vs CON model. Afterwards, those classified as IDC patients were analyzed based on the LR vs HR model to predict their risk level.

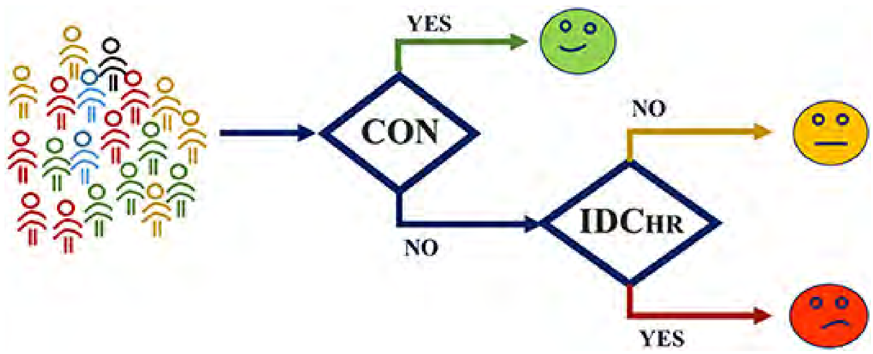

Figure 6.1. Cascade model structure. The subject is evaluated in the IDC vs CON model, and resulting IDC patient's level of risk is evaluated by means of the LR vs HR model.

6.4 Results

The calculated indices were used to analyze the cardiovascular coupling in 91 idiopathic dilated cardiomyopathy patients (IDC) and 49 healthy subjects (CON). Four different comparisons were performed:

- The high-risk IDC patients (IDC_{HR}) vs the low-risk IDC patients (IDC_{LR})
- The IDC patients vs the CON subjects
- The high-risk IDC patients (IDC_{HR}) vs the CON subjects
- The low-risk IDC patients (IDC_{LR}) vs the CON subjects

- IDC_{LR} patients vs IDC_{HR} patients compared with CON subjects

We obtained statistically significant differences in the symbolic dynamic analysis for both the cardio-diastolic (BBI–DBP) and diastolic-systolic (DBP-SBP) couplings. Figures 6.2 and 6.3 present an example of the three-dimensional plots of the word distribution density matrix of the couplings using the JSD and HRJSD methods from IDC_{LR} (Figures 6.2a, 6.2c, 6.3a and 6.3c) and IDC_{HR} (Figures 6.2b, 6.2d, 6.3b and 6.3d) patients, respectively.

Figure 6.4 shows an example of the Poincaré plot method applied to a patient for each analyzed group considering the systogram from a) a CON subject, b) an IDC_{LR} patient, and c) an IDC_{HR} patient. Figure 6.5 represents the averaged NSTPDC applied to the BBI, SBP, and DBP time series couplings, for a) the CON, b) IDC_{LR}, and c) IDC_{HR} groups. Figure 6.6 presents the relationships between all three analyzed groups, where the arrows represent the coupling direction and the arrow thickness indicates the coupling strength. The level of statistical significance is also represented ($p \leq 0.01$).

In the comparison of the IDC_{LR} and IDC_{HR} groups, 96 indices presented statistically significant differences, corresponding to: 76 indices from the HRJSD, 12 from the SPPA, and 7 from the NSTPDC. After the correlation analysis, a total of 36 statistically significant indices were chosen for the classification process. Some of the most relevant indices, expressed in mean value and a 95% confidence interval, are shown in Table 6.4.

- IDC patients vs CON subjects

When comparing IDC patients vs CON subjects, 261 indices presented statistically significant differences between the two groups: 169 from the HRJSD, 76 from the SPPA, and 13 from NSTPDC. A total of 82 indices remained after discarding the highly correlated indices. Table 6.5 shows the most relevant of these.

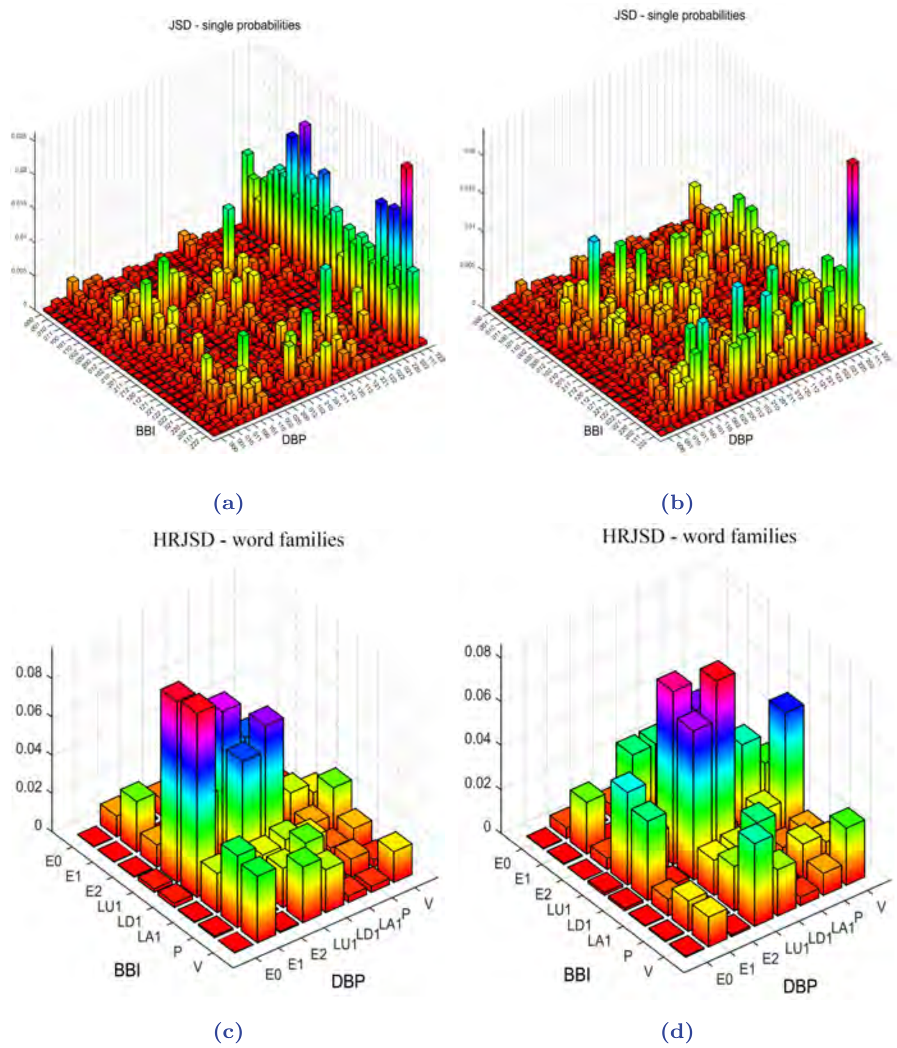

Figure 6.2. Three-dimensional plots of the word distribution density matrix using the JSD and HRJSD methods (single word probabilities, word families) from an **(a,c)** IDC_{LR} and **(b,d)** IDC_{HR} patient, respectively, for cardio-diastolic coupling.

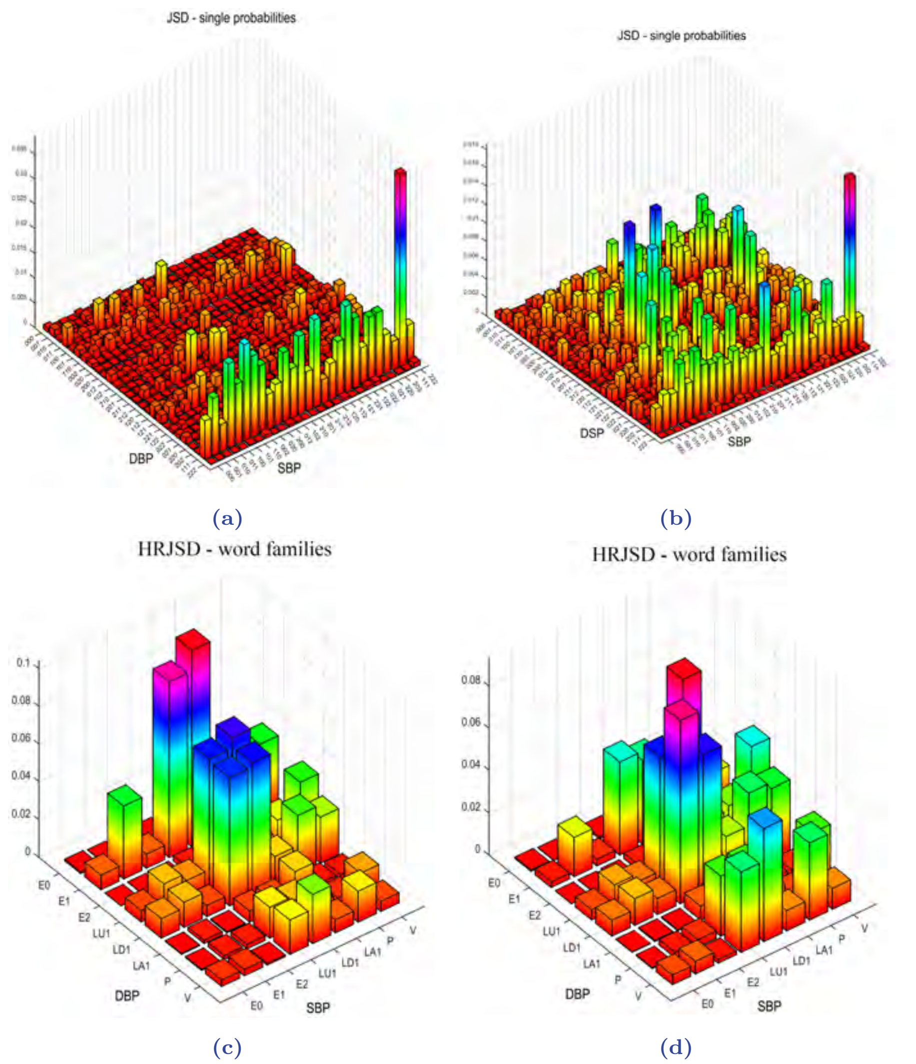

(a) (b) (c) (d)

Figure 6.3. Three-dimensional plots of the word distribution density matrix using the JSD and HRJSD methods (single word probabilities, word families), from an **(a,c)** $\mathrm{IDC_{LR}}$ and **(b,d)** $\mathrm{IDC_{HR}}$ patient, respectively, for diastolic-systolic coupling.

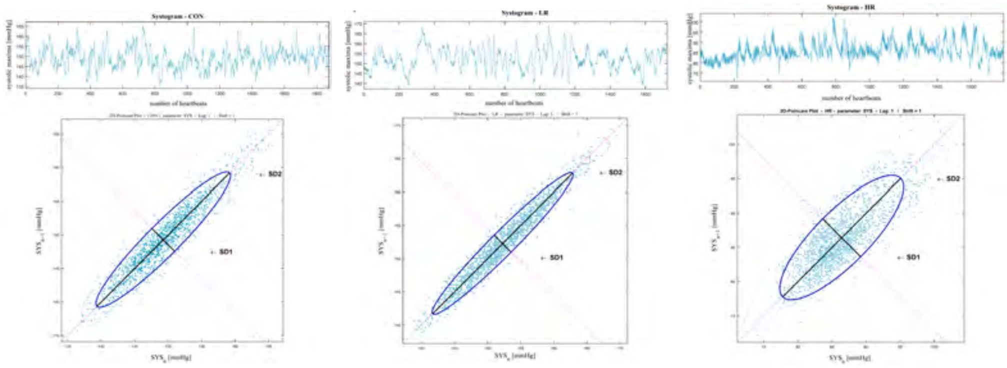

(a) (b) (c)

Figure 6.4. Systolic blood pressure Poincaré plot analysis results from **(a)** a CON subject, **(b)** an IDC_{LR} patient, and **(c)** an IDC_{HR} patient.

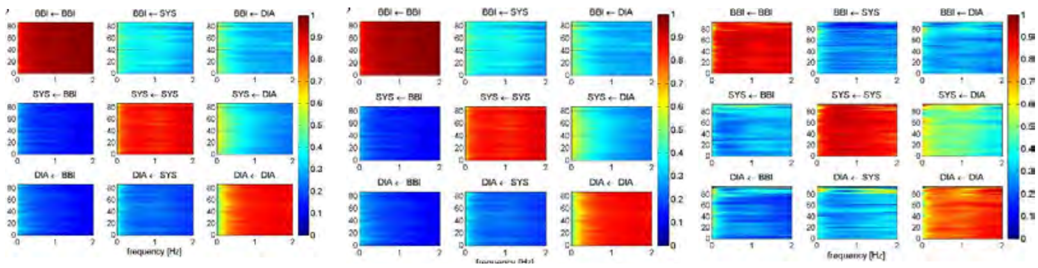

(a) (b) (c)

Figure 6.5. Averaged NSTPDC plots for cardiovascular coupling analyses for **(a)** the CON, **(b)** the IDC_{LR}, and **(c)** the IDC_{HR} group. Arrows indicate the causal coupling direction from one time series to another, e.g., SYS ← BBI, indicates the causal link from BBI to SYS. Coupling strength ranges from blue (0, no coupling) to red (1, maximum coupling) where BBI are beat-to-beat intervals, and SYS are successive end-systolic blood pressure amplitude values over time.

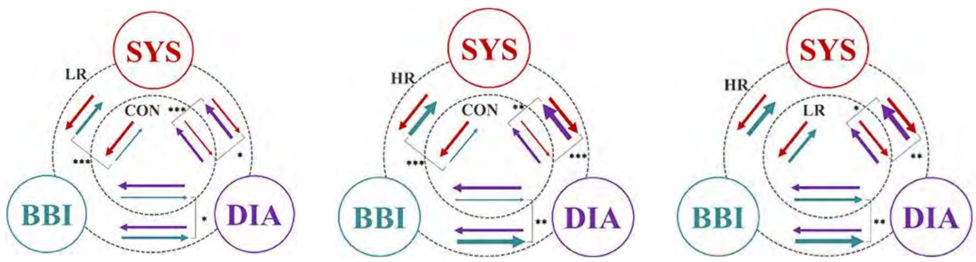

(a) (b) (c)

Figure 6.6. Schematic representation of the entire cardiovascular coupling structure (coupling strengths and directions) among the cardiac (BBI), systolic blood pressure (SYS), and diastolic blood pressure (DIA) systems, when comparing **(a)** CON vs IDC_{LR}, **(b)** CON vs IDC_{HR}, and **(c)** IDC_{HR} vs IDC_{LR}. The arrow directions indicate the causal coupling direction and the thickness the coupling strength. * indicates that the NSTPDC index associated to the coupling represented by the arrow is statistically significant when * $p \leq 0.01$; ** $p \leq 0.001$; *** $p \leq 0.0000167$.

Table 6.4. Mean value and 95% confidence interval of the most significant indices when comparing IDC_{LR} and IDC_{HR} patients.

Index	IDC_{HR}(N=14)	IDC_{LR}(N=77)	$p-value$
PPAs_SD1/SD2	0.26 [0.22 ; 0.30]	0.20 [0.18 ; 0.22]	*
PPAd_SD1/SD2	0.27 [0.25 ; 0.28]	0.19 [0.17 ; 0.20]	**
PPAd_SD1	1.21 [1.15 ; 1.26]	0.92 [0.85 ; 0.98]	**
SPPAcd_Column5	13.97 [13.54 ; 14.39]	12.09 [12.01 ; 13.02]	*
SPPAcd_Column8	13.77 [13.53 ; 14.03]	12.71 [12.35 ; 13.06]	n.s.
HRJSDcd_E1-LD1	0.03 [0.024 ; 0.035]	0.09 [0.081 ; 0.091]	**
HRJSDcd_LD1-V	0.056 [0.039 ; 0.073]	0.025 [0.021 ; 0.028]	**
HRJSDds_P-LU1	0.028 [0.022 ; 0.034]	0.016 [0.013 ; 0.019]	**
HRJSDds_V-LD1	0.050 [0.040 ; 0.060]	0.026 [0.022 ; 0.029]	**
NSTPDCcd_NF	-0.15 [-0.44 ; 0.14]	-0.71 [-0.85 ; -0.56]	*
NSTPDCcd_Area_c-d	0.26 [0.23 ; 0.29]	0.20 [0.18 ; 0.21]	**

*$p \leq 0.01$;**$p \leq 0.001$; n.s. $p > 0.01$; IDC_{HR}, idiopathic cardiomyopathic patients at high risk of sudden cardiac death; IDC_{LR}, idiopathic cardiomyopathic patients at low risk of sudden cardiac death; PPA, Poincaré plot analysis; SPPA, segmented Poincaré plot analysis; HRJSD, high resolution joint symbolic dynamics; NSTPDC, normalized short-time partial directed coherence; cd, cardio-diastolic coupling; ds, diastolic-systolic coupling

Table 6.5. Mean value and 95% confidence interval of the most significant indices comparing IDC patients and CON subjects.

Index	IDC(N=91)	CON(N=49)	$p-value$
HRJSDds_E0d	0.018 [0.014 ; 0.021]	0.0064 [0.0048 ; 0.0071]	***
NSTPDCcs_Area_c-s	0.25 [0.23 ; 0.28]	0.15 [0.13 ; 0.17]	***
PPAc_SD1	14.18 [10.44 ; 17.93]	23.27 [20.70 ; 25.84]	**
PPAc_SD1/SD2	0.29 [0.23 ; 0.34]	0.36 [0.33 ; 0.38]	**
HRJSDcd_E2d	0.02 [0.18 ; 0.21]	0.05 [0.045 ; 0.054]	*
HRJSDcd-LD1d	0.23 [0.22 ; 0.24]	0.28 [0.027 ; 0.29]	**
HRJSDds_LD1-E2	0.0014 [0.0010 ; 0.0018]	0.0053 [0.0035 ; 0.0071]	***
HRJSDcd_E0-LA1	0.0004 [0.00028 ; 0.00053]	0.00014 [0.00010 ; 0.00019]	***
HRJSDds_LD1-LD1	0.069 [0.063 ; 0.074]	0.093 [0.086 ; 0.10]	***

*$p \leq 0.01$;**$p \leq 0.001$; n.s. $p > 0.01$; IDC, idiopathic cardiomyopathic patients; CON, control group; PPA, Poincaré plot analysis; HRJSD, high resolution joint symbolic dynamics; NSTPDC, normalized short-time partial directed coherence; cd, cardio-diastolic coupling; ds, diastolic-systolic coupling

- IDC_{LR} and IDC_{HR} patients vs CON subjects

The comparison of IDC_{LR} patients vs CON subjects, and IDC_{HR} patients vs CON subjects yielded differences in 247 and 182 indices, respectively. After the correlation analysis, 85 and 61 remaining indices were chosen for the classification step. Summaries of the most relevant indices are shown in Tables 6.6 and 6.7.

- HRV and BPV standard indices and DSM results

No statistically significant indices were found when the HRV and BPV standard indices and the DSM were evaluated in the IDC_{LR} vs IDC_{HR} comparison. These results suggests that these indices are not suitable for SCD risk stratification

Table 6.6. Mean value and 95% confidence interval of the most significant indices comparing the IDC_{HR} patients and CON subjects.

Index	IDC_{HR}(N=14)	CON(N=49)	$p-value$
HRJSDds_LD1-V	0.05 [0.040 ; 0.066]	0.02 [0.020 ; 0.027]	***
NSTPDCcs_Area_c → s	0.29 [0.24 ; 0.35]	0.15 [0.13 ; 0.17]	***
NSTPDCcd_Area_c → d	0.31 [0.27 ; 0.36]	0.22 [0.20 ; 0.24]	**
SPPAds_Column_2-6	27.23 [25.73 ; 28.72]	22.44 [21.26 ; 23.63]	**
HRJSDcd_LD1-E2	0.003 [0.001 ; 0.006]	0.012 [0.010 ; 0.015]	**

**$p \leq 0.001$; *** $p \leq 0.0000167$; IDC_{HR}, idiopathic cardiomyopathic patients at high risk of sudden cardiac death; CON, control group; SPPA, segmented Poincaré plot analysis; HRJSD, high resolution joint symbolic dynamics; NSTPDC, normalized short-time partial directed coherence; cd, cardio-diastolic coupling; cs, cardio-systolic coupling; ds, diastolic-systolic coupling

Table 6.7. Mean value and 95% confidence interval for the most significant indices comparing the IDC_{LR} patients and CON subjects.

Index	IDC_{LR}(N=77)	CON(N=49)	$p-value$
HRJSDcd_E1d	0.33 [0.29 ; 0.37]	0.21 [0.17 ; 0.026]	**
NSTPDCcs_Area_c → s	0.25 [0.22 ; 0.27]	0.15 [0.13 ; 0.17]	***
SPPAcd_Column_1-8	5.40 [4.95 ; 5.85]	7.19 [6.56 ; 7.82]	**
HRJSDcd_E0-LA1	0.0004 [0.0002 ; 0.0005]	0.0014 [0.0010 ; 0.0019]	***
HRJSDds_LD1-LD1	0.070 [0.064 ; 0.075]	0.093 [0.086 ; 0.101]	***

**$p \leq 0.001$; *** $p \leq 0.0000167$; IDC_{LR}, idiopathic cardiomyopathic patients at low risk of sudden cardiac death; CON, control group; SPPA, segmented Poincaré plot analysis; HRJSD, high resolution joint symbolic dynamics; NSTPDC, normalized short-time partial directed coherence; cd, cardio-diastolic coupling; cs, cardio-systolic coupling; ds, diastolic-systolic coupling

in idiopathic cardiomyopathy patients. When comparing patients and control subjects, seven indices presented statistical significance: two from the DSM and five from the HRV and BPV standard indices. A summary of these results is shown in Table 6.8.

- Classification results

After the SVM classification step, the PPAs_SD1/SD2 and HRJSDds_LU1-P indices were deemed the optimal choices for the Laplace kernel SVM model having achieved accuracy of 98.9% and an AUC of 0.96 for the IDC_{LR} vs IDC_{HR} comparison. The HRJSDds-E0d and NSTPDCcs_Area_c-s allowed us to classify IDC patients from the CON group with 93.6% accuracy and an AUC of 0.94 using the Laplace kernel. Meanwhile, the HRJSDds_LD1-V and the NSTPDCcs_Area_c-s were able to differentiate between IDC_{HR} patients and the CON group with 96.9% accuracy and an AUC of 0.95 with the application of the Gaussian kernel. Finally, the HRJSDds-E1d and the NSTPDCcs_Area_c-s were found to be the best indices to classify IDC_{LR} patients from the CON group, obtaining 89.6% accuracy and a 0.85 AUC with the Laplace kernel. The classification plots and the results are shown in Figure 6.7 and Table 6.9, respectively.

Table 6.8. Mean value and 95% confidence interval of the HRV and BPV standard indices and the dual sequence method across all comparisons.

Index	**IDC_{HR}(N=14)**	**IDC_{LR}(N=77)**	**CON(N=49)**
bslope	5.3 [3.4 ; 7.2]	7.81 [6.8 ; 8.7]	10.2 [9.0 ; 11.4]
tslope	5.5 [3.7 ; 7.2]	7.94 [7.0 ; 8.83]	11.0 [9.8 ; 12.2]
BBI_meanNN	828.4 [775.2 ; 881.5]	906.9 [879.2 ; 934.6]	883.79 [853.3 ; 914.2]
BBI_sdNN	33.4 [25.0 ; 41.8]	36.9 [32.8 ; 41.0]	47.8 [43.4 ; 52.2]
BBI_rmssd	17.4 [12.0 ; 22.8]	20.5 [18.2 ; 22.8]	32.9 [28.2 ; 37.5]
BBI_pNN50	2.48 [1.4 ; 3.5]	3.44 [2.7 ; 4.1]	0.14 [0.1 ; 0.1]
BBI_HFn	0.6 [0.6 ; 0.7]	0.6 [0.6 ; 0.7]	0.6 [0.6 ; 0.6]
BBI_LFn	0.3 [0.3 ; 0.4]	0.3 [0.3 ; 0.3]	0.3 [0.3 ; 0.4]
BBI_LF/HF	2.5 [1.5 ; 3.5]	3.4 [2.7 ; 4.1]	2.5 [2.0 ; 3.0]
SYS_meanNN	121.3 [107.6 ; 135]	112.6 [108.3 ; 117]	122.5 [116.7 ; 128.2]
DIA_meanNN	61.5 [55.2 ; 67.9]	58.5 [55.8 ; 61.2]	60.6 [56.7 ; 64.5]
DIA_VLF	0.5 [0.4 ; 0.5]	0.5 [0.5 ; 0.5]	0.4 [0.3 ; 0.4]

	p − value IDC_{LR} vs IDC_{HR}	***p − value*** IDC vs CON	***p − value*** IDC_{HR} vs CON	***p − value*** IDC_{LR} vs CON
bslope	n.s.	**	**	*
tslope	n.s.	**	**	*
BBI_meanNN	n.s.	n.s.	n.s.	n.s.
BBI_sdNN	n.s.	**	*	**
BBI_rmssd	n.s.	**	*	**
BBI_pNN50	n.s.	**	*	**
BBI_HFn	n.s.	n.s.	n.s.	n.s.
BBI_LFn	n.s.	n.s.	n.s.	n.s.
BBI_LF/HF	n.s.	n.s.	n.s.	n.s.
SYS_meanNN	n.s.	n.s.	n.s.	**
DIA_meanNN	n.s.	n.s.	n.s.	n.s.
DIA_VLF	n.s.	**	n.s.	**

*$p \leq 0.01$; **$p \leq 0.001$; n.s. $p > 0.01$; IDC_{HR}, idiopathic cardiomyopathic patients at high risk of sudden cardiac death; IDC_{LR}, idiopathic cardiomyopathic patients at low risk of sudden cardiac death; CON, control group; bslope, bradycardic fluctuations; tslope, tachycardic fluctuations; BBI, beat-to-beat cardiac interval; SYS, systolic blood pressure; DIA, diastolic blood pressure.

Table 6.9. Accuracy (Acc), sensitivity (Sn), specificity (Sp), and area under the curve (AUC) obtained with the best SVM model for each comparison.

Indices	**IDC_{HR} vs IDC_{LR}** PPAs_SD1/Sd2 HRJSDds_LU1-P	**IDC vs CON** HRJSDds-E0d NSTPDCcs_Area_c-s	**IDC_{HR} vs CON** HRJSDds_LD1-V NSTPDCcs_Area_c-s	**IDC_{LR} vs CON** HRJSDds-E1d NSTPDCs_Area_c-s
C	7	5.5	1	0.3
Kernel	Laplace	Laplace	Gaussian	Laplace
σ	1	1.5	0.3	1
Acc (%)	98.9	93.6	96.8	84.9
Sn (%)	100	93.7	92.9	89.6
Sp (%)	93.1	95.5	98.0	79.5
AUC	0.96	0.94	0.95	0.85

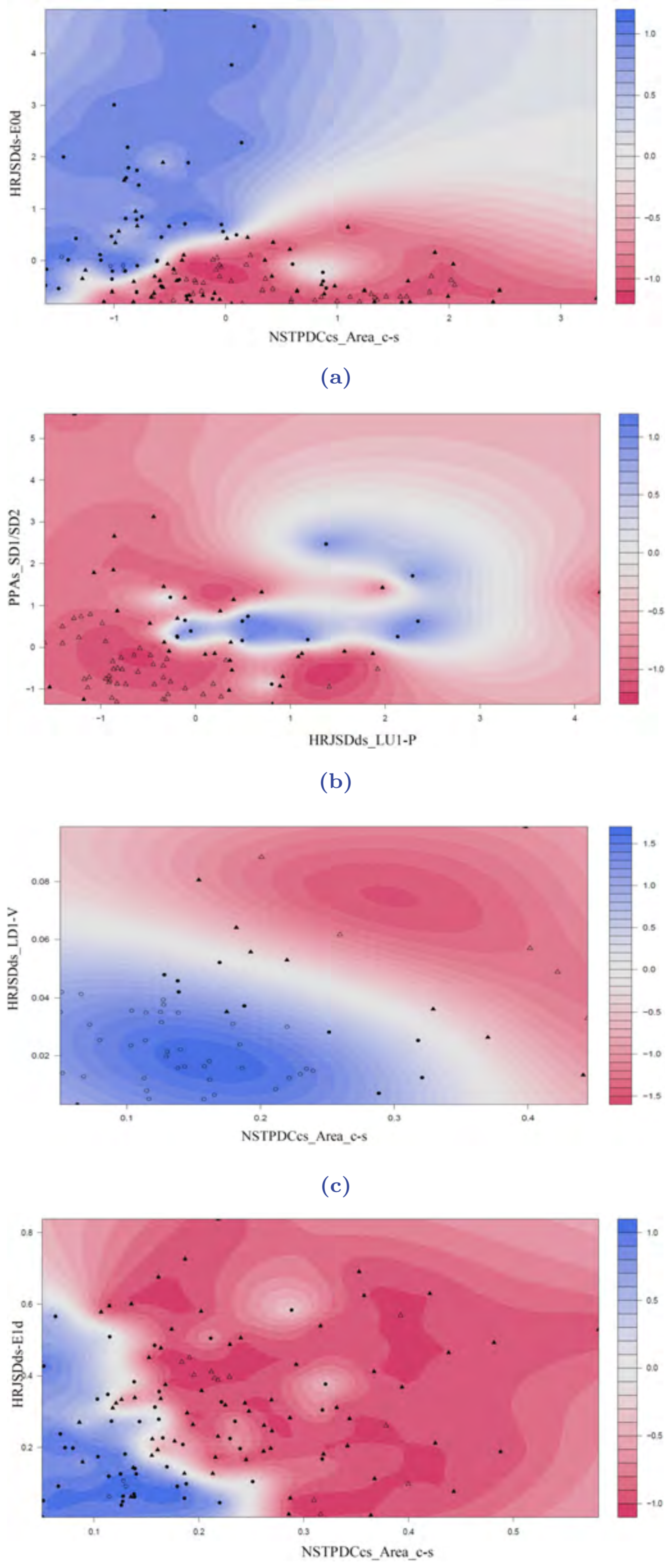

(a)

(b)

(c)

(d)

Figure 6.7. SVM classification plots: **(a)** IDC vs CON using Laplace kernel, **(b)** IDC_{LR} vs IDC_{HR} using Laplace kernel, **(c)** IDC_{HR} vs CON using Gaussian kernel, and (d) IDC_{LR} vs CON using Laplace kernel.

The cascade model achieved 94.4% accuracy. A One vs All approach yielded 86.1% sensitivity and 92.8% specificity for the CON group, 93.2% sensitivity and 94.5% specificity for the HR group, and 98.8% sensitivity and 89.0% specificity for the LR group.

6.5 Discussion

The aim of this study was to find indices capable of stratifying sudden cardiac death (SCD) risk in idiopathic cardiomyopathy patients. In order to achieve this, we obtained indices extracted from BBI (ECG) and systolic and diastolic blood pressure (BP) time series using linear and non-linear univariate and bivariate (coupling analysis) techniques. The indices extracted from these techniques showed patterns that behave differently in patients at high risk of SCD. These indices (mainly from coupling analyses) were used to train several SVM models in order to classify the subjects based on different levels of SCD risk.

Our findings showed that cardio-diastolic coupling (NSTPDC_cd_NF) is bidirectional with diastolic activity as a driver in IDC_{LR} patients. In addition, the coupling strength of cardiac activity over both systolic and diastolic blood pressure (NSTPDCcs_Area_c→s, NSTPDCcs_Area_c→d) increases when the patients are at high risk, suggesting that cardiac activity significantly dominates over blood pressure. This type of relationship has been previously observed in congestive heart failure patients [37].

Our results also indicated that systolic pressure activity significantly increases in response to the alternant activity of diastolic pressure in patients at risk of SCD (HRJSDds_P-LU_1). Similar patterns were also observed in cardio-diastolic coupling (HRJSDcd_LD_1-P), suggesting that the deterioration of autonomic regulation is more severe in patients at high risk of SCD. Earlier studies indicated that symmetric patterns in the HRJSD could be related to baroreflex-like response patterns. This suggests that this kind of behavior is also more pronounced in patients at high risk [4, 57].

The Poincaré plot analysis showed that the patients from the HR group have higher short-term systolic blood pressure deviation than the patients from the LR group and the CON subjects. This pathological behavior is also reflected in the PPAs_SD1/SD2 index, which becomes less balanced as the illness progresses. Diastolic blood pressure behaved in a similar way: the short-term diastolic blood pressure deviation was significantly lower in HR patients and their PPAd_SD1/SD2 was less balanced as well, indicating higher BPV in patients with critical conditions. Previous studies have found that higher short-term BPV is associated with several cardiac diseases, such as left ventricular systolic dysfunction and atherosclerosis, among others [64, 49]. This BPV behavior was also present in sinoaortic denervated cats [13]. In addition, baroreflex effectiveness has been studied in paraplegic subjects, and their BPV was found to be higher than that of CON subjects [9].

The aforementioned patterns were also present when the IDC patients were compared to the CON group. In general, the indices found in the PPA suggest that short-term BPV is higher in patients with pathological conditions [36, 39]. In relation to BBI, the PPA indices showed that short-term deviation and the short- and long- term deviation ratio of the heart rate is higher in the CON group, suggesting that the HRV in this group is higher than in IDC patients. On the other hand, the BBI_rmssd index suggests that the HRV is lower in IDC patients than in CON subjects [61]. Reduced HRV is a recognized predictor of an adverse prognosis in patients with cardiac disease [63, 22]. Several studies have related low HRV with heart failure [12, 43, 52, 46]. In addition, an increased complexity in BBI randomness and a lower fractal-like behavior have been associated with SDC [27].

The DSM revealed that both the tslope and bslope are significantly lower in IDC patients compared to CON subjects, and lower values of these sequences are associated with baroreflex dysfunction [14, 33]. A trend appeared in these indices when the patients were compared by their level of risk: $\mathrm{IDC_{HR}}$ patients showed lower tslopes and bslopes.

The segmented approach of the Poincaré plot analysis showed that some patterns in the cardiovascular coupling are more common in HR patients. There was a significantly higher concentration of these patterns in columns 5 and 8 in both cardio-diastolic and cardio-systolic couplings in patients at higher risk of SDC, indicating a lower variability in their baroreflex activity compared to patients at low risk. SPPA patterns (SPPAcd_Column_5, SPPAcd_Column_8) occurred more frequently and were more concentrated in low-risk patients, suggesting that these patients present a higher HRV compared to patients at higher risk of SCD. The viability of HRV as a reliable predictor of SCD in IDC patients was explored in a previous study [25], but the findings did not support the hypothesis that HRV is a reliable predictor of SCD in IDC patients. However, those results were based on a time domain analysis of HRV only, whereas the significant indices analyzed in our work come primarily from non-linear methods. These characterization methods are more suitable for describing the non-linear behavior of HRV in pathological conditions.

The HRJSD results suggest that patients at high risk adapt less frequently to changes in blood pressure, reflected in the lower presence of decreasing patterns of BBI ($\mathrm{E_0}$) in response to decreasing patterns in diastolic blood pressure ($\mathrm{LD_1}$). This may be a result of the vagal response causing less recurring parasympathetic activity, which leads to a less effective control of blood pressure, and consequently of heart rate, in patients at higher risk.

These results were consistent when CON subjects were compared with IDC patients: decreasing patterns (E_0) in diastolic BPV were reflected in decreasing heart rates at higher frequencies in CON subjects. The DIA_LF/HF was higher in patients than in the CON group. Higher levels of this index reflect efferent sympathetic activity [38]. Additionally, a higher prevalence of unchanging patterns (E_1) was found in the IDC patients compared with the CON group, indicating that changes in blood pressure are frequently not reflected in changes in heart rate, in patients with pathological conditions.

In addition, the HRJSDcd-E_2d and HRJSDcd-LD_1d indices showed that steady (E_2) and low decreasing (LD_1) diastolic blood pressure patterns, independent from all BBI patterns, are more recurrent in CON subjects. These indices suggest a worsened circulatory homeostasis in IDC patients, and support the idea of the influence of baroreflex activity in pathological conditions [29].

Some studies [23, 53] have stated that the relationship between systolic and diastolic blood pressure should be coherent: if one increases, the other is expected to increase as well. The results of the systolic-diastolic coupling revealed that patterns that are opposing in nature (sLU_1-dP, sLD_1-dV) are more recurrent in the HR group. This suggests that the relationship between systolic and diastolic blood pressure loses linearity as the pathological condition worsens.

The coupling strength of the cardiovascular and diastolic-systolic couplings was stronger in pathological conditions. In addition, the symmetric patterns of the diastolic-systolic coupling activity were less recurrent in the patients than in the control subjects. This may be caused by the effect of autonomic regulation mechanisms in pathological conditions [20, 30].

To summarize, our results suggest that there is a gradual loss of HRV as SCD risk increases and, at the same time, BPV increases in keeping with SCD risk. There is great controversy surrounding the prognostic value of linear time and frequency domain HRV indices for risk stratification among this type of patient [25, 26, 41, 66, 68, 67]. The results of this work suggest that commonly used techniques for analyzing the time and frequency domain of HRV are not suitable for risk stratification. However, the combination of non-linear HRV analysis and linear as well as non-linear coupling analysis seems to be a promising tool for risk assessment in IDC patients [69, 65, 19]. The processes involved in circulatory homeostasis are by nature non-linear. Therefore, the differences between the stages of this process can be more adequately shown by the quantification of the signal properties rather than by the assessment of their magnitude.

We hypothesize that a dysfunction of the vagal activity, and in general of the baroreflex mechanism as a whole, prevents the body from correctly maintaining circulatory homeostasis. This reduction in vagal activity and increase in sympathetic influence exposes the cardiovascular system to frequent states of stress that contribute to the further deterioration of the condition over time. The gradual deterioration of heart rate and blood pressure variability in the different SDC risk stages considered here supports this assumption. This kind of impairment has also been associated with other cardiac pathological conditions like ventricular fibrillation during myocardial ischemia [32]. Abnormal sympathetic neural firing has been associated with SCD and the onset of ventricular tachyarrhythmias [16]. A similar behavior has been observed in elderly mice [21], which presented a reduced baroreflex bradycardic response compared to younger mice.

This study has some limitations that are important to consider. The average age in the CON group was lower than in the IDC group, and the influence of age in the study of HRV has been widely studied in other works [70]. However, this limitation does not affect our results for HR vs LR comparisons. A higher number of indices were analyzed than the number of patients in the database. In order to minimize problems due to possible overfitting, we established different levels of statistical significance to reduce the dataset dimensionality, including the Bonferroni-Holm correction criterion.

The characterization of linear and non-linear coupling could be also analyzed based on linear and non-linear Granger causality in time- and frequency- domains [55]. The objective of this study was to evaluate the general behavior of the underlying coupling through the average of all the features (windows) over time. Nevertheless, it is uncertain if another time-invariant time domain measure based on Granger causality would be more appropriate and would have more discriminative power [47]. It would be an interesting objective for an ongoing study.

Another limitation of this work is related to comorbidities and confounding factors influencing the autonomic regulation system. Therefore, these exclusion criteria make risk stratification not yet applicable to every patient.

6.6 Conclusion

The results of this research suggest that indices from coupling analysis and non-linear HRV and BPV can contribute to the development of risk stratification in IDC patients. We have introduced a novel cascade model that successfully classified subjects into different levels of SCD risk (CON, $\mathrm{IDC_{LR}}$, and $\mathrm{IDC_{HR}}$). Further, this study allowed us to reveal, for the first time, some of the complex interactions that take place within autonomic regulation, leading to more accurate modeling and interpretation of these processes in pathological conditions. Our findings suggest that HRV gradually decreases and BPV increases as the SCD risk increases. We conclude that patients at high risk of SCD can no longer consistently maintain circulatory homeostasis, leading to states of stress that worsen the condition over time.

However, these results should be validated with a greater number of patients, especially in the high-risk group. Therefore, the results presented in this work are more of a hypothesis-generating nature than confirmatory.

Chapter 6 bibliography

[1] F. Adochiei, S. Schulz, I. Edu, H. Costin, and A. Voss. "A new normalised short time PDC for dynamic coupling analyses." In: (2013). DOI: 10.1515/bmt-2013-4167.

[2] Saour B., Ji Y., Philbin E., Tan H., Nguyen D.and O'Brien J., Sidhu S., Steckman A., and Torosoff M. "Following theraoeutic hypothermia in patients with sudden cardiac death due to ventricular tachycardia or fibrillation." In: *International Journal of Clinical Medicine* 8 (2017), pp. 293–305.

[3] L. A. Baccala and K. Sameshima. "Partial directed coherence: a new concept in neural structure determination". In: *Biol Cybern* 84.6 (2001), pp. 463–74. ISSN: 0340-1200 (Print) 0340-1200 (Linking). DOI: 10.1007/PL00007990. URL: https://www.ncbi.nlm.nih.gov/pubmed/11417058.

[4] M. Baumert, V. Baier, S. Truebner, A. Schirdewan, and A. Voss. "Short- and long-term joint symbolic dynamics of heart rate and blood pressure in dilated cardiomyopathy". In: *IEEE Trans Biomed Eng* 52.12 (2005), pp. 2112–5. ISSN: 0018-9294 (Print) 0018-9294 (Linking). DOI: 10.1109/TBME.2005.857636. URL: https://www.ncbi.nlm.nih.gov/pubmed/16366235.

[5] M. Baumert, T. Walther, J. Hopfe, R. Stepan H.and Faber, and A. Voss. "Joint symbolic dynamic analysis of beat-to-beat interactions of heart rate and systolic blood pressure in normal pregnancy." In: (2002). DOI: 10.1007/BF02348131.

[6] A. Ben-Hur, C. S. Ong, S. Sonnenburg, B. Scholkopf, and G. Ratsch. "Support vector machines and kernels for computational biology". In: *PLoS Comput Biol* 4.10 (2008), e1000173. ISSN: 1553-7358 (Electronic) 1553-734X (Linking). DOI: 10.1371/journal.pcbi.1000173. URL: https://www.ncbi.nlm.nih.gov/pubmed/18974822.

[7] G. Bertinieri, M. Di Rienzo, A. Cavallazzi, A. U. Ferrari, A. Pedotti, and G. Mancia. "Evaluation of baroreceptor reflex by blood pressure monitoring in unanesthetized cats." In: *Am. J. Physiol.* (1988). DOI: 10.1152/ajpheart.1988.254.2.H377.

[8] M. R. Bristow, L. A. Saxon, J. Boehmer, S. Krueger, D. A. Kass, T. De Marco, P. Carson, L. DiCarlo, D. DeMets, B. G. White, D. W. DeVries, A. M. Feldman, Pacing Comparison of Medical Therapy, and Investigators Defibrillation in Heart Failure. "Cardiac-resynchronization therapy with or without an implantable defibrillator in advanced chronic heart failure". In: *N Engl J Med* 350.21 (2004), pp. 2140–50. ISSN: 1533-4406 (Electronic) 0028-4793 (Linking). DOI: 10.1056/NEJMoa032423. URL: https://www.ncbi.nlm.nih.gov/pubmed/15152059.

[9] P. Castiglioni, M. Di Rienzo, A. Veicsteinas, G. Parati, and G. Merati. "Mechanisms of blood pressure and heart rate variability: an insight from low-level paraplegia". In: *Am J Physiol Regul Integr Comp Physiol* 292.4 (2007), R1502–9. ISSN: 0363-6119 (Print) 0363-6119 (Linking). DOI: 10.1152/ajpregu.00273.2006. URL: https://www.ncbi.nlm.nih.gov/pubmed/17122332.

[10] S. S. Chugh. "Sudden cardiac death in 2017: Spotlight on prediction and prevention". In: *Int J Cardiol* 237 (2017), pp. 2–5. ISSN: 1874-1754 (Electronic) 0167-5273 (Linking). DOI: 10.1016/j.ijcard.2017.03.086. URL: https://www.ncbi.nlm.nih.gov/pubmed/28365183.

[11] C. Cortes and V. Vapnik. "Support vector networks". In: *Machine Learning* 20 (1995), pp. 273–297.

[12] J. M. Dekker, R. S. Crow, A. R. Folsom, P. J. Hannan, D. Liao, C. A. Swenne, and E. G. Schouten. "Low heart rate variability in a 2-minute rhythm strip predicts risk of coronary heart disease and mortality from several causes: the ARIC Study. Atherosclerosis Risk In Communities". In: *Circulation* 102.11 (2000), pp. 1239–44. ISSN: 1524-4539 (Electronic) 0009-7322 (Linking). URL: https://www.ncbi.nlm.nih.gov/pubmed/10982537.

[13] M. Di Rienzo, G. Parati, P. Castiglioni, S. Omboni, A. U. Ferrari, A. J. Ramirez, A. Pedotti, and G. Mancia. "Role of sinoaortic afferents in modulating BP and pulse-interval spectral characteristics in unanesthetized cats". In: *Am J Physiol* 261.6 Pt 2 (1991), H1811–8. ISSN: 0002-9513 (Print) 0002-9513 (Linking). DOI: 10.1152/ajpheart.1991.261.6.H1811. URL: https://www.ncbi.nlm.nih.gov/pubmed/1750537.

[14] M. Di Rienzo, G. Parati, P. Castiglioni, R. Tordi, G. Mancia, and A. Pedotti. "Baroreflex effectiveness index: an additional measure of baroreflex control of heart rate in daily life". In: *Am J Physiol Regul Integr Comp Physiol* 280.3 (2001), R744–51. ISSN: 0363-6119 (Print) 0363-6119 (Linking). DOI: 10.1152/ajpregu.2001.280.3.R744. URL: https://www.ncbi.nlm.nih.gov/pubmed/11171653.

[15] G. Duray, C. W. Israel, and S. H. Hohnloser. "Recent primary prevention implantable cardioverter defibrillator trials". In: *Curr Opin Cardiol* 21.1 (2006), pp. 15–9. ISSN: 0268-4705 (Print) 0268-4705 (Linking). URL: https://www.ncbi.nlm.nih.gov/pubmed/16355024.

[16] M. D. Esler, J. M. Thompson, D. M. Kaye, A. G. Turner, G. L. Jennings, H. S. Cox, G. W. Lambert, and D. R. Seals. “Effects of aging on the responsiveness of the human cardiac sympathetic nerves to stressors”. In: *Circulation* 91.2 (1995), pp. 351–8. ISSN: 0009-7322 (Print) 0009-7322 (Linking). URL: https://www.ncbi.nlm.nih.gov/pubmed/7805237.

[17] L. Faes, S. Erla, and G. Nollo. “Measuring connectivity in linear multivariate processes: definitions, interpretation, and practical analysis”. In: *Comput Math Methods Med* 2012 (2012), p. 140513. ISSN: 1748-6718. DOI: 10.1155/2012/140513. URL: https://www.ncbi.nlm.nih.gov/pubmed/22666300.

[18] L. Faes, A. Porta, G. Nollo, and M. Javorka. “Information Decomposition in Multivariate Systems: Definitions, Implementation and Application to Cardiovascular Networks”. In: *Entropy* 19.5 (2017), pp. 1–28. DOI: 10.3390/e19010005.

[19] C. Fischer and A. Voss. “Three-Dimensional Segmented Poincare Plot Analyses SPPA3 Investigates Cardiovascular and Cardiorespiratory Couplings in Hypertensive Pregnancy Disorders”. In: *Front Bioeng Biotechnol* 2 (2014), p. 51. ISSN: 2296-4185 (Print) 2296-4185 (Linking). DOI: 10.3389/fbioe.2014.00051. URL: https://www.ncbi.nlm.nih.gov/pubmed/25429364.

[20] J. S. Floras. “Sympathetic nervous system activation in human heart failure: clinical implications of an updated model”. In: *J Am Coll Cardiol* 54.5 (2009), pp. 375–85. ISSN: 1558-3597 (Electronic) 0735-1097 (Linking). DOI: 10.1016/j.jacc.2009.03.061. URL: https://www.ncbi.nlm.nih.gov/pubmed/19628111.

[21] J. L. Freeling and Y. Li. “Age-related attenuation of parasympathetic control of the heart in mice”. In: *Int J Physiol Pathophysiol Pharmacol* 7.3 (2015), pp. 126–35. ISSN: 1944-8171 (Print) 1944-8171 (Linking). URL: https://www.ncbi.nlm.nih.gov/pubmed/26823961.

[22] Y. Gang and M. Malik. “Heart rate variability analysis in general medicine”. In: *Indian Pacing Electrophysiol J* 3.1 (2003), pp. 34–40. ISSN: 0972-6292 (Electronic) 0972-6292 (Linking). URL: https://www.ncbi.nlm.nih.gov/pubmed/16943988.

[23] B. Gavish, I. Z. Ben-Dov, and M. Bursztyn. “Linear relationship between systolic and diastolic blood pressure monitored over 24 h: assessment and correlates”. In: *J Hypertens* 26.2 (2008), pp. 199–209. ISSN: 0263-6352 (Print) 0263-6352 (Linking). DOI: 10.1097/HJH.0b013e3282f25b5a. URL: https://www.ncbi.nlm.nih.gov/pubmed/18192832.

[24] B. F. Giraldo, J. Rodriguez, P. Caminal, A. Bayes-Genis, and A. Voss. “Cardiorespiratory and cardiovascular interactions in cardiomyopathy patients using joint symbolic dynamic analysis”. In: *Conf Proc IEEE Eng Med Biol Soc* 2015 (2015), pp. 306–9. ISSN: 1557-170X (Print) 1557-170X (Linking).

DOI: 10.1109/EMBC.2015.7318361. URL: https://www.ncbi.nlm.nih.gov/pubmed/26736261.

[25] W. Grimm, I. Herzum, H. H. Muller, and M. Christ. "Value of heart rate variability to predict ventricular arrhythmias in recipients of prophylactic defibrillators with idiopathic dilated cardiomyopathy". In: *Pacing Clin Electrophysiol* 26.1 Pt 2 (2003), pp. 411–5. ISSN: 0147-8389 (Print) 0147-8389 (Linking). URL: https://www.ncbi.nlm.nih.gov/pubmed/12687856.

[26] S. H. Hohnloser, T. Klingenheben, D. Bloomfield, O. Dabbous, and R. J. Cohen. "Usefulness of microvolt T-wave alternans for prediction of ventricular tachyarrhythmic events in patients with dilated cardiomyopathy: results from a prospective observational study". In: *J Am Coll Cardiol* 41.12 (2003), pp. 2220–4. ISSN: 0735-1097 (Print) 0735-1097 (Linking). URL: https://www.ncbi.nlm.nih.gov/pubmed/12821251.

[27] H. V. Huikuri, T. H. Makikallio, C. K. Peng, A. L. Goldberger, U. Hintze, and M. Moller. "Fractal correlation properties of R-R interval dynamics and mortality in patients with depressed left ventricular function after an acute myocardial infarction". In: *Circulation* 101.1 (2000), pp. 47–53. ISSN: 0009-7322 (Print) 0009-7322 (Linking). URL: https://www.ncbi.nlm.nih.gov/pubmed/10618303.

[28] M. Javorka, J. Krohova, B. Czippelova, Z. Turianikova, Z. Lazarova, K. Javorka, and L. Faes. "Basic cardiovascular variability signals: mutual directed interactions explored in the information domain". In: *Physiol Meas* 38.5 (2017), pp. 877–894. ISSN: 1361-6579. DOI: 10.1088/1361-6579/aa5b77. URL: https://www.ncbi.nlm.nih.gov/pubmed/28140353.

[29] T. Kishi. "Disruption of Central Antioxidant Property of Nuclear Factor Erythroid 2-Related Factor 2 Worsens Circulatory Homeostasis with Baroreflex Dysfunction in Heart Failure". In: *Int J Mol Sci* 19.3 (2018). ISSN: 1422-0067 (Electronic) 1422-0067 (Linking). DOI: 10.3390/ijms19030646. URL: https://www.ncbi.nlm.nih.gov/pubmed/29495326.

[30] T. Kishi. "Heart failure as an autonomic nervous system dysfunction". In: *J Cardiol* 59.2 (2012), pp. 117–22. ISSN: 1876-4738 (Electronic) 0914-5087 (Linking). DOI: 10.1016/j.jjcc.2011.12.006. URL: https://www.ncbi.nlm.nih.gov/pubmed/22341431.

[31] L. Kober, J. J. Thune, J. C. Nielsen, J. Haarbo, L. Videbaek, E. Korup, G. Jensen, P. Hildebrandt, F. H. Steffensen, N. E. Bruun, H. Eiskjaer, A. Brandes, A. M. Thogersen, F. Gustafsson, K. Egstrup, R. Videbaek, C. Hassager, J. H. Svendsen, D. E. Hofsten, C. Torp-Pedersen, S. Pehrson, and Danish Investigators. "Defibrillator Implantation in Patients with Nonischemic Systolic Heart Failure". In: *N Engl J Med* 375.13 (2016), pp. 1221–30. ISSN: 1533-4406 (Electronic) 0028-4793 (Linking). DOI: 10.1056/NEJMoa1608029. URL: https://www.ncbi.nlm.nih.gov/pubmed/27571011.

[32] M. T. La Rovere, G. D. Pinna, S. H. Hohnloser, F. I. Marcus, A. Mortara, R. Nohara, Jr. Bigger J. T., A. J. Camm, P. J. Schwartz, Atrami Investigators. Autonomic Tone, and Infarcton Reflexes After Myocardial. "Baroreflex sensitivity and heart rate variability in the identification of patients at risk for life-threatening arrhythmias: implications for clinical trials". In: *Circulation* 103.16 (2001), pp. 2072–7. ISSN: 0009-7322 (Print) 0009-7322 (Linking). URL: https://www.ncbi.nlm.nih.gov/pubmed/11319197.

[33] M. T. La Rovere, G. D. Pinna, and G. Raczak. "Baroreflex sensitivity: measurement and clinical implications". In: *Ann Noninvasive Electrocardiol* 13.2 (2008), pp. 191–207. ISSN: 1542-474X (Electronic) 1082-720X (Linking). DOI: 10.1111/j.1542-474X.2008.00219.x. URL: https://www.ncbi.nlm.nih.gov/pubmed/18426445.

[34] H. Malberg, N. Wessel, A. Hasart, K. J. Osterziel, and A. Voss. "Advanced analysis of spontaneous baroreflex sensitivity, blood pressure and heart rate variability in patients with dilated cardiomyopathy." In: *Clin. Sci.* (2002). DOI: 10.1042/cs1020465.

[35] H. Malberg, N. Wessel, A. Schirdewan, K. J. Osterziel, and A. Voss. "Dual sequence method for analysis of spontaneous baroreceptor reflex sensitivity in patients with dilated cardiomyopathy." In: *Z. Kardiol.* (1999). DOI: 10.1007/s003920050294.

[36] G. Mancia, A. Ferrari, L. Gregorini, G. Parati, G. Pomidossi, G. Bertinieri, G. Grassi, M. di Rienzo, A. Pedotti, and A. Zanchetti. "Blood pressure and heart rate variabilities in normotensive and hypertensive human beings". In: *Circ Res* 53.1 (1983), pp. 96–104. ISSN: 0009-7330 (Print) 0009-7330 (Linking). URL: https://www.ncbi.nlm.nih.gov/pubmed/6861300.

[37] D. Marinazzo, M. Pellicoro, and S. Stramaglia. "Nonlinear parametric model for Granger causality of time series". In: *Phys Rev E Stat Nonlin Soft Matter Phys* 73.6 Pt 2 (2006), p. 066216. ISSN: 1539-3755. DOI: 10.1103/PhysRevE.73.066216. URL: https://www.ncbi.nlm.nih.gov/pubmed/16906955.

[38] R. McCraty and F. Shaffer. "Heart Rate Variability: New Perspectives on Physiological Mechanisms, Assessment of Self-regulatory Capacity, and Health risk". In: *Glob Adv Health Med* 4.1 (2015), pp. 46–61. ISSN: 2164-957X. DOI: 10.7453/gahmj.2014.073. URL: https://www.ncbi.nlm.nih.gov/pubmed/25694852.

[39] M. H. Mehlum, K. Liestol, S. E. Kjeldsen, S. Julius, T. A. Hua, P. M. Rothwell, G. Mancia, G. Parati, M. A. Weber, and E. Berge. "Blood pressure variability and risk of cardiovascular events and death in patients with hypertension and different baseline risks". In: *Eur Heart J* 39.24 (2018), pp. 2243–2251. ISSN: 1522-9645 (Electronic) 0195-668X (Linking). DOI: 10.1093/eurheartj/ehx760. URL: https://www.ncbi.nlm.nih.gov/pubmed/29365085.

[40] T. Milde, K. Schwab, M. Walther, M. Eiselt, C. Schelenz, and A Voss. "Time-variant partial directed coherence in analysis of the cardiovascular system. A methodological study." In: *Physiol. Meas.* (2011). DOI: `10.1088/0967-3334/32/11/S06`.

[41] O. Minamihaba, M. Yamaki, H. Tomoike, and I. Kubota. "Severity in myocardial dysfunction contributed to long-term fluctuation of heart rate, rather than short-term fluctuations". In: *Ann Noninvasive Electrocardiol* 8.2 (2003), pp. 132–8. ISSN: 1082-720X (Print) 1082-720X (Linking). URL: `https://www.ncbi.nlm.nih.gov/pubmed/12848794`.

[42] D. Mozaffarian, E. J. Benjamin, A. S. Go, D. K. Arnett, M. J. Blaha, M. Cushman, S. de Ferranti, J. P. Despres, H. J. Fullerton, V. J. Howard, M. D. Huffman, S. E. Judd, B. M. Kissela, D. T. Lackland, J. H. Lichtman, L. D. Lisabeth, S. Liu, R. H. Mackey, D. B. Matchar, D. K. McGuire, 3rd Mohler E. R., C. S. Moy, P. Muntner, M. E. Mussolino, K. Nasir, R. W. Neumar, G. Nichol, L. Palaniappan, D. K. Pandey, M. J. Reeves, C. J. Rodriguez, P. D. Sorlie, J. Stein, A. Towfighi, T. N. Turan, S. S. Virani, J. Z. Willey, D. Woo, R. W. Yeh, M. B. Turner, Committee American Heart Association Statistics, and Subcommittee Stroke Statistics. "Heart disease and stroke statistics–2015 update: a report from the American Heart Association". In: *Circulation* 131.4 (2015), e29–322. ISSN: 1524-4539 (Electronic) 0009-7322 (Linking). DOI: `10.1161/CIR.0000000000000152`. URL: `https://www.ncbi.nlm.nih.gov/pubmed/25520374`.

[43] A. Musialik-Lydka, B. Sredniawa, and S. Pasyk. "Heart rate variability in heart failure". In: *Kardiol Pol* 58.1 (2003), pp. 10–6. ISSN: 0022-9032 (Print) 0022-9032 (Linking). URL: `https://www.ncbi.nlm.nih.gov/pubmed/14502297`.

[44] A. Neumaier and T. Schneider. "Estimation of parameters and eigenmodes of multivariate autoregressive models." In: *ACM Trans. Math. Softw.* (2001). DOI: `10.1145/382043.382304`.

[45] M. Parati G.and Di Rienzo and G. Mancia. "How to measure baroreflex sensitivity: from the cardiovascular laboratory to daily life." In: *J. Hypertens.* (2000). DOI: `10.1097/00004872-200018010-00003`.

[46] V. N. Patel, B. R. Pierce, R. K. Bodapati, D. L. Brown, D. G. Ives, and P. K. Stein. "Association of Holter-Derived Heart Rate Variability Parameters With the Development of Congestive Heart Failure in the Cardiovascular Health Study". In: *JACC Heart Fail* 5.6 (2017), pp. 423–431. ISSN: 2213-1787 (Electronic) 2213-1779 (Linking). DOI: `10.1016/j.jchf.2016.12.015`. URL: `https://www.ncbi.nlm.nih.gov/pubmed/28396041`.

[47] A. Porta and L. Faes. "Wiener-granger causality in network physiology with applications to cardiovascular control and neuroscience." In: *Proc. IEEE.* (2016). DOI: `10.1109/JPROC.2015.2476824`.

[48] A. Porta, L. Faes, V. Bari, A. Marchi, T. Bassani, G. Nollo, N. M. Perseguini, J. Milan, V. Minatel, A. Borghi-Silva, A. C. Takahashi, and A. M. Catai. “Effect of age on complexity and causality of the cardiovascular control: comparison between model-based and model-free approaches”. In: *PLoS One* 9.2 (2014), e89463. ISSN: 1932-6203. DOI: 10.1371/journal.pone.0089463. URL: https://www.ncbi.nlm.nih.gov/pubmed/24586796.

[49] A. H. Ribeiro, P. A. Lotufo, A. Fujita, A. C. Goulart, D. Chor, J. G. Mill, I. M. Bensenor, and I. S. Santos. “Association Between Short-Term Systolic Blood Pressure Variability and Carotid Intima-Media Thickness in ELSA-Brasil Baseline”. In: *Am J Hypertens* 30.10 (2017), pp. 954–960. ISSN: 1941-7225 (Electronic) 0895-7061 (Linking). DOI: 10.1093/ajh/hpx076. URL: https://www.ncbi.nlm.nih.gov/pubmed/28475663.

[50] J. Rodriguez, S. Schulz, B.F. Giraldo, and A. Voss. “Risk Stratification in idiopathic dilated cardiomyopathy patients using cardiovascular coupling analysis.” In: *Frontiers in physiology.* (2019).

[51] J. B. Rundle, A. Giguere, D. L. Turcotte, J. P. Crutchfield, and A. Donnellan. “Global Seismic Nowcasting With Shannon Information Entropy”. In: *Earth Space Sci* 6.1 (2019), pp. 191–197. ISSN: 2333-5084. DOI: 10.1029/2018EA000464. URL: https://www.ncbi.nlm.nih.gov/pubmed/30854411.

[52] G. R. Sandercock and D. A. Brodie. “The role of heart rate variability in prognosis for different modes of death in chronic heart failure”. In: *Pacing Clin Electrophysiol* 29.8 (2006), pp. 892–904. ISSN: 0147-8389 (Print) 0147-8389 (Linking). DOI: 10.1111/j.1540-8159.2006.00457.x. URL: https://www.ncbi.nlm.nih.gov/pubmed/16923007.

[53] G. Schillaci and G. Pucci. “The dynamic relationship between systolic and diastolic blood pressure: yet another marker of vascular aging?” In: *Hypertens Res* 33.7 (2010), pp. 659–61. ISSN: 1348-4214 (Electronic) 0916-9636 (Linking). DOI: 10.1038/hr.2010.95. URL: https://www.ncbi.nlm.nih.gov/pubmed/20520611.

[54] T. Schneider and A. Neumaier. “Algorithm 808: ARfit&mdash: a matlab package for the estimation of parameters and eigenmodes of multivariate autoregressive models.” In: *ACM Trans. Math. Softw.* (2001). DOI: 10.1145/382043.382316.

[55] S. Schulz, F. C. Adochiei, R. Schroeder, H. Costin, K. J. Bar, and A. Voss. “Cardiovascular and cardiorespiratory coupling analyses: a review.” In: *Philosophical Transactions A Math. Phys. Eng. SCi.* (2013). DOI: 10.1098/rsta.2012.0191.

[56] S. Schulz, K. J. Bär, and A. Voss. “Analyses of heart rate, respiration and cardiorespiratory coupling in patients with schizophrenia.” In: (2015). DOI: 10.3390/e17020483.

[57] S. Schulz, M. Bolz, K. J. Bar, and A. Voss. “Central- and autonomic nervous system coupling in schizophrenia”. In: *Philos Trans A Math Phys Eng Sci* 374.2067 (2016). ISSN: 1364-503X (Print) 1364-503X (Linking). DOI: 10.1098/rsta.2015.0178. URL: https://www.ncbi.nlm.nih.gov/pubmed/27044986.

[58] S. Schulz, J. Haueisen, K. J. Bar, and V. Andreas. “High-resolution joint symbolic analysis to enhance classification of the cardiorespiratory system in patients with schizophrenia and their relatives”. In: *Philos Trans A Math Phys Eng Sci* 373.2034 (2015). ISSN: 1364-503X (Print) 1364-503X (Linking). DOI: 10.1098/rsta.2014.0098. URL: https://www.ncbi.nlm.nih.gov/pubmed/25548266.

[59] S. Schulz, N. Tupaika, S. Berger, J. Haueisen, K. J. Bar, and A. Voss. “Cardiovascular coupling analysis with high-resolution joint symbolic dynamics in patients suffering from acute schizophrenia”. In: *Physiol Meas* 34.8 (2013), pp. 883–901. ISSN: 1361-6579 (Electronic) 0967-3334 (Linking). DOI: 10.1088/0967-3334/34/8/883. URL: https://www.ncbi.nlm.nih.gov/pubmed/23859938.

[60] A. Seeck, M. Baumert, C. Fischer, A. Khandoker, R. Faber, and A. Voss. “Advanced Poincare plot analysis differentiates between hypertensive pregnancy disorders”. In: *Physiol Meas* 32.10 (2011), pp. 1611–22. ISSN: 1361-6579 (Electronic) 0967-3334 (Linking). DOI: 10.1088/0967-3334/32/10/009. URL: https://www.ncbi.nlm.nih.gov/pubmed/21896969.

[61] F. Shaffer and J. P. Ginsberg. “An Overview of Heart Rate Variability Metrics and Norms”. In: *Front Public Health* 5 (2017), p. 258. ISSN: 2296-2565 (Print) 2296-2565 (Linking). DOI: 10.3389/fpubh.2017.00258. URL: https://www.ncbi.nlm.nih.gov/pubmed/29034226.

[62] A. Silvani, D. Grimaldi, S. Vandi, G. Barletta, R. Vetrugno, F. Provini, G. Pierangeli, C. Berteotti, P. Montagna, G. Zoccoli, and P. Cortelli. “Sleep-dependent changes in the coupling between heart period and blood pressure in human subjects”. In: *Am J Physiol Regul Integr Comp Physiol* 294.5 (2008), R1686–92. ISSN: 0363-6119. DOI: 10.1152/ajpregu.00756.2007. URL: https://www.ncbi.nlm.nih.gov/pubmed/18272662.

[63] Task-Force-of-the-European-Society-of-Cardiology-the-North-American-Society-of-Pacing-Electrophysiology. “Heart rate variability: standards of measurement, physiological interpretation and clinical use. Task Force of the European Society of Cardiology and the North American Society of Pacing and Electrophysiology”. In: *Circulation* 93.5 (1996), pp. 1043–65. ISSN: 0009-7322 (Print) 0009-7322 (Linking). URL: https://www.ncbi.nlm.nih.gov/pubmed/8598068.

[64] A. Tatasciore, M. Zimarino, R. Tommasi, G. Renda, G. Schillaci, G. Parati, and R. De Caterina. "Increased short-term blood pressure variability is associated with early left ventricular systolic dysfunction in newly diagnosed untreated hypertensive patients". In: *J Hypertens* 31.8 (2013), pp. 1653–61. ISSN: 1473-5598 (Electronic) 0263-6352 (Linking). DOI: 10.1097/HJH.0b013e328361e4a6. URL: https://www.ncbi.nlm.nih.gov/pubmed/23811997.

[65] J. F. Valencia, M. Vallverdu, A. Porta, A. Voss, R. Schroeder, R. Vazquez, A. Bayes de Luna, and P. Caminal. "Ischemic risk stratification by means of multivariate analysis of the heart rate variability". In: *Physiol Meas* 34.3 (2013), pp. 325–38. ISSN: 1361-6579 (Electronic) 0967-3334 (Linking). DOI: 10.1088/0967-3334/34/3/325. URL: https://www.ncbi.nlm.nih.gov/pubmed/23399982.

[66] J. F. Valencia, M. Vallverdu, R. Schroeder, A. Voss, R. Vazquez, A. Bayes de Luna, and P. Caminal. "Complexity of the short-term heart-rate variability". In: *IEEE Eng Med Biol Mag* 28.6 (2009), pp. 72–8. ISSN: 1937-4186 (Electronic) 0739-5175 (Linking). DOI: 10.1109/MEMB.2009.934621. URL: https://www.ncbi.nlm.nih.gov/pubmed/19914891.

[67] A. Voss, C. Fischer, R. Schroeder, H. R. Figulla, and M. Goernig. "Lagged segmented Poincare plot analysis for risk stratification in patients with dilated cardiomyopathy". In: *Med Biol Eng Comput* 50.7 (2012), pp. 727–36. ISSN: 1741-0444 (Electronic) 0140-0118 (Linking). DOI: 10.1007/s11517-012-0925-5. URL: https://www.ncbi.nlm.nih.gov/pubmed/22689265.

[68] A. Voss, C. Fischer, R. Schroeder, H. R. Figulla, and M. Goernig. "Segmented Poincare plot analysis for risk stratification in patients with dilated cardiomyopathy". In: *Methods Inf Med* 49.5 (2010), pp. 511–5. ISSN: 2511-705X (Electronic) 0026-1270 (Linking). DOI: 10.3414/ME09-02-0050. URL: https://www.ncbi.nlm.nih.gov/pubmed/20526525.

[69] A. Voss, M. Goernig, R. Schroeder, S. Truebner, A. Schirdewan, and H. R. Figulla. "Blood pressure variability as sign of autonomic imbalance in patients with idiopathic dilated cardiomyopathy". In: *Pacing Clin Electrophysiol* 35.4 (2012), pp. 471–9. ISSN: 1540-8159 (Electronic) 0147-8389 (Linking). DOI: 10.1111/j.1540-8159.2011.03312.x. URL: https://www.ncbi.nlm.nih.gov/pubmed/22268614.

[70] A. Voss, R. Schroeder, A. Heitmann, A. Peters, and S. Perz. "Short-term heart rate variability–influence of gender and age in healthy subjects". In: *PLoS One* 10.3 (2015), e0118308. ISSN: 1932-6203 (Electronic) 1932-6203 (Linking). DOI: 10.1371/journal.pone.0118308. URL: https://www.ncbi.nlm.nih.gov/pubmed/25822720.

7

Cardiorespiratory and cardiovascular variability analysis

7.1 Introduction

One of the most relevant challenges in biomedical research is the analysis of system response variability. This is true not only because a system's response variability represents the description of the patient's state, but also because it can mask comorbidities. Diseases like cardiomyopathies, which affect a large segment of the elderly population, are of particular interest, as they constitute one of the most common causes of death.

These pathologies may originate in an ischemic (ICM) or dilated (DCM) process of the heart. The reaction to this process, however, may be related to the variability of the cardiorespiratory and cardiovascular system response, which is associated with the baroreflex mechanism. Therefore, these systems can help in differentiating between these cardiomyopathies, which can lead to an improved and earlier diagnosis for these patients [8, 13].

Despite the symptomatic similarities between ischemic and dilated cardiomyopathies, they differ in etiology. For instance, ischemic cardiomyopathy is related to coronary artery disease, while dilated cardiomyopathy is characterized by the enlargement and weakening of the left ventricle. Several studies have proposed linear and non-linear techniques as a means to analyze these differences from a signal processing perspective [15, 14, 1]. An early study explored the differences in cardiovascular autonomic regulation between patients with ischemic and those with dilated cardiomyopathy [3].

Analyzing the interactions between the cardiovascular and respiratory systems could provide new insights into these cardiomyopathies, and contribute to the more accurate diagnosis of these diseases. In our previous work, we proposed analyzing the cardiovascular activity through the use of coupling analysis [12]. In this work, we introduce cardiorespiratory interaction as a means by which to analyze the behavior of the systems associated with ICM and DCM cardiomyopathies. We proposed a three-dimensional analysis that considered the relationship between the cardiac, respiratory and vascular systems. Based on vascular activity as the input and output of the baroreflex response, we evaluated the variability of these interactions. This novel approach introduces new information about the homeostatic control system and other internal relationships. The aim of this study was to analyze the suitability of cardiorespiratory and vascular interactions for the classification of ICM and DCM patients. However, we also characterized these interactions through features extracted from ECG, respiratory flow and blood pressure signals.

7.2 Database

A sample of 41 cardiomyopathy patients from the Heris dataset, presented in Chapter 3 (section 3.1), was used to explore the method described in this chapter. All of the patients selected had a New York heart association index (NYHA) ≥ 2, and were diagnosed with either ischemic cardiomyopathy (ICM - 24 patients) or dilated cardiomyopathy (DCM - 17 patients). In addition, 39 healthy subjects (CON) from the Healthy data set, also presented in Chapter 3 (section 3.4), were used as a reference. The clinical information of the patients from the Heris database is summarized in Table 7.1.

- Signal processing

For this study, we used the ECG, blood pressure (BP) and respiratory flow (RF) signals from the Heris and Healthy databases. Linear trends were removed, and in-house preprocessing tools were used to reduce noise, artifacts and spikes. All outliers were eliminated.

The beat-to-beat interval time series (BBI, ms) was extracted from the ECG signal by calculating the time between two consecutive R peaks. The systolic (SBP, mmHg) and diastolic (DBP, mmHg) blood pressure time series were cal-

Table 7.1. Clinical parameters of the Heris database (mean and standard deviation).

	ICM	**DCM**
Patients	24	17
Age [years]	65.54 ± 10.53	61.54 ± 12.27
Weight [Kg]	78.14 ± 14.22	77.40 ± 16.47
BMI [Kg/m^2]	27.55 ± 3.89	27.76 ± 5.77
NYHA	2.07 ± 0.28	2.00 ± 0.57
LVDD [mm]	60.83 ± 8.78	62.75 ± 4.27
AD [mm]	46.22 ± 7.67	44.62 ± 3.47
ProBNP	881.78 ± 1424.40	441.84 ± 1535.76
LVEF [%]	33.40 ± 11.49	33.47 ± 6.68

BMI: body mass index; **NYHA**: New York Heart Association functional classification; **LVDD**: left ventricular diastolic dimension; **AD**: auricular diameter; **ProBNP**: brain natriuretic peptide; **LVEF**: left ventricular ejection fraction.

culated by defining the maximum and minimum values of the BP in each heartbeat. The breathing duration (TT, s) time series was obtained by calculating the time between two consecutive respiratory cycles. Next, all of the time series were inspected and edited, if necessary. To analyze the interaction between these time series, they were resampled and synchronized using the linear interpolation method to 1 Hz. The new signals were then decimated to 0.25 Hz to analyze the changes in respiratory activity.

7.3 Methodology

To analyze the interaction between the cardiac, respiratory and vascular systems, we took the difference between two consecutive events as a new time series values, represented by,

$$\Delta X = X_{n+1} - X_n, \quad \forall n = 1, \; \dots \; , \; N, \tag{7.1}$$

being X either the BBI, SBP, DBP or TT time series, and N the total number of time series values.

To determine vascular activity, we defined a threshold associated with the increase, decrease or absence of change of the SBP or DBP variability, defined by:

$$ThX_v = \frac{\alpha \; (|max(\Delta X_v)| - |min(\Delta X_v)|)}{2}, \tag{7.2}$$

where ΔX_v is either ΔSBP or ΔDBP time series, and α is a factor that defines the percentage of the boundary value at which blood pressure values are considered as 'no change'. The dataset was normalized (zero mean and unit variance), and centered to zero. In this study, we defined $\alpha = 15\%$.

To analyze the variability of the vascular system, three new sub-spaces were defined in accordance with the ThX_v threshold: 'up' referred to increasing values, 'no change' referred to values between the negative and positive threshold, and 'down' referred to decreasing values. Thus, the values of each ΔX_v are classified as:

- *Up* (u): $\Delta X_v > ThX_v$

- *No change* (nc): $-ThX_v \leq \Delta X_v \leq ThX_v$

- *Down* (d): $\Delta X_v < -ThX_v$

7.3.1 Three-dimensional representation

To evaluate the variability of cardiorespiratory activity associated with vascular behavior, a three-dimensional representation was generated for each sub-space: 'up', 'no change' and 'down'. This representation presents the relationship between changes in the ΔBBI, ΔTT, ΔSBP and ΔDBP time series. Figure 7.1 is an example of the representation of these relationships for a subject from the control group (CON), an ischemic patient (ICM), and a dilated patient (DCM) based on ΔSBP.

Several parameters were extracted from this three-dimensional representation in order to characterize their interactions. For each subject/patient scatterplot, a polygon that represents the projection of the cardiac and respiratory activity based on vascular behavior (ΔSBP and ΔDBP) was fitted. The vertices of the polygon were defined including 95% of each set of values. To characterize the geometry of each polygon, its area (ΔXY_A) and centroid (C_x,C_y) were defined by:

$$\Delta XY_A = \frac{1}{2}\sum_{i=0}^{n-1}(V_{X_i}V_{Y_{i+1}} - V_{X_{i+1}}V_{Y_i}),$$

$$C_x = \frac{1}{6A}\sum_{i=0}^{n-1}(V_{X_i} + V_{X_{i+1}})(V_{X_i}V_{Y_{i+1}} - V_{X_{i+1}}V_{Y_i}),$$

$$C_y = \frac{1}{6A}\sum_{i=0}^{n-1}(V_{Y_i} + V_{Y_{i+1}})(V_{X_i}V_{Y_{i+1}} - V_{X_{i+1}}V_{Y_i}), \tag{7.3}$$

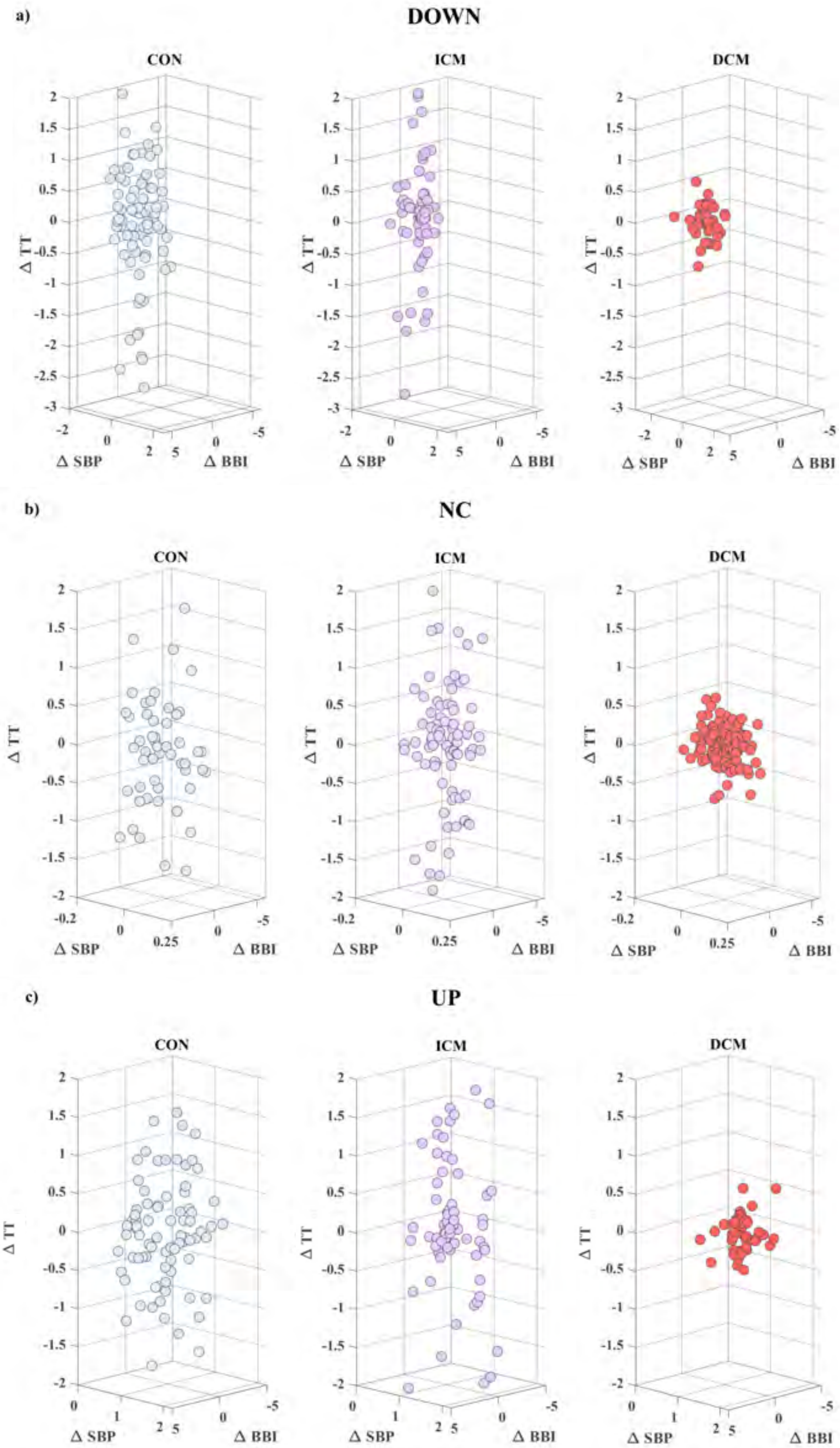

Figure 7.1. Cardiac (ΔBBI) vs respiratory (ΔTT) time series considering (ΔSBP) a) down, b) no change, and c) up activity, for a CON subject, an ICM patient and a DCM patient.

where V_{X_i} and V_{Y_i} are coordinates of the ith vertex, and n is the total number of vertices. The area was normalized in accordance with the number of vertices (ΔXY_{A_v}) and samples (ΔXY_{A_n}). In addition, the mean distance between each sample and centroid was measured (ΔXY_{dc}), and the probability of occurrence of samples for each triangle of the polygon (ΔX_p) was calculated.

The morphology of the polygon was also analyzed using all the triangles that form it. First, the mean area of all triangles (ΔXY_{A_r}) and the probability of occurrence of the samples (ΔXY_{pr}) were calculated, and then the mean angles formed were calculated: one in the centroid with two consecutive vertices (ΔXY_β) and a second in the vertex with the centroid (ΔXY_θ). Figure 7.2 is an example of the morphological characterization of a scatterplot for cardiorespiratory activity, when systolic vascular activity decreased, illustrated for a CON subject. In addition, for the ΔBBI and ΔTT time series, statistical parameters like mean (ΔX_m), standard deviation (ΔX_{sd}), kurtosis (ΔX_K), skewness (ΔX_{Sk}), interquartile range (ΔX_{IQR}), and coefficient of variation (ΔX_{CV}) were obtained for each sub-space (up, no-change, and down). Table 7.2 shows a summary of the indices considered.

Table 7.2. Index description

Index	**Description**
ΔX_m-z	ΔX time series mean value
ΔX_{sd}-z	ΔX time series standard deviation
ΔX_K-z	ΔX time series kurtosis
ΔX_{Sk}-z	ΔX time series skewness
ΔX_{CV}-z	ΔX time series coefficient of variation
ΔX_{IQR}-z	ΔX time series interquartile range
ΔX_p-z	ΔX time series probability of occurrence
ΔX_d-z	ΔX time series mean distance
ΔXY_A-z	Area of the fitting polygon for the X and Y time series
ΔXY_{A_n}-z	Area of the fitting polygon normalized by the number of points
ΔXY_{A_v}-z	Area of the fitting polygon normalized by the number of vertices
ΔXY_n-z	Number of vertices of the fitted polygon
ΔXY_{dc}-z	Mean distance between each sample and the centroid
ΔXY_θ-z	Mean angle formed by one vertex and by the centroid
ΔXY_β-z	Mean angle formed by the centroid and by two vertices
$\Delta XY_{\theta\beta}$-z	Mean difference between ΔXY_θ-z and ΔXY_β-z
ΔXY_{pr}-z	Mean number of points inside of each triangle formed by two vertices and the centroid
ΔXY_{A_r}-z	Mean area of triangles formed by two vertices and the centroid

X and Y refers to either, BBI or TT time series; z refers to increasing (up), no change (nc) or decreasing activity (d).

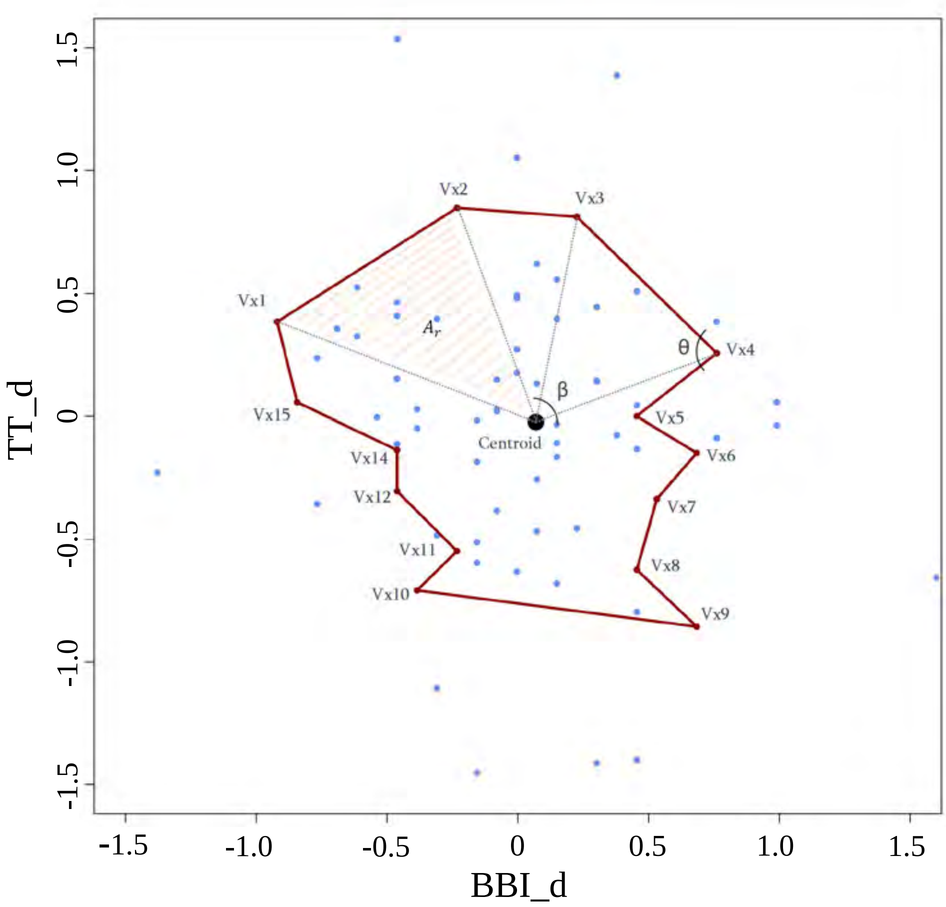

Figure 7.2. Scatterplot of cardiorespiratory activity for decreasing systolic vascular activity in a CON subject. $V_{x1} - V_{x15}$: vertices of the polygon; A_r: area of the triangle formed by vertices V_{x1} and V_{x2}, and the centroid; θ and β: angles formed on the V_{x4} vertex and the centroid, respectively.

7.3.2 Classification and statistical analysis

A mathematical description of the support vector machines (SVM) classifier is presented in Chapter 5 (Section 5.3.2). The classification models were optimized as described in Chapter 6 (Section 6.3.8). The kernels considered for the SVM optimization were the Gaussian, Laplace, and ANOVA. The indices with statistically significant differences and low correlations were used in pairs to build a series of SVM models.

A Mann-Whitney non-parametric statistical test was applied to evaluate the statistically significant differences between all the indices. Any index with a p-value $\leq$ 0.05 was considered statistically significant. The leave-one-out cross-validation method was used to validate the results. The classification results are presented in terms of accuracy (Acc), sensitivity (Sn), and specificity (Sp).

7.4 Results

This work aimed to characterize the cardiovascular and cardiorespiratory activity of patients with ischemic or dilated cardiomyopathy. A total of 168 indices were obtained during the characterization process. The results were analyzed considering the following comparisons:

- Ischemic vs dilated cardiomyopathy patients (ICM vs DCM)

- Cardiomyopathy patients vs control subjects (CMP vs CON)

- Ischemic cardiomyopathy patients vs control subjects (ICM vs CON)

- Dilated cardiomyopathy patients vs control subjects (DCM vs CON)

Figure 7.3 provides an example of the characterization of cardiorespiratory activity based on systolic blood pressure activity according to the different subspaces: down (a, b, c), no-change (d, e, f), and up (g, h, i) for a CON subject (a, d, g), an ICM patient (b, e, h), and a DCM patient (c, f, i).

In the comparison of ICM and DCM patients, 9 indices presented statistically significant differences, and relatively low correlation. For the CMP patients vs CON group, 13 indices presented statistical differences. When each pathology was compared to the CON group, 10 indices presented differences when compared to ICM patients, and 19 when compared to DCM patients. These indices were used to build different SVM models, determining the best classifiers in each case. Tables 7.3 and 7.4 present the most relevant indices for each comparison in terms of mean value and standard deviation.

Table 7.3. ICM vs DCM significant indices, in terms of mean and standard deviation.

ICM vs DCM			
Index	**ICM (24)**	**DCM (17)**	**p-value**
SBP-ΔTT_m-d	0.007 ± 0.12	-0.07 ± 0.07	0.02
SBP-ΔTT_{sd}-u	1.00 ± 0.17	0.89 ± 0.14	0.02
SBP-ΔBBI_{sd}-nc	0.85 ± 0.28	1.09 ± 0.18	0.009
SBP-ΔBBI_TT_θ-u	76.25 ± 29.47	49.23 ± 39.59	0.01
SBP-ΔTT_{CV}-d	-3.15 ± 31.10	-31.2 ± 52.2	0.002
DBP-ΔTT_{CV}-d	1.05 ± 0.15	0.96 ± 0.14	0.03

The SBP-ΔTT_m-d and SBP-ΔTT_{sd}-u were the indices used to build the optimal SVM model for the ICM vs DCM comparison, achieving 92.7% accuracy, 94.1% sensitivity and 91.7% specificity. The optimal model for the CMP vs

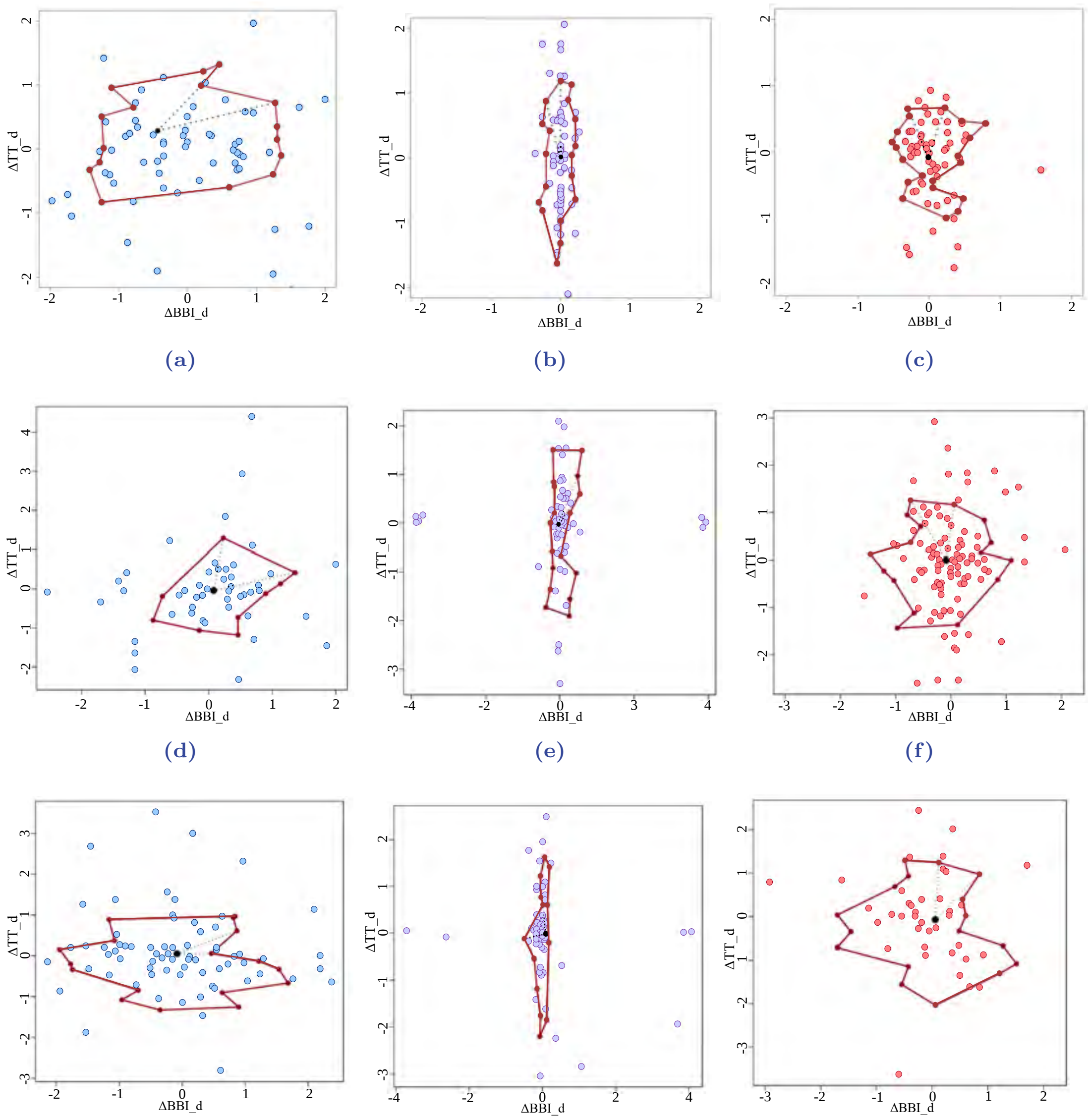

(a) **(b)** **(c)**

(d) **(e)** **(f)**

(g) **(h)** **(i)**

Figure 7.3. Characterization of cardiorespiratory activity based on the sub-space for systolic blood pressure activity: down for a) CON subject, b) ICM and c) DCM patients; no-change for d) CON subject, e) ICM and f) DCM patients; and up for g) CON subject, h) ICM and i) DCM patients.

Table 7.4. Significant indices for CMP vs CON, ICM vs CON, and DCM vs CON comparisons, presented in terms of mean value and standard deviation.

	CMP vs CON		
	CMP (41)	**CON(39)**	**p-value**
DBP-ΔBBI_p-u	61.60 ± 18.73	87.43 ± 13.18	$<$ 0.00001
DBP-$\Delta BBI\_TT_{A_v}$-u	0.17 ± 0.15	0.27 ± 0.09	0.004
SBP-ΔBBI_{IQR}-u	0.66 ± 0.53	1.09 ± 0.45	0.00006
SBP-ΔBBI_{IQR}-nc	0.60 ± 0.47	1.04 ± 0.43	0.00007
SBP-ΔBBI_{IQR}-d	0.62 ± 0.48	1.03 ± 0.45	0.0003
	ICM vs CON		
	ICM (24)	**CON (39)**	**p-value**
SBP-ΔBBI_K-nc	14.70 ± 24.17	4.19 ± 8.55	0.01
DBP-ΔBBI_p-u	61 ± 15.16	87.43 ± 13.18	$<$ 0.00001
SBP-ΔBBI_{IQR}-d	0.74 ± 0.57	1.09 ± 0.45	0.004
SBP-ΔTT_{CV}-d	-3.15 ± 31.10	-8.43 ± 54.18	n.s
	DCM vs CON		
	DCM (17)	**CON (39)**	**p-value**
SBP-ΔTT_{IQR}-u	0.63 ± 0.20	0.75 ± 0.21	0.03
SBP-ΔBBI_TT_A-u	1.78 ± 1.73	4.02 ± 1.80	0.00009
SBP-ΔBBI_{IQR}-d	0.54 ± 0.46	1.09 ± 0.45	0.0001
SBP-ΔTT_{CV}-d	-31.2 ± 52.2	-8.43 ± 54.18	0.006

CON comparison was built with the DBP-ΔBBI_p-u and DBP-$\Delta BBI\_TT_{A_v}$-u, obtaining 86.2% accuracy, 82.9% sensitivity and 89.7% specificity. The indices for the optimal ICM vs CON model were the SBP-ΔBBI_K-nc and DBP-ΔBBI_p-u, achieving 88.9% accuracy, 87.5% sensitivity and 89.7% specificity. The SBP-ΔTT_{IQR}-u and SBP-ΔBBI_TT_A-u indices were used to build the SVM model for DCM vs CON, obtaining 87.5% accuracy, 76.5% sensitivity and 92.3% specificity. The Gaussian kernel was used in both the ICM vs DCM and the DCM vs CON SVM models; the Laplace kernel was used in the CMP vs CON and the ICM vs CON comparisons. The classification results and the SVM scoreplot are shown in Table 7.5 and Figure 7.4, respectively.

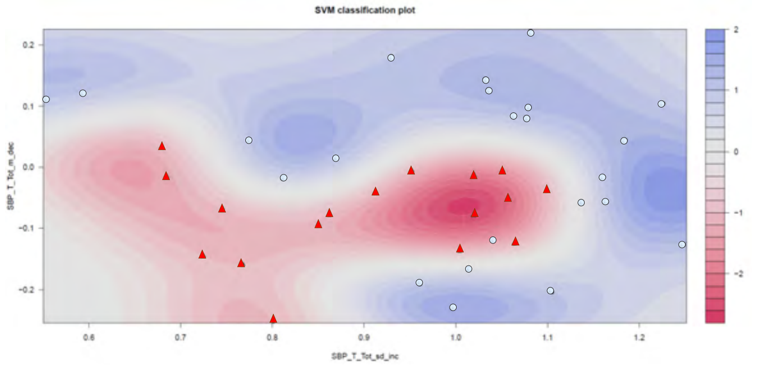

(a)

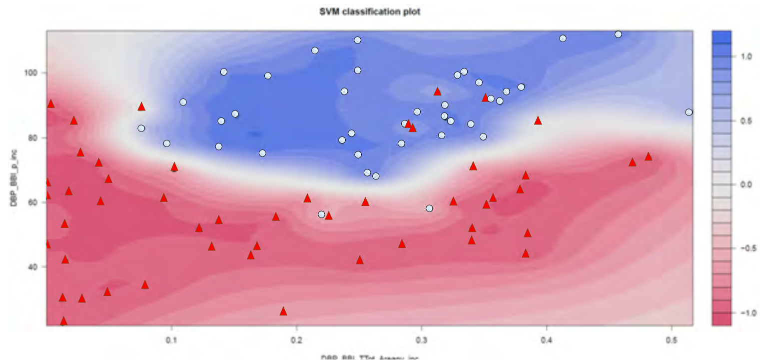

(b)

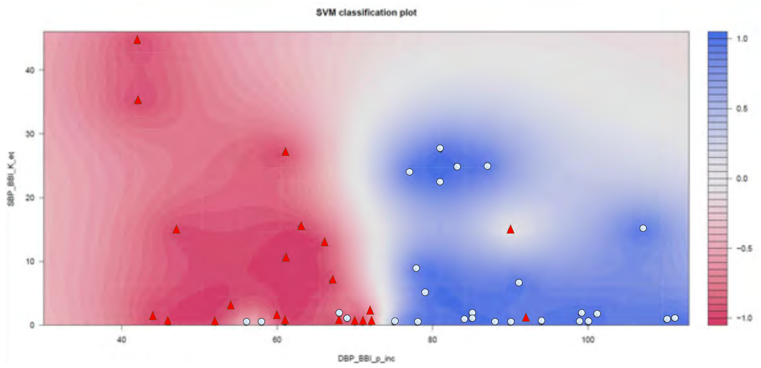

(c)

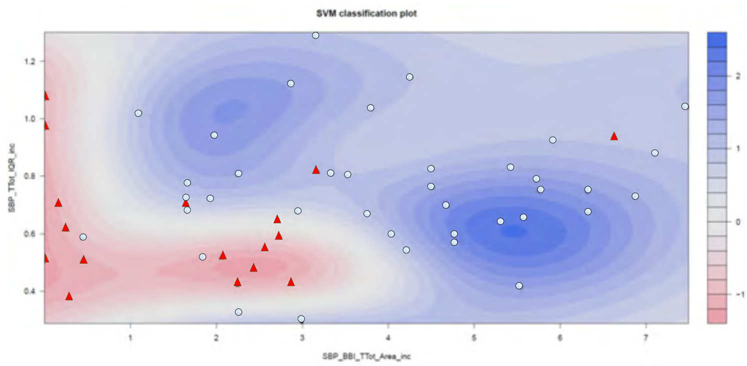

(d)

Figure 7.4. SVM classification plots considering: **(a)** ICM vs DCM patients, **(b)** CMP patients vs CON subjects, **(c)** ICM patients vs CON subjects, and (d) DCM patients vs CON subjects.

Table 7.5. Accuracy (Acc), sensitivity (Sn), and specificity (Sp), obtained with the best SVM model for each classification group.

Groups	C	σ	Acc(%)	Sn(%)	Sp(%)
ICM vs DCM	2.2	1.5	92.7	94.1	91.7
CMP vs CON	1	1.5	86.2	82.9	89.7
ICM vs CON	1	2	88.9	87.5	89.7
DCM vs CON	5	0.8	87.5	76.5	92.3

7.5 Discussion and conclusions

A novel method to analyze the three-dimensional relationships between the cardiac, vascular and respiratory systems was proposed. The interaction between cardiorespiratory and vascular activity was explored and characterized to analyze the behavior of these systems in patients diagnosed with ischemic or dilated cardiomyopathy. Based on indices related to geometrical representation and statistical measurements from the time series that describe these systems, this method proposes to reduce the complexity of the analysis in contrast with other non-linear methods. From a three-dimensional representation of these time series, a bivariate behavior of two of them is analyzed in function of the dynamical changes of the third. Afterwards, the best indices were used to classify these patients, through the introduction of new information about the response of the cardiac and respiratory systems, based on vascular activity.

Our results indicate a decreasing respiratory response in DCM patients when systolic blood pressure activity decreases (SBP-ΔTT_m-d), in contrast to the more stable response in ICM patients. In addition, ICM patients exhibited higher variance in respiratory activity a as response to decreased systolic or diastolic blood pressure activity (SBP-ΔTT_{CV}-d,DBP-ΔTT_{CV}-d).

The decreased respiratory activity observed during drops in systolic blood pressure in DCM patients suggests a faster breathing response to decreasing blood pressure. Changes in breathing rhythm are known to affect blood pressure levels [11]. We hypothesize that the respiratory activity in DCM patients compensates for the impaired cardiac-dependent regulation of blood pressure.

The comparison of SBP activity when the values corresponds to 'no change' revealed that cardiac response was more stable in ICM patients (SBP-ΔBBI_{sd}-nc), than in DCM patients. This may be a sign of healthier autonomic regulation in ICM patients, who have retained some parasympathetic responsiveness [7]. Some studies have reported that DCM patients experience impairment of cardiac autonomic regulation [4, 9]. Therefore, this impairment may explain the differences observed in the cardiac behavior of DCM patients vs ICM patients in contrast to the ischemic-related etiology in ICM patients. [7].

In the presence of increased SBP activity, the respiratory response is more disperse in ICM patients than in DCM patients (SBP-ΔTT_{sd}-u). These differences could be attributed to stimulation of the vagal pulmonary mechanoreceptors, which, mechanical in origin, are not influenced by ischemic stimulus [6]. As increased respiratory variability has been observed in elderly people in a previous work [5], we suggest that the differences found in DCM patients are due to a more pronounced impairment of their autonomous regulation.

In addition, in cases of increased in SBP activity, the mean angle formed by each vertex and the centroid of its fitting cloud of points associated with cardiorespiratory activity (SBP-ΔBBI_TT_{Θ}-u) had higher values in ICM patients, while the values of DCM patients were more scattered. These patterns suggest that ICM patients tend to have more stable cardiorespiratory activity than DCM patients.

An analysis of overall cardiac behavior among CMP patients, in general showed a reduced response to increasing DBP activity (DBP-ΔBBI_p-u) compared to CON subjects. The differences found in the DBP-$\Delta BBI\_TT_{A_v}$-u indicated lower cardiac and respiratory variability in CMP patients when DBP activity increases. The interquartile range of the cardiac activity of CMP patients across every SBP pattern considered (SBP-ΔBBI_{IQR}-u, SBP-ΔBBI_{IQR}-nc, SBP-ΔBBI_{IQR}-d) presented lower values when compared to the subjects of the CON group. The results of these indices indicate lower heart rate variability in patients with cardiomyopathies. Lower cardiac and respiratory variabilities are typically associated with a cardiovascular dysfunction [2, 10]. We hypothesize that the cardiac and respiratory systems in CMP patients have a more limited ability to regulate incremental changes in BP compared to CON subjects.

A similar behavior was observed for increased DBP activity, when ICM patients were compared to the CON subjects (DBP-ΔBBI_p-u), and the cardiac activity was lower in ICM patients. The overall observations regarding the interquartile range of the cardiac activity for decreasing blood pressure were also present in the ICM vs CON (SBP-ΔBBI_{IQR}-d) and DCM vs CON (SBP-ΔBBI_{IQR}-d) comparisons. These indices suggest that cardiac activity is diminished in both ICM and DCM patients when compared with the CON subjects.

Cardiac and respiratory variability differences were also found when the DCM patients were compared to the CON subjects for increased SBP activity (SBP-ΔBBI_TT_A-u), and lower values were recorded in DCM patients. We found no significant differences between respiratory variance (SBP-ΔTT_{CV}-d) when comparing ICM patients and CON subjects for decreasing blood pressure activity. In contrast, differences were recorded in respiratory variance between DCM patients and CON subjects. These results suggest specific patterns among DCM patients in their respiratory response to decreasing blood pressure activity.

In conclusion, the analysis of the interaction between cardiac and respiratory activity and blood pressure provides novel insight into the classification of patients with this type of disease. We found respiratory patterns that are present only in dilated cardiomyopathy patients. In general, the cardiac and respiratory variabilities presented lower values in these patients. The work presented in this chapter may provide physicians with new symptom-independent information about these types of cardiomyopathies, which could help to improve the diagnosis of these patients. This method not only serves to analyze the behavior of ischemic and dilated cardiomyopathy patients, but also introduces a new procedure with which to analyze the dynamic behavior between other related systems. The results discussed in this chapter should be validated using a larger dataset.

Chapter 7 bibliography

[1] C. Davos, L. Davies, and M. Piepoli. “The Effect of Baroreceptor Activity on Cardiovascular Regulation.” In: *Hellemoc journal of cardiology* (2002).

[2] J. Dekker, R. Crow, A. Folsom, P. Hannan, D. Liao, C. Swenne, and E. Schouten. “Low heart rate variability in a 2-minute rhythm strip predicts risk of coronary heart disease and mortality from several causes: the ARIC Study. Atherosclerosis Risk In Communities.” In: *Circulation* (2008).

[3] J. Freeman, F. Dewey, D. Hadley, J. Myers, and V. Froelicher. “Autonomic Nervous System Interaction With the Cardiovascular System During Exercise.” In: *Progress in Cardiovascular Diseases* (2006).

[4] Y. Goldman and J. Keeling. “Heart rate variability in idiopathic dilated cardiomyopathy: relation to disease severity and prognosis.” In: *Heart.* (1997).

[5] D Kaplan, M. Furman, S. Pincus, S. Ryan, S. Lewis, A. Lipsitz, and A. Goldberger. “Aging and the complexity of cardiovascular dynamics.” In: *Biophysiological Journal.* (1991).

[6] F. Lombardi, C. Casalone, G. Malfatto, M. Pagani, and A. Malliani. “Global versus regional myocardial ischaemia: differences in cardiovascular and sympathetic responses in cats.” In: *Cardiovascular Research.* (1984).

[7] G. Malfatto, G. Branzi, S. Gritti, L. Sala, R. Bragato, G. Battista, L. Gastone, and M. Facchini. “Different baseline sympathovagal balance and cardiac autonomic responsiveness in ischemic and non-ischemic congestive heart failure.” In: *European Journal of Heart Failure.* (2001).

[8] R. Medina, I. Panidis, J. Morganroth, M. Kotler, and G. Mintz. “The value of echocardiographic regional wall motion abnormalities in detecting coronary artery disease in patients with or without a dilated left ventricle.” In: *American Heart Journal* (1985).

[9] M. Momose, L. Tyndale-Hines, F. Bengel, and M. Schwaiger. “How heterogeneous is the cardiac autonomic innervation?” In: *Basic Research in Cardiology.* (2001).

[10] A. Musialik-Lydka, B. Sredniawa, and S. Pasyk. “Heart rate variability in heart failure.” In: *Kardiol Pol* (2003).

[11] M. Nuckowska, M. Gruszecki, J. Kot, J. Wolf, W. Guminski, A. Frydrychowski, J. Worek, K. Narkiewicz, and P. Winklewski. "Impact of slow breathing on the blood pressure and subarachnoid space width oscillations in humans." In: *Scientific Reports.* (2019).

[12] J. Rodriguez, S. Schulz, A. Voss, and B. Giraldo. "Cardiovascular Coupling-Based Classification of Ischemic and Dilated Cardiomyopathy Patients." In: *41st Annual International Conference of the IEEE Engineering in Medicine and Biology Society (EMBC)* (2019).

[13] S. Sawada, T. Ryan, D. Segar, L. Atherton, N. Fineberg, C. Davis, and H. Feigenbaum. "Distinguishing ischemic cardiomyopathy from nonischemic dilated cardiomyopathy with coronary echocardiography." In: *Journal of the American College of Cardiology* (1985).

[14] P. Stein, P. Domitrovich, N. Hui, P. Rautaharju, and J. Gottdiener. "Sometimes Higher Heart Rate Variability Is Not Better Heart Rate Variability: Results of Graphical and Nonlinear Analyses." In: *Journal of Cardiovascular Electrophysiology* (2005).

[15] A. Voss, R. Schroeder, P. Caminal, M. Vallverdú, H. Brunel, I. Cygankiewicz, R Vázquez, and A. Bayés de Luna. "Segmented Symbolic Dynamics for Risk Stratification in Patients with Ischemic Heart Failure." In: *Cardiovascular Engineering and Technology* (2010).

8
Conclusions

This research has focused on the study, characterization and interpretation of the cardiac, vascular and respiratory patterns of cardiomyopathy patients with different etiologies and at different levels of sudden cardiac death risk. We analyzed the characteristics extracted from electrocardiographic, blood pressure and respiratory flow signals, and to do this more effectively, we developed an artifact reconstruction method that allowed us to improve the quality of signals corrupted by artifacts. A range of studies were conducted for the purpose of extracting new information about the cardiac, vascular and respiratory systems as well as autonomic control mechanisms to help improve the sudden cardiac death risk stratification of heart failure patients, and to contribute to the diagnosis of cardiomyopathy patients considering the etiology of their disease.

In order to extract this new information, we characterized time series extracted from ECG, blood pressure and respiratory flow signals by means of various advanced signal processing techniques, including time-frequency analysis, linear and non-linear analysis, coupling analysis, as well as techniques based on the variability of the interaction between the cardiovascular and cardiorespiratory systems.

The first part of this research aimed to design of a novel automatic artifact reconstruction method for quasi-periodic signals. We have proposed a technique that allows artifact events to be replaced by nearby physiological cycles, maintaining the dynamic variability of the reconstructed signal. The method was tested using simulated and real biomedical signals. In addition, we performed both an automatic and visual validation of the reconstruction, considering the possible artifacts missing, incorrectly reconstructed cycles, and the quality of the reconstruction. In all cases, the method detected more than 97% of the artifacts present in the signals, and incorrectly reconstructed cycles and low-quality reconstructions occurred in less than 1% of the reconstructions.

In the second part, two different studies were conducted to classify patients with different cardiomyopathies according to their cardiovascular risk stratification. The first is based on the cardiac death risk stratification of patients according to their left ventricular ejection fraction, through the Poincaré plot analysis. Based on the left ventricular ejection fraction index, a cardiac death risk level was assigned as either low risk (LR, LVEF $> 35\%$) or high risk (HR, LVEF $\leq 35\%$). Parameters related to the electrophysiological behavior of the cardiac, vascular and respiratory systems, based on their time series (BBI, SBP and TT, respectively) were extracted. New indices associated with cardiorespiratory and vascular variabilities were used to characterize the patients and predict their cardiovascular risk based on their left ventricular ejection fraction. These indices could contribute to improve the clinical studies associated with the HRV in the diagnostic of these pathologies.

Statistical and correlation analyses were performed in order to determine the most relevant indices. The support vector machines and the linear discriminant analysis pattern recognition methods were applied to classify the patients by their cardiovascular LVEF-based risk. Our results suggest that high risk patients (LVEF $\leq 35\%$) have reduced parasympathetic activity which is compensated by the sympathetic autonomic response.

The second study we report here was about the risk stratification of idiopathic cardiomyopathy patients through coupling analysis. Based on a two year follow-up period, the patients who died due to cardiac related episodes were stratified as at high risk of sudden cardiac death. The cardiac and vascular variabilities were explored through the coupling analysis of the cardiac, vascular, and respiratory systems by means of several linear and non-linear characterization techniques. This new indices allowed to classify the risk of sudden cardiac death, without prior characterization of patients, using a cascade model.

Statistical and correlation analyses were used to determine the most relevant indices. The support vector machines method was used to predict which patients were at high risk of sudden cardiac death. Our results suggest that a gradual decrease in heart rate variability and a simultaneous increase in blood pressure variability could be related to an increased risk of sudden cardiac death.

We hypothesize that a dysfunction of the vagal activity, and in general of the baroreflex mechanism as a whole, prevents the body from correctly maintaining circulatory homeostasis. This reduction in vagal activity and increase in the sympathetic influence exposes the cardiovascular system to recurrent states of stress, which contribute to further worsening the condition over time.

The third part relates to the classification of ischemic and dilated cardiomyopathy patients by etiology through the analysis of their cardiac, vascular, and respiratory variabilities. The patients considered in this research were diagnosed as having either ischemic or dilated cardiomyopathy. Vascular activity was analyzed as both the input and output of the baroreflex and chemoreflex mechanisms by looking at changes in their responses and considering three different stages: increasing, unchanged, and decreasing values. The cardiorespiratory variability for these stages was analyzed using statistical and geometrical methods. A new method to analyze multivariate three-dimensional coupling systems was proposed. New indices based on the geometrical distribution of the interaction between these coupled systems allowed to describe the bivariate behavior of two of them in function of the dynamical changes of the third.

Statistical and correlation analyses were performed in order to identify the most significant indices. The support vector machines method was used to classify the patients into either the ischemic or dilated cardiomyopathy group. Our results suggest that dilated cardiomyopathy patients exhibit specific patterns in their respiratory responses in the presence of decreasing blood pressure activity.

The original contributions of this thesis focus on the identification and interpretation of new indices that make the risk stratification and etiology classification of cardiomyopathy patients possible. This has allowed us to develop tools that could help improve the earlier diagnosis of these patients, and introduce new knowledge about these pathologies.

One of the limitations of this research is the size of datasets used. Thence, we used the leave-one-out cross-validation method to validate our results. Nevertheless, the results seem significantly promising, and should be validated with a larger dataset. Another limitation of this work is the great variability in the physiological response that patients of these pathologies present. The complex interactions between the cardiac, vascular and respiratory systems impose major limitations and give rise to different levels of complexity in the analysis of their responses. But, at the same time, these challenges make conducting this type of research more interesting, and give impetus to the pursuit of answers beyond the obvious.

8.1 Artifact reconstruction

When analyzing physiological signals with pseudo-cycles, it is sometimes necessary to apply solutions to mitigate the effects of artifact events present in the signals. In this thesis, we present a novel method for artifact reconstruction applied to biomedical signals that allows for the recovery of segments affected by the disconnection of the device during recording, by noise caused by the instrumentation, or other types of erratic records, caused by processes unrelated to the physiological function being studied. Below, we summarize our contributions on the automatic artifact reconstruction method.

In [11], we presented the first part of this work, the reconstruction method applied to blood pressure signals (a quasi-periodic signal) to recover segments affected by calibration episodes. The proposed method was successful in detecting the calibration episodes and reconstructing these segments in each tested signal.

In contrast to previous studies related to artifact reconstruction methods [3, 10, 6, 9], this novel method consists of a completely automatic reconstruction process using only the affected signal, and not requiring additional channels or devices. This is possible because it uses the information of the morphology of the signal to perform the whole analysis, detection and reconstruction processes. So, the performance of the method relies on the morphological differences between the artifacts and the physiological cycles. This method is therefore recommended for application in signals whose artifacts differ morphologically from the pseudo-cycles. Introducing a reconstruction step, if necessary, before the study of these types of physiological signals could contribute not only improving studies associated with these cycles, but also to guaranteeing the integrity of the information associated with the dynamic responses of the related systems.

8.2 Risk stratification

The study, characterization, and interpretation of cardiac, vascular and respiratory interactions and their variabilities, and the effect of the baroreflex control mechanisms on blood pressure, provide improved information through new indices related to sudden cardiac death risk of patients with cardiomyopathies. The pathological values of these indices have been compared to values of healthy subjects. Below, we summarize our contributions in relation to the risk stratification of sudden cardiac death patients.

Our studies based on the characterization of the Poincaré plot analysis [17, 16, 18] examined the risk stratification of cardiomyopathy patients by their left ventricular ejection fraction level. Electrocardiographic, blood pressure, and respiratory flow signals were analyzed through time series related to heart and respiratory rates and blood pressure variability. Using the Poincaré plot method applied to these time series, several indices were identified as means to characterize the variability and dispersion of cardiac, vascular and respiratory system response in heart failure patients. These indices were analyzed to determine which ones presented statistically significant differences for subsequent use in building support vector machine-based models. Through this analysis, we obtained powerful indices to predict the cardiovascular risk of cardiomyopathy patients by means of their left ventricular ejection fraction.

In general, patients with a lower left ventricular ejection fraction exhibited lower heart rate variability. Compared to the control subjects, all the system responses analyzed in the patients occurred at a slower rate. The results suggest that patients with lower ejection fractions have reduced parasympathetic activity, and that this impairment is being compensated by the sympathetic autonomic response. Therefore, the study of the cardiac, vascular and respiratory systems through the Poincaré plot analysis can assess indices that may be useful in stratifying cardiovascular risk based on the left ventricular ejection fraction.

In our coupling analysis-based studies [19, 13], we proposed a methodology for the sudden cardiac death risk stratification of idiopathic cardiomyopathy patients using coupling analysis. In this study, according to the database used, the cardiac death risk of each patient was determined from the result of a two year follow-up period. Patients who died during this period were stratified as at high risk of sudden cardiac death. Through the coupling analysis of the time series extracted from the ECG and blood pressure signals, several indices were extracted using different non-linear techniques. These indices were analyzed to determine their statistical power to differentiate between these groups of patients. Afterwards, the most significant indices were used to build support vector machine-based classification models.

Our findings revealed some of the complex interactions that take place within autonomic regulation. For instance, our results suggest that there is a gradual decrease in heart rate variability and an increase in blood pressure variability as sudden cardiac death risk increases. We found that the strength of the cardiovascular and diastolic-systolic coupling was stronger in pathological conditions, suggesting an autonomic pathological behavior [2, 8]. Our results support the idea that the commonly used techniques for the analysis of the time and frequency domain of HRV are insufficient for the effective risk stratification of idiopathic cardiomyopathy patients. However, the combination of linear and non-linear HRV analysis as well as non-linear coupling analysis seems to be a promising tool for risk assessment in idiopathic cardiomyopathy patients [21, 20, 1].

We conclude that the pathological behaviors described in this study are caused mainly by the inability of the cardiac and vascular systems of high risk patients to maintain circulatory homeostasis, leading to states of cardiovascular stress that trigger compensatory mechanisms that increasingly worsen their condition. On the other hand, we introduced a novel cascade model that successfully classified subjects into different levels of sudden cardiac death risk. Therefore, the coupling analysis-based indices introduced could be a suitable means with which to improve the sudden cardiac death risk stratification of idiopathic cardiomyopathy patients.

8.3 Cardiomyopathy classification

Through the non-linear analysis of cardiac, vascular and respiratory activity we were able to classify cardiomyopathy patients by the etiology of their disease. The observed differences between the pathological patterns associated with the most relevant indices were studied, and their physiological implications interpreted.

In our studies based on joint symbolic dynamics [5, 12, 4], patients who suffered from either ischemic or dilated cardiomyopathy were successfully classified by etiology. The time series extracted from the electrocardiographic and blood pressure signals were characterized using the joint symbolic dynamics method. The indices obtained were statistically analyzed and the most suitable for classification tasks were chosen. The support vector machines and principal component analysis methods were used to build classification models.

We found a monotonous pattern in the cardiovascular interaction that is less prevalent in dilated cardiomyopathy patients. We speculate that this difference may occur due to the degeneration of the autonomous baroreflex control, which is typical in this etiology. Therefore, joint symbolic dynamics could provide indices that are useful for classifying patients with different cardiomyopathies.

In our coupling-based etiology classification study [15], ischemic and dilated cardiomyopathy patients were classified by etiology. The cardiovascular and respiratory systems were studied in terms of couplings. Several non-linear methods were applied to characterize the time series extracted from electrocardiographic, blood pressure and respiratory flow signals. The most significant indices were obtained using statistical analysis, and the etiologies of the patients were classified through support vector machine models.

Our results suggest that there are behavioral baroreflex differences between ischemic and dilated cardiomyopathy patients, with lower short-term variability in ischemic patients. The values of the tachycardic fluctuations were lower in cardiomyopathy patients. Therefore, the coupling analysis of the cardiac, vascular, and respiratory systems could provide indices that are useful for cardiomyopathy etiology classification.

In our most recent publication [14], we analyzed the blood pressure as both the input and output of the baroreflex and chemoreflex autonomic mechanisms to identify indices that could help to classify patients with ischemic and dilated cardiomyopathy. Vascular activity was divided into sub-spaces considering three different types of vascular response increasing, no-change, and decreasing based on an activity threshold. The signals were analyzed through cardiac and respiratory time series considering the vascular sub-spaces using a scatter plot representing the local difference between two consecutive physiological cycles. The resulting plots were studied by extracting indices obtained by statistical and geometrical analyses. Then, a reduced dimensionality process was applied, and the indices with high statistical significance and low correlation between them were chosen. The best indices were used to build support vector machine-based classification models.

We found recurring respiratory patterns related to decreasing blood pressure in dilated cardiomyopathy patients. We hypothesize that the differences observed in respiratory system behavior are related to respiratory compensation for the impaired cardiac regulation associated with blood pressure. These differences were observed when dilated cardiomyopathy patients were compared to the ischemic patients, and also when they were compared to the control group. Additionally, the dispersion of the respiratory activity in ischemic patients is significantly higher when blood pressure increases.

The differences reflected in these results point to a more pronounced deterioration of autonomic regulation in dilated cardiomyopathy patients, since the vagal pulmonary mechanoreceptors are not influenced by ischemic stimulus [7]. In general, the cardiac and respiratory variabilities presented lower values in patients than in control subjects. Therefore, the analysis of the interaction between cardiac and respiratory activity and blood pressure could constitute a novel breakthrough in the classification of patients by etiology. It is worth mentioning that this method could not only be used to analyze the cardiorespiratory behavior in cardiomyopathy patients, but also introduces a novel procedure with which to analyze the dynamic behavior of other related systems.

8.4 Future extension

Future research could expand the classification of heart failure patients to include other type of cardiomyopathies and heart diseases in general. The non-linear analysis of the cardiac, vascular and respiratory activity could contribute to the detection of etiology-specific patterns, which could aid in improving the prognosis of the patient, especially in cases where the diagnosis is unclear.

One limitation of this research is the sample size of the population used in the different studies. Therefore, one of the main areas of focus for future research would be the acquisition of a dataset that includes all the signals as well as a greater number of patients. This new larger dataset would enable the validation of all the studies proposed in this thesis.

The analysis of other signals like pulse pressure or the pulse transit time using the methods and procedures presented in this research could help to introduce new knowledge in the breakdown of physiological responses. Another area for future exploration is related to the introduction of clinical information that would help to add to our understanding of the complex interactions of cardiovascular regulation. The sum of all these contributions can facilitate the earlier and more accurate analysis of symptoms and evidence of these diseases. We hope to have advanced the research into biomedical signal processing, especially with regard to pseudo-periodic events.

8.5 Publications derived from this thesis

- International publications

[Giraldo 2015a] Giraldo, B.F., Rodriguez, J., Caminal, P., Bayés-Genis, A., Voss, A. (2015) "Cardiorespiratory and Cardiovascular Interactions in Cardiomyopathy Patients using Joint Symbolic Dynamic Analysis" *Engineering in Medicine and Biology Society, 2015. EMBC'15. Annual International Conference of the IEEE.*

[Rodriguez 2016a] Rodriguez, J., Giraldo, B.F., Caminal, P., Bayés-Genis, A., Voss, A. (2016) "Cardiorespiratory and Cardiovascular Interactions in Cardiomyopathy Patients using Joint Symbolic Dynamic Analysis" *9th IBEC Symposium for Active Ageing*, Barcelona, Spain, June 29

[Rodriguez 2017] Rodriguez, J., Voss, A., Caminal, P., Bayés-Genis, A., Giraldo, B.F. (2017) "Characterization and classification of patients with different levels of cardiac death risk by using Poincaré plot analysis." *Engineering in Medicine and Biology Society, 2017. EMBC'17. Annual International Conference of the IEEE.* pp. 1332-1335

[Rodriguez 2018a] Rodriguez, J., Giraldo, B.F. (2018) "A Novel Artifact Reconstruction Method Applied to Blood Pressure Signals." *Engineering in Medicine and Biology Society, 2018. EMBC'18. Annual International Conference of the IEEE.* pp. 4864-4867

[Rodriguez 2018b] Rodriguez, J., Voss, A., Schultz, S., Fischer, C., Giraldo, B. (2018) ”Sudden cardiac death risk stratification of idiopathic cardiomyopathy patients” *11th IBEC Symposium*, Barcelona, Spain, October 2

[Rodriguez 2019a] Rodriguez, J., Schulz, S., Giraldo, B.F. and Voss, A. (2019) Risk Stratification in Idiopathic Dilated Cardiomyopathy Patients Using Cardiovascular Coupling Analysis. *Frontiers in Physiology.* 10:841. doi: 10.3389/fphys. 2019.00841

[Rodriguez 2019b] Rodriguez, J., Schulz, S., Voss, A., Giraldo, B.F. (2019) ”Cardiovascular coupling-based classification of ischemic and dilated cardiomyopathy patients” *Engineering in Medicine and Biology Society, 2019. EMBC'19. Annual International Conference of the IEEE.*

[Rodriguez 2020] Rodriguez, J., Schulz, S., Voss, A., Giraldo, B.F. (2020) ”Cardiorespiratory and vascular variability analysis to classify patients with ischemic and dilated cardiomyopathy.” *Engineering in Medicine and Biology Society, 2020. EMBC'20. Annual International Conference of the IEEE.* (In press)

- National publications

[Giraldo 2015b] Giraldo, B. F., Rodríguez, J., Arcentales, A., Voss, A., Caminal, P., Bayes-Genis, A., (2015). “Caracterización de pacientes isquémicos y dilatados a partir de las señales ECG y de presión sanguínea” *XXXIII Congreso Anual de la Sociedad Española de Ingeniería Biomédica*, Madrid, November 4-6, 2015., pp. 31-34.

[Rodriguez 2016b] Rodriguez, J., Voss, A., Caminal, P., Bayés-Genis, A., Giraldo, B.F. (2016) “Caracterización de pacientes con diferentes niveles de riesgo cardiovascular mediante diagramas de Poincaré” *XXXIV Congreso Anual de la Sociedad Española de Ingeniería Biomédica*, Valencia, November 23-25, 2016., pp. 396-399.

[Rodriguez 2018c] Rodriguez, J., Voss, A., Caminal, P., Bayés-Genis, A., Giraldo, B.F. (2018) “Poincaré plot used to characterize and classify patients with different levels of cardiovascular risk” *Jornadas del grupo Ingenieria de sistemas automática e informática industrial (ESAII)*, Barcelona, February 9, 2018.

[Rodriguez 2018d] Rodriguez, J., Giraldo, B.F. (2018) “Reconstrucción de artefactos de calibración para señales de presión sanguínea” *25 Seminario anual de automática, electrónica industrial e instrumentación*, Barcelona, July 4-6, 2018.

Chapter 8 bibliography

[1] C. Fischer and A. Voss. "Three-Dimensional Segmented Poincare Plot Analyses SPPA3 Investigates Cardiovascular and Cardiorespiratory Couplings in Hypertensive Pregnancy Disorders". In: *Front Bioeng Biotechnol* 2 (2014), p. 51. ISSN: 2296-4185 (Print) 2296-4185 (Linking). DOI: `10.3389/fbioe.2014.00051`. URL: `https://www.ncbi.nlm.nih.gov/pubmed/25429364`.

[2] J. S. Floras. "Sympathetic nervous system activation in human heart failure: clinical implications of an updated model". In: *J Am Coll Cardiol* 54.5 (2009), pp. 375–85. ISSN: 1558-3597 (Electronic) 0735-1097 (Linking). DOI: `10.1016/j.jacc.2009.03.061`. URL: `https://www.ncbi.nlm.nih.gov/pubmed/19628111`.

[3] V. Fox, J. Hightower, Liao Lin, D. Schulz, and G. Borriello. "Bayesian filtering for location estimation". In: *IEEE Pervasive Computing* 2.3 (2003), pp. 24–33. ISSN: 1536-1268. DOI: `10.1109/MPRV.2003.1228524`.

[4] B. F. Giraldo, J. Rodríguez, A. Arcentales, A. Voss, P. Caminal, and A. Bayes-Genis. "Caracterización de pacientes isquémicos y dilatados a partir de las señales ECG y de presión sanguínea." In: *XXXIII Congreso Anual de la Sociedad Española de Ingeniería Biomédica.* (2015).

[5] B.F. Giraldo, J. Rodriguez, P. Caminal, A. Bayés-Genis, and A. Voss. "Cardiorespiratory and Cardiovascular Interactions in Cardiomyopathy Patients using Joint Symbolic Dynamic Analysis." In: *Engineering in Medicine and Biology Society, 2015. EMBC'15. Annual International Conference of the IEEE.* (2015).

[6] M. Izzetoglu, A. Devaraj, S. Bunce, and B. Onaral. "Motion artifact cancellation in NIR spectroscopy using Wiener filtering". In: *IEEE Transactions on Biomedical Engineering* 52.5 (2005), pp. 934–938. ISSN: 0018-9294. DOI: `10.1109/TBME.2005.845243`.

[7] D Kaplan, M. Furman, S. Pincus, S. Ryan, S. Lewis, A. Lipsitz, and A. Goldberger. "Aging and the complexity of cardiovascular dynamics." In: *Biophysiological Journal.* (1991).

[8] T. Kishi. "Heart failure as an autonomic nervous system dysfunction". In: *J Cardiol* 59.2 (2012), pp. 117–22. ISSN: 1876-4738 (Electronic) 0914-5087 (Linking). DOI: `10.1016/j.jjcc.2011.12.006`. URL: `https://www.ncbi.nlm.nih.gov/pubmed/22341431`.

[9] Hongxia Pan and Jifang Men. “De-noising method research on bearing fault signal based on particle filter”. In: *2010 Second World Congress on Nature and Biologically Inspired Computing (NaBIC)*, pp. 311–315. DOI: 10.1109/NABIC.2010.5716353.

[10] M. Zia Ur Rahman, R. A. Shaik, and D. V. R. K. Reddy. “Cancellation of artifacts in ECG Signals using sign based normalized adaptive filtering technique”. In: *2009 IEEE Symposium on Industrial Electronics & Applications*. Vol. 1, pp. 442–445. DOI: 10.1109/ISIEA.2009.5356413.

[11] J. Rodriguez and B.F. Giraldo. “A Novel Artifact Reconstruction Method Applied to Blood Pressure Signals.” In: *Engineering in Medicine and Biology Society, 2018. EMBC’18. Annual International Conference of the IEEE.* (2018).

[12] J. Rodriguez, B.F. Giraldo, P. Caminal, A. Bayés-Genis, and A. Voss. “Cardiorespiratory and Cardiovascular Interactions in Cardiomyopathy Patients using Joint Symbolic Dynamic Analysis.” In: *9th IBEC symposium for active ageing.* (2016).

[13] J. Rodriguez, S. Schulz, B.F. Giraldo, and A. Voss. “Risk Stratification in idiopathic dilated cardiomyopathy patients using cardiovascular coupling analysis.” In: *Frontiers in physiology.* (2019).

[14] J. Rodriguez, S. Schulz, A. Voss, and B.F. Giraldo. “Cardiorespiratory and vascular variability analysis to classify patients with ischemic and dilated cardiomyopathy.” In: *Engineering in Medicine and Biology Society, 2020. EMBC’20. Annual International Conference of the IEEE.* (2020).

[15] J. Rodriguez, S. Schulz, A. Voss, and B.F. Giraldo. “Cardiovascular coupling-based classification of ischemic and dilated cardiomyopathy patients.” In: *Engineering in Medicine and Biology Society, 2019. EMBC’19. Annual International Conference of the IEEE.* (2019).

[16] J. Rodriguez, A. Voss, P. Caminal, A. Bayés-Genis, and B.F. Giraldo. “Caracterización de pacientes con diferentes niveles de riesgo cardiovascular mediante diagramas de Poincaré.” In: *XXXIV Congreso Anual de la Sociedad Española de Ingeniería Biomédica.* (2016).

[17] J. Rodriguez, A. Voss, P. Caminal, A. Bayés-Genis, and B.F. Giraldo. “Characterization and classification of patients with different levels of cardiac death risk by using Poincaré plot analysis.” In: *Engineering in Medicine and Biology Society, 2017. EMBC’17. Annual International Conference of the IEEE.* (2017).

[18] J. Rodriguez, A. Voss, P. Caminal, A. Bayés-Genis, and B.F. Giraldo. “Poincaré plot used to characterize and classify patients with different levels of cardiovascular risk.” In: *Jornadas del grupo Ingenieria de sistemas automática e informática industrial (ESAII).* (2018).

[19] J. Rodriguez, A. Voss, S. Schultz, C. Fischer, and B. Giraldo. "Sudden cardiac death risk stratification of idiopathic cardiomyopathy patients." In: *11th IBEC symposium.* (2018).

[20] J. F. Valencia, M. Vallverdu, A. Porta, A. Voss, R. Schroeder, R. Vazquez, A. Bayes de Luna, and P. Caminal. "Ischemic risk stratification by means of multivariate analysis of the heart rate variability". In: *Physiol Meas* 34.3 (2013), pp. 325–38. ISSN: 1361-6579 (Electronic) 0967-3334 (Linking). DOI: 10.1088/0967-3334/34/3/325. URL: https://www.ncbi.nlm.nih.gov/pubmed/23399982.

[21] A. Voss, M. Goernig, R. Schroeder, S. Truebner, A. Schirdewan, and H. R. Figulla. "Blood pressure variability as sign of autonomic imbalance in patients with idiopathic dilated cardiomyopathy". In: *Pacing Clin Electrophysiol* 35.4 (2012), pp. 471–9. ISSN: 1540-8159 (Electronic) 0147-8389 (Linking). DOI: 10.1111/j.1540-8159.2011.03312.x. URL: https://www.ncbi.nlm.nih.gov/pubmed/22268614.